CRCLEME
Cooperative Research Centre for
Landscape Evolution & Mineral Exploration

AMIRA
Australian Mineral Industries Research Association Limited ACN 004 448 266

OPEN FILE
REPORT
SERIES

ATLAS OF FERRUGINOUS AND SILICEOUS MATERIALS, NORTH QUEENSLAND

C. Phang, R.R. Anand, J.E. Wildman and I.D.M. Robertson

CRC LEME OPEN FILE REPORT 136

May 2002

(CSIRO Exploration and Mining Report 450R/CRC LEME Report 66R, 1998.
Second impression 2002)

CRC LEME is an unincorporated joint venture between CSIRO-Exploration & Mining, and Land & Water, The Australian National University, Curtin University of Technology, University of Adelaide, University of Canberra, Geoscience Australia, Bureau of Rural Sciences, Primary Industries and Resources SA, NSW Department of Mineral Resources-Geological Survey and Minerals Council of Australia, established and supported under the Australian Government's Cooperative Research Centres Program.

CRC

AMIRA
Australian Mineral Industries Research Association Limited ACN 004 448 266

CRCLEME
Cooperative Research Centre for
Landscape Evolution & Mineral Exploration

ATLAS OF FERRUGINOUS AND SILICEOUS MATERIALS, NORTH QUEENSLAND

C. Phang, R.R. Anand, J.E. Wildman and I.D.M. Robertson

CRC LEME OPEN FILE REPORT 136

May 2002

(CSIRO Exploration and Mining Report 450R/CRC LEME Report 66R, 1998.
Second impression 2002)

CRC LEME is an unincorporated joint venture between CSIRO-Exploration & Mining, and Land & Water, The Australian National University, Curtin University of Technology, University of Adelaide, University of Canberra, Geoscience Australia, Bureau of Rural Sciences, Primary Industries and Resources SA, NSW Department of Mineral Resources-Geological Survey and Minerals Council of Australia.
Headquarters: CRC LEME c/o CSIRO Exploration and Mining, PO Box 1130, Bentley WA 6102, Australia

CSIRO/CRC LEME/AMIRA PROJECT P417
GEOCHEMICAL EXPLORATION IN REGOLITH-DOMINATED TERRAIN, NORTH QUEENSLAND 1994-1997

In 1994, CSIRO commenced a multi-client research project in regolith geology and geochemistry in North Queensland, supported by 11 mining companies, through the Australian Mineral Industries Research Association Limited (AMIRA). This research project, "Geochemical Exploration in Regolith-Dominated Terrain, North Queensland" had the aim of substantially improving geochemical methods of exploring for base metals and gold deposits under cover or obscured by deep weathering in selected areas within (a) the Mt Isa region and (b) the Charters Towers - North Drummond Basin region.

In July 1995, this project was incorporated into the research programs of CRC LEME, which provided an expanded staffing, not only from CSIRO but also from the Australian Geological Survey Organisation, University of Queensland and the Queensland Department of Minerals and Energy. The project, operated from nodes in Perth, Brisbane, Canberra and Sydney, was led by Dr R.R. Anand. It was commenced on 1st April 1994 and concluded in December 1997. The project involved regional mapping (three areas), district scale mapping (seven areas), local scale mapping (six areas), geochemical dispersion studies (fifteen sites) and geochronological studies (eleven sites). It carried the experience gained from the Yilgarn (see CRC LEME Open File Reports 1-75 and 86-112) across the continent and expanded upon it.

Although the confidentiality period of Project P417 expired in mid 2000, the reports have not been released previously. CRC LEME acknowledges the Australian Mineral Industries Research Association and CSIRO Division of Exploration and Mining for authority to publish these reports. It is intended that publication of the reports will be a substantial additional factor in transferring technology to aid the Australian mineral industry.

This report (CRC LEME Open File Report 136) is a second impression (second printing) of CSIRO, Division of Exploration and Mining Restricted Report 450R, first issued in 1998, which formed part of the CSIRO/AMIRA Project P417.

Copies of this publication can be obtained from:
The Publication Officer, c/- CRC LEME, CSIRO Exploration and Mining, P.O. Box 1130, Bentley, WA 6102, Australia.. Information on other publications in this series may be obtained from the above or from http://leme.anu.edu.au/

Cataloguing-in-Publication:

Atlas of ferruginous and siliceous materials, North Queensland.
ISBN 0 643 06841 4
1. Regolith - North Queensland 2. Landfoirms - North Queensland 3. Geochemistry - North Queensland
I. Phang, C II. Title
CRC LEME Open File Report 136.
ISSN 1329-4768

PREFACE AND EXECUTIVE SUMMARY

The CRC LEME-AMIRA Project 417 *Geochemical exploration in regolith-dominated terrain of North Queensland* has an overall aim of substantially improving geochemical methods of exploring for base metals and gold deposits under cover or obscured by deep weathering. Regolith-geochemical dispersion studies were undertaken in a variety of geomorphological and sedimentary settings with particular emphasis on distribution, characteristics and origin of the regolith.

This Atlas fulfils one of the specific objectives of this project that is to determine a field scheme for the identification and classification of sample types for use with exploration drilling and surface sampling. The Atlas depicts ferruginous and siliceous regolith materials that are found in the Mount Isa and Charters Towers - north Drummond Basin regions in North Queensland. Each group of regolith materials is subdivided into different regolith types and sub-types. The classification is based on field relationships and morphology of sliced hand specimens. Wherever feasible, regolith types are related to photographically illustrated geomorphological settings.

R.R. Anand
Project Leader

I.D.M. Robertson
Deputy Project Leader

CONTENTS

1. INTRODUCTION 1

1.1 Background 1
1.2 Regolith evolution 1
1.3 Atlas classification scheme and scope 4
1.4 Ferruginous versus siliceous materials - implications for exploration 4

2. FERRUGINOUS MATERIALS 12

2.1 Selected field perspectives of ferruginous duricrusts, nodules and pisoliths 12
2.2 Hand specimens and photomicrographs of ferruginous duricrusts 16
Pisolitic ferruginous duricrust 17
Pisolitic-nodular ferruginous duricrust 17
Nodular-vermiform ferruginous duricrust 18
Brecciated-pisolitic ferruginous duricrust 18
Vermiform ferruginous duricrust 19
Mottled ferruginous duricrust 19
Speckled ferruginous duricrust 19
Speckled-brecciated ferruginous duricrust 20
Variegated ferruginous duricrust 20
Gritty ferruginous duricrust 20
Conglomeratic ferruginous duricrust 21
Massive ferruginous duricrust 21
2.3 Hand specimens and photomicrographs of ferruginous pisoliths and nodules 23
Complex ferruginous pisolith 24
Variegated ferruginous pisolith 24
Oblate ferruginous nodules 24
2.4 Selected field perspectives of ferruginous saprolite 25
2.5 Hand specimens and photomicrographs of ferruginous saprolite 27
Brecciated/collapsed, Fe oxide-stained saprolite 28
Blocky ferruginous saprolite 28
Massive ferruginous saprolite 28
Laminated ferruginous saprolite 29
2.6 Selected field perspectives of cemented sands, grits and silts 30
2.7 Hand specimens and photomicrographs of cemented sands, grits and silts 33
2.8 Selected field perspectives of ironstones 35
2.9 Hand specimens and photomicrographs of ironstones 38
Massive ironstone 39
Variegated ironstone 39
Vesicular ironstone 39
Stratiform ironstone 40
2.10 Selected field perspectives of ferruginous veins and bands 41
2.11 Hand specimens and photomicrographs of ferruginous veins and bands 43
Massive ferruginous vein 44
Variegated ferruginous vein 44
Striated ferruginous vein 44
Fragmental ferruginous vein 45
Sinuous ferruginous band 45
Striated ferruginous band 45

3. SILICEOUS MATERIALS 46

3.1 Selected field perspectives of silcrete 46
3.2 Hand specimens and photomicrographs of silcrete 50
Nodular-massive silcrete 51
Terrazzo silcrete 51
Brecciated silcrete 51
Fragmental silcrete 52
Massive silcrete 52
Columnar silcrete 53
3.3 Selected field perspectives of silicified saprolite and mottled, silicified saprolite 54
3.4 Hand specimens and photomicrographs of silicified saprolite 55
Laminated silicified saprolite 56
Folded silicified saprolite 56
Speckled silicified saprolite 56
3.5 Hand specimens and photomicrographs of mottled, silicified saprolite 57
3.6 Selected field perspectives of cherty breccia 59
3.7 Hand specimens and photomicrographs of cherty breccia 60

4. ACKNOWLEDGMENTS 62

5. REFERENCES 62

APPENDICES

Appendix I : Geochemistry of ferruginous and siliceous materials.

Appendix II : Petrography and geochemistry of bedrocks and ironstones from Grey Ghost and Gordon prospects.
Table 1 : Geochemistry of fresh rocks, saprolite and stratiform ironstones from Grey Ghost and Gordon prospects.

1. INTRODUCTION

1.1 Background

Mineral exploration in the Mount Isa and Charters Towers - north Drummond Basin regions in North Queensland is now focussing on mineralisation under deeply weathered or transported cover, including Mesozoic and older sediments. Weathering, erosion and sedimentation have concealed, altered or weakened the geological, geochemical and geophysical expression of the underlying ore deposits.

To address these exploration problems, CSIRO-AMIRA Project 417, was initiated to develop suitable geochemical exploration methods for regolith covered areas, based on an improved knowledge of the nature and evolution of the regolith and landscape. Regolith-geochemical dispersion studies were undertaken in a variety of geomorphological and sedimentary settings with particular emphasis on distribution, characteristics and origin of the regolith. The locations of districts and sites studied are shown in Figure 1.1. This Atlas is a compilation describing the principal ferruginous and siliceous materials that are found in these two regions to assist field explorationists.

1.2 Regolith evolution

The summary of the regolith-landform synthesis of the Mt Isa and Charters Towers - north Drummond Basin regions, presented here, is derived from Anand *et al.*, (1996) and Anand *et al.*, (1997).

Mt Isa Region

The effects of weathering, cycles of erosion, deposition and induration of regolith materials have produced diverse landforms. Field relationships and dating of Mn oxides suggest that the evolution of weathering profiles spans the Tertiary, possibly extending into the Cretaceous.

The details of the Mt Isa landsurface are intimately related to differential weathering and erosion of the various lithologies. Quartzite forms upstanding masses; siltstone and claystone tend to offer little resistance and were eroded relatively easily, to form lowlands and valleys. The flat summits (420-520 amsl), preserved on quartzite, lack weathering profiles. However, in places, soil and colluvia in depressions contain ferruginous pisoliths, suggesting that even these summits may have been blanketed by weathering profiles, now eroded.

In the Mt Isa region, Proterozoic basement may be overlain by Cambrian, Mesozoic and Cainozoic sediments. The Mesozoic cover extended over a very large part of the Mt Isa region but, now, Mesozoic sediments are more widespread in the southeast and to the north than in the centre of the Mt Isa Inlier. Weathering profiles have developed on Proterozoic bedrock, Cambrian and Mesozoic sediments and extend to variable depths below the present landsurface. The depth of weathering is largely controlled by landscape position, bedrock, structural features and overlying sediments at the time of weathering. Palaeoplains and topographic lows are more deeply weathered than the erosional plains and hill belts. At many locations, Proterozoic bedrock is weathered to greater depths where overlying Cambrian or Mesozoic sediments have been removed or were never deposited.

Weathering has resulted in regolith profiles capped, in places, by ferruginous or siliceous duricrust. Saprolite is generally present, but the upper ferruginous or siliceous horizons may be absent, due to incomplete formation or erosion. In places, ferruginous duricrust is developed on

Fe-rich bedrock (e.g., basalt, gabbro, dolomitic siltstone, and shale). They are more common in the Western Succession than in the Eastern Succession. Silcrete has developed on siliceous bedrock (e.g., stromatolitic shale and siltstone), indicating a lithological control. Ferruginous duricrust and silcrete may occur within a few hundreds metres of each other.

The ferruginous profile on Proterozoic bedrock consists of ferruginous duricrust, mottled saprolite, saprolite, saprock and bedrock. Mottled saprolite, 2-5 m thick, which overlies the saprolite, is characterised by hematite- and goethite-rich mottles in a kaolinite-rich matrix and becomes more indurated towards the top of the profile. There is a gradual transition between mottled saprolite and overlying duricrust. In places, higher in the profile, soft, clay-rich masses in the mottled saprolite have been dissolved, leading to its collapse (*collapsed mottled saprolite*).

A variety of ferruginous duricrusts were identified and their pathways of formation are shown in Figure 1.2. There is a gradual transition between mottled saprolite and overlying duricrust. The *massive, fragmental and nodular duricrusts* have formed *in situ* on weathered rocks by accumulation of ferruginous material from the mottled saprolite, left by down-wasting of the profile as clays and soluble elements were removed. The Fe oxide mineralogy and field relationships suggest that *slabby duricrusts* formed on the lower slopes by induration of locally derived gritty colluvium and upper saprolite. Iron in slabby duricrust is thought to be enriched by absolute accumulation, derived from weathering of a local, upland area, lateral chemical transport and precipitation in a low landscape position. Subsequently, induration by ferruginisation allowed differential erosion and relief inversion to its current topographic position.

Goethite- and hollandite-rich *vesicular duricrust* is probably the youngest duricrust in the landscape. Iron and Mn in vesicular duricrust are interpreted to be derived from degradation of regolith up slope.

Ferruginous duricrusts have developed on some Mesozoic sediments. The *massive and slabby duricrusts*, which developed on Mesozoic sediments (claystone and sandstone), closely resemble those developed on Proterozoic bedrocks in that their Fe oxide mineralogy is similar to those developed on Proterozoic bedrock. However, they are relatively enriched in Si, Zr and Ti. Duricrusts, in many places, have resulted from absolute accumulation of Fe oxide because most contain more Fe oxide than normally would be obtainable from their Fe-poor parent rocks by relative accumulation.

An idealised *silcrete profile on Proterozoic bedrock* consists, from top to base, of silcrete, silicified saprolite, saprolite, saprock and bedrock. Kaolinitic saprolite is overlain by a bleached quartz- and kaolinite-rich, silicified saprolite with rock structures and fabrics at least partially preserved. Silcrete overlying silicified saprolite is an indurated, grey, massive or columnar horizon rich in quartz and microcrystalline quartz with small amounts of anatase. Silica increases in abundance up the profile in the sites examined and Al decreases. Zirconium and Ti are enriched relative to the underlying saprolite.

The *massive silcretes* may be due to groundwater precipitation of silica. However, other structures within some silcretes, including columnar jointing patterns and candlestick beading, could be indicative of a pedogenic origin. Jointing may reflect columnar peds in a palaeosol and candlestick beading may relate to movement of solute particles down an old soil profile which has since been silicified. Loss of the primary fabric from the silcrete suggests that they have formed close to the surface.

In places, silica has cemented alluvial sands or sheet wash sands and gravels. Silicification is probably associated with fluxes of silica-rich groundwaters when the sediments were low in the

landscape. Silicified alluvial sands and gravels now occupy topographically high areas because of relief inversion since induration. The inversion can be very subtle with only a few metres elevation difference between an older, silicified alluvium and a modern channel. In other places (e.g., the Grey Ghost area), the silicified sediments are some 40 m above the present drainages.

Silicification appears to be occurring at present, with siliceous hardpans developing within extensive, low-lying, colluvial plains. Both ferruginous and siliceous secondary cements are common within the same weathering profile. Either silicification overprints ferruginous materials or the reverse, suggesting that conditions favourable for both silicification and ferruginisation have occurred recently.

Weathering of Cambrian sediments forms a profile comprising cherty breccia or silcrete over mottled Proterozoic saprolite. In places, silcrete on Cambrian sediments is overlain by massive, ferruginous duricrust on Mesozoic sediments.

Charter Towers - north Drummond Basin region

In the Charters Towers - north Drummond Basin region, the cover rocks are Cainozoic sediments, the older, Southern Cross and Suttor Formations, and the younger, Campaspe Formation, overlying Palaeozoic rocks.

The *Southern Cross Formation* forms an extensive blanket over the northern Drummond Basin and the Lolworth-Ravenswood Block. The weathering profile on the Southern Cross Formation is variable. In some places, the Southern Cross Formation is partly eroded into breakaways, exposing underlying mottled sediments and mottled basement (Campbell, 1996) but, in other areas, deep red or yellow earths are underlain by mottled sediments. The basal Southern Cross Formation contains clay and lithic clasts of the basement rocks. Pisolitic duricrust is limited to the local high areas on the plateaux and mesas, where incision of the plateau has increased the drainage locally. Ferruginisation occurs throughout the top few metres of the profile but pisoliths are present in the top half metre. Some pisoliths are detrital, being derived from older profiles, and others have formed *in situ*.

The *Campaspe Formation* is dominated by sands with minor interbedded silts and clays and covers much of the northern Drummond Basin and the Lolworths-Ravenswood Block. In many areas, the Campaspe Formation has limited outcrop as it occurs in low parts of the landscape and lacks breakaways.

The profile exposed at Red Falls is one of the few places where the Campaspe Formation overlies the Southern Cross Formation. Here, the Campaspe Formation is about 14 m thick and consists of yellow earths, ferruginous gravels, mottled, quartz-rich sediments and sands within a clay-rich matrix. The sands unconformably overlie the red, mottled Southern Cross Formation and show bedding and cross-bedding. Cementing of quartz-grains by Fe oxides occurs at the top of the profile. This ferruginous horizon degrades to a lag composed mainly of ferruginous gravel (2-25 mm), mainly of Fe oxide-stained and cemented sandstone with some large, angular quartz fragments, pisoliths and nodules which, in places, are cemented by goethite into nodular duricrust. In contrast, the mottled Southern Cross Formation consists of gritty sandstone and lacks sedimentary structures. A similar profile in the Campaspe Formation occurs at the Waterloo Prospect and many parts of the Charters Tower - north Drummond Basin. There appears to be two types of nodules and pisoliths developed in the upper part of the Campaspe formation. Some are detrital, with broken edges, but the majority was formed *in situ* in the soil or its substrate. The surfaces of nodules and pisoliths have goethite-rich cutans. In places, massive duricrust has formed instead of pisoliths over relatively fresh sediments, without any deep, weathered profile.

The minor weathering of the substrate suggests that Fe oxide in these pisoliths and duricrusts came from the surrounding uplands rather than from the basement below the Campaspe Formation.

Discontinuities in feldspar and kaolinite abundances, rounding of quartz grains and geochemical parameters such as Ti/Zr ratios can be used to distinguish the Campaspe Formation from weathered basement volcanics (Scott, 1997).

The *Suttor Formation* is thought to be equivalent to the Southern Cross Formation in the Charters Towers area (Li Shu, 1997). Ferruginisation and silicification occur throughout the profile, with duricrusts developed at the top. Where silica or iron has been moved hydromorphically, the bleached sediments have been transformed to silcrete; in places, some silcretes have been subsequently been de-silicified.

In the Pajingo area, *profiles on basement rocks* are characterised by Fe oxide-rich pisolitic duricrust similar to that developed on the Tertiary sediments but lacking cobbles. The duricrust is dominantly hematite, with some goethite, gibbsite and kaolinite cementing the pisoliths. Mottled saprolite on volcanic rocks is equivalent to mottled Tertiary sediments. Mottles are confined to one horizon and the mottling is much more intense than on the Tertiary sediments. The mineralogy is similar to that of the mottled sediments; distinguishing between the two can be difficult. Generally the vegetation on this unit tends to be sparser than on the mottled sediments. In places, mottles have been broken into a very coarse lag.

In the Mt Coolon area, profiles on basement rocks, in particular the metamorphosed sandstones and siltstones of the Anakie Formation have weathered to mottled saprolite or silcrete. Similarly, the Tertiary sediments have also weathered to mottled saprolite and silcrete which form mesas. This provides a dilemma when mapping using aerial photographs.

1.3 Atlas classification scheme and scope

The Atlas illustrates ferruginous and siliceous regolith materials, classified according to the scheme shown in Figures 1.3 and 1.4. Each group is subdivided into different regolith types and sub-types. This classification and nomenclature are based on field relationships and morphology of sliced hand specimens. The stratigraphic relationship between regolith types is illustrated in Figure 1.5. Geochemical, and mineralogical characteristics are displayed in charts. Explanatory notes for reading these charts are given in Figure 1.6. The geochemical data are in Appendix I. Mineralogical interpretations are principally based on XRD data. Photomicrographs have been taken of samples either in thin section, polished thin section, polished block or magnified view and are depicted in Figure FM series (Ferruginous Materials) and Figure SM series (Siliceous Materials). Wherever feasible, regolith types are related to photographically illustrated geomorphological settings.

1.4 Ferruginous versus siliceous materials - implications for exploration

Many residual ferruginous materials may accumulate pathfinder elements from mineralisation and have potential application as sampling media in exploration. However, different materials occur, in different environments, so it is difficult to achieve sample uniformity. Each type of ferruginous material has to be assessed in terms of its origin, e.g., residual nodules and pisoliths and duricrust, ferruginised sediments, Fe leakage ironstones, gossans or fault ironstones, ferruginous bands formed at water-tables or redox fronts or structurally controlled ferruginous veins. Dispersion can then be described in terms of bedrock, hydrology and landscape, and an exploration strategy developed (Anand *et al.*, 1997).

Siliceous materials tend to be developed on siliceous bedrock (e.g. stromatolitic shale and siltstone) and silcrete may occur within a few hundred metres from a ferruginous duricrust (Anand *et al.*, 1996). Ferruginous materials can coexist in a siliceous environment such as the ferruginous cherty breccia at the Drifter Prospect where Fe-rich fluid is channeled through fault lines and, in the case of silcrete at the Grey Ghost Prospect, the formation of ferruginous skin on the silcrete. Some siliceous materials can become potential sampling media where associated with Fe-oxides.

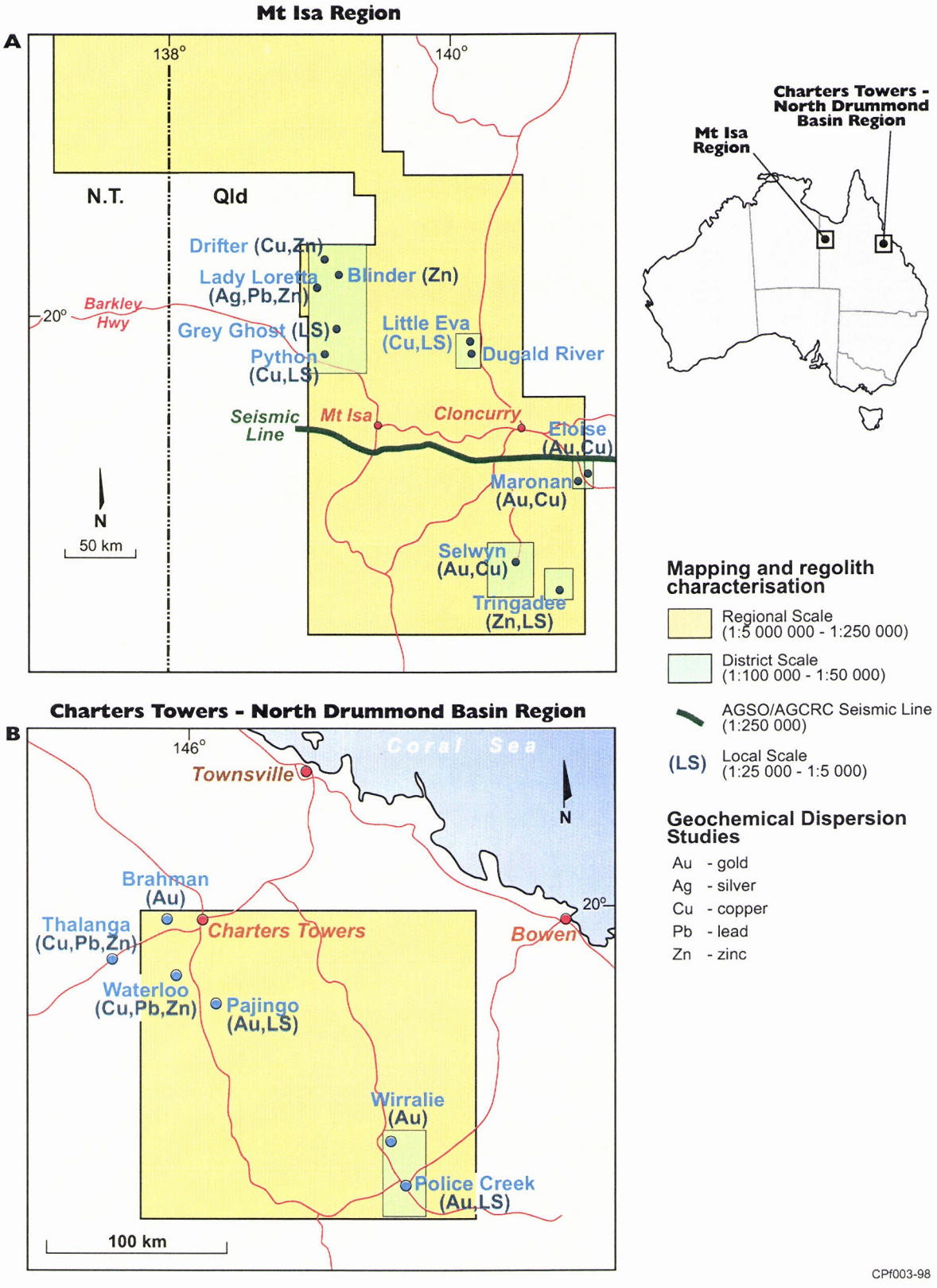

Figure 1.1. Location of study areas in (A) Mt Isa Region and (B) the Charters Towers - north Drummond Basin Region (after Anand *et al.*, 1997).

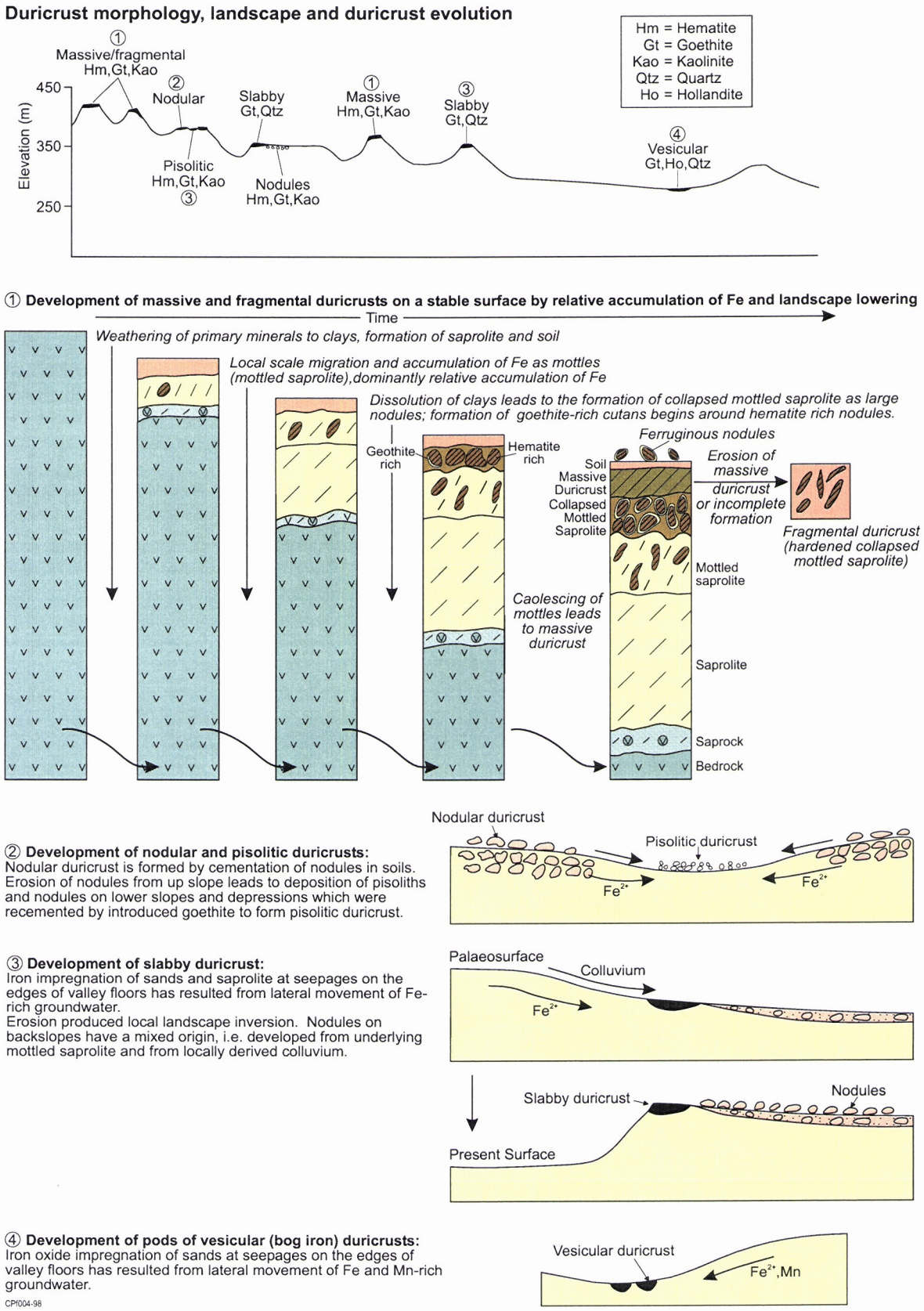

Figure 1.2. Pathways of evolution of ferruginous duricrusts in the Mt Isa region (after Anand *et al.*, 1997).

CLASSIFICATION SCHEME

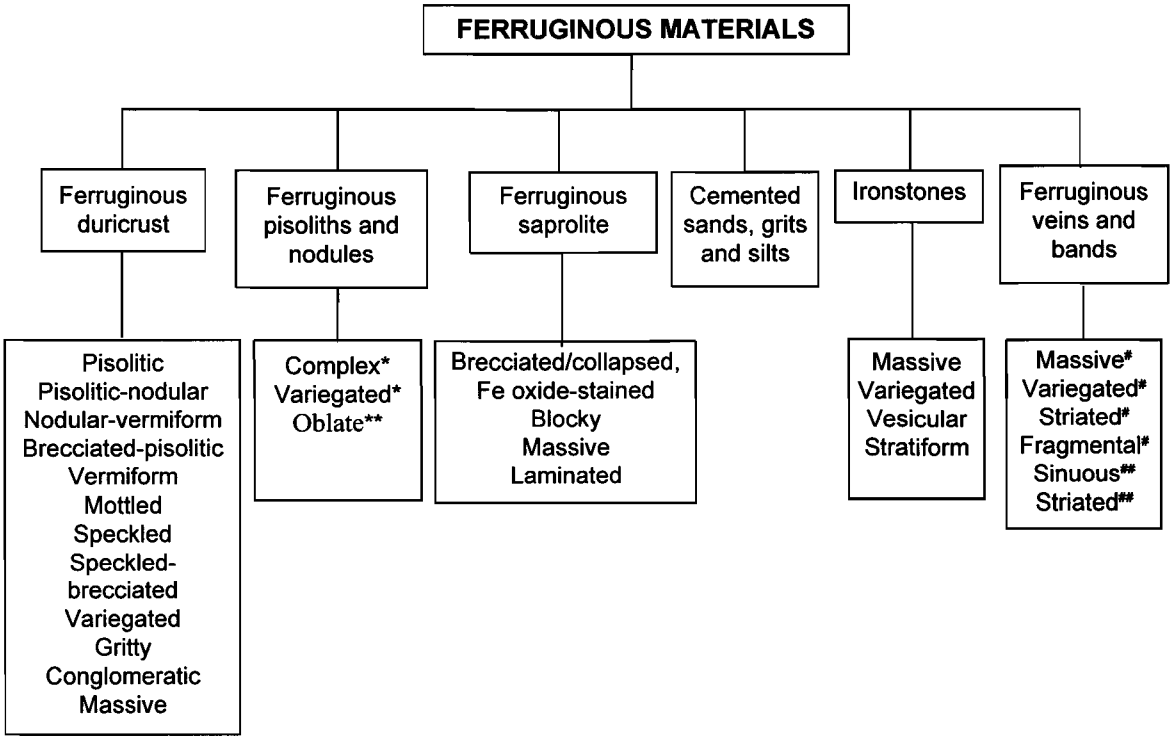

* ferruginous pisoliths
** ferruginous nodules
\# ferruginous veins
\#\# ferruginous bands

Figure 1.3. Classification scheme for ferruginous materials.

CLASSIFICATION SCHEME

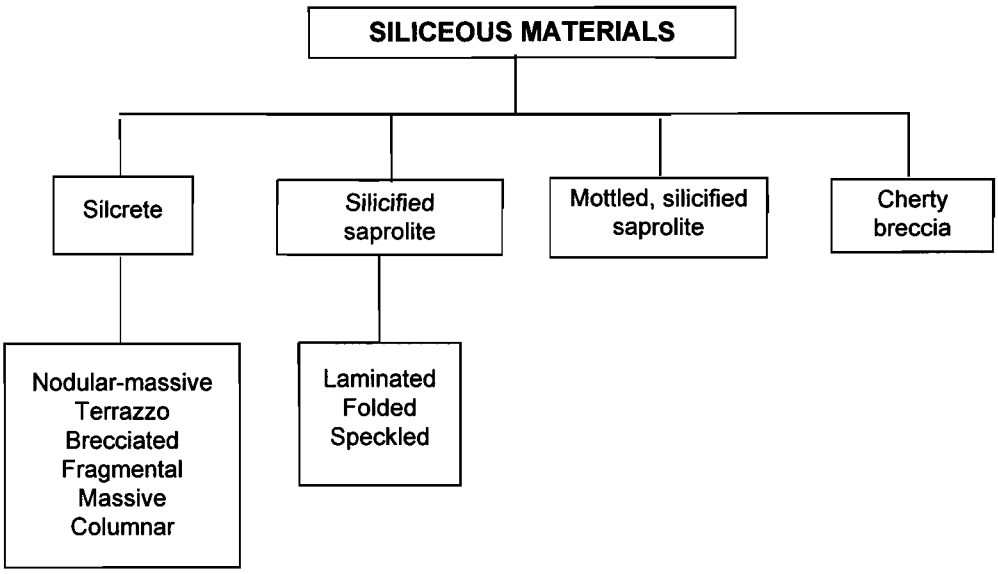

Figure 1.4. Classification scheme for siliceous materials.

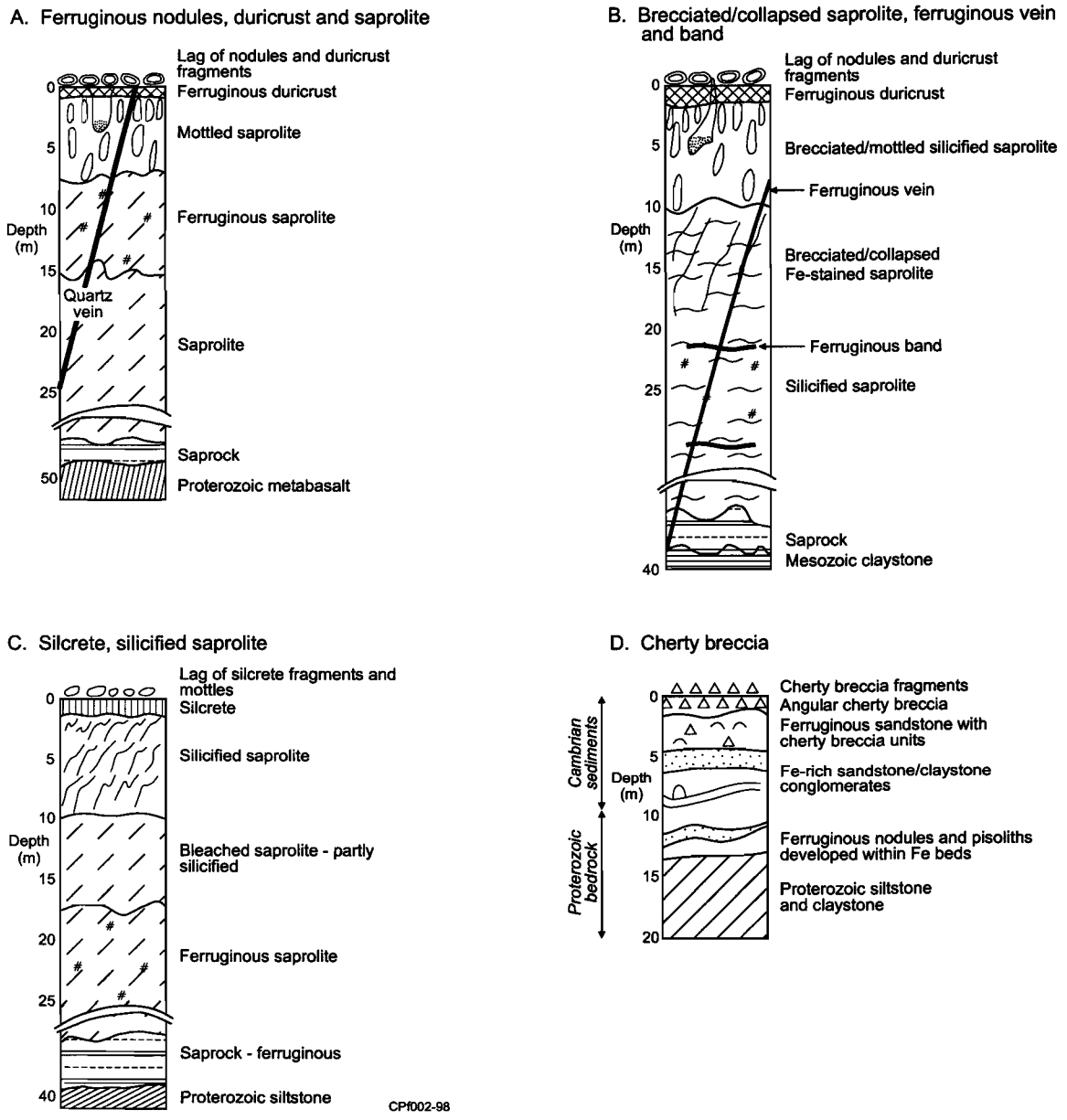

Figure 1.5. Illustrations of stratigraphic relationship between regolith types (adapted from Anand et *al.*, 1997)

1. Mineralogical abbreviations

Ana	Anatase	Hm	Hematite
Ap	Apatite	K	Kaolinite
Ca	Calcite	Li	Lithiophorite
Crt	Cryptomelane	M	Mica
F	Feldspar/plagioclase	Q	Quartz
Gt	Goethite	Rt	Rutile
Ha	Halite	Sm	Smectite
Ho	Hollandite		
	-am amorphous component is present		

2. Mineral species relative abundance

2.1. The relative abundance is indicated by an index in superscript.

>90%	1	30-50%	4
70-90%	2	10-30%	5
50-70%	3	<10%	6

2.2. Examples

e.g., 1 **Hm-Gt^3,K^5,M^5**
Implies hematite is more abundant than goethite, but their combined presence is in the range of 50-70%; kaolinite and mica are in the same range of 10-30% but kaolinite is more abundant than mica. The relative abundance between minerals increases towards the left of the series of abbreviations.

e.g., 2 **Q-am^1,Ana-Rt^6**
Implies quartz also has an amorphous component with combined presence of >90%; anatase is relative more abundant than rutile with combined presence is in the range of <10%. The relative abundance between minerals also increases towards the left of the series of abbreviations.

For an element with concentration below detection limit of the instrument, half value of detection limit for that element is used in this plot. Detection limits are :

	SiO2	Al2O3	Fe2O3	MnO	MgO	CaO	Na2O
Unit	%	%	%	%	%	%	%
Detection limit	0.01	0.01	0.005	0.002	0.01	0.001	0.01

	K2O	P2O5	TiO2	Zr	Ba	Cu	Pb	Zn
Unit	%	%	%	ppm	ppm	ppm	ppm	ppm
Detection limit	0.001	0.002	0.003	5	30	10	5	5

Vertical axis (logarithmic scale)
% : for major oxides
ppm : for trace elements

To be read as 10.8 % Al_2O_3

To be read as 32 ppm Zr

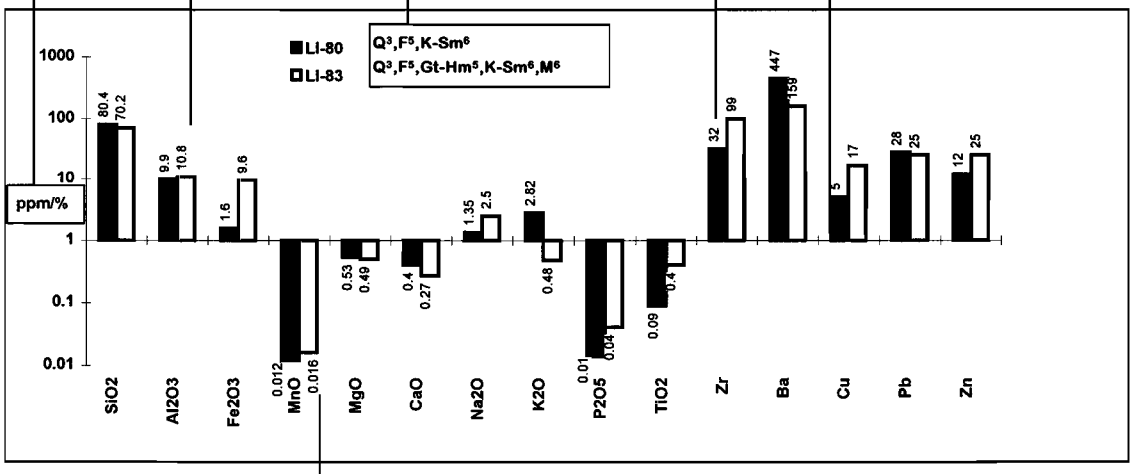

For concentration of major oxides < 1%, bar graphs are plotted below horizontal axis. Bar graph height is inversely related to concentration.

Figure 1.6. Explanatory notes on geochemical chart.

2.1. SELECTED FIELD PERSPECTIVES OF FERRUGINOUS DURICRUSTS, NODULES AND PISOLITHS

Ferruginous duricrust can be part of the weathering profile (*lateritic duricrust*) or formed on transported material through cementation of weathering detritus with poor or even negligible profile development (*ferruginised sediments or ferricrete*). The ferruginous duricrust is associated with Fe-rich bedrock (*e.g.*, basalt, gabbro, pyritic siltstone and shale) and is more common in the Eastern than the Western Succession of the Mt Isa region (Anand *et al.*, 1997).

Guidelines for distinguishing residual *versus* transported ferruginous duricrust, nodules and pisoliths (after Anand *et al.*, 1997).

Requires combined interpretation of field relationships, morphology, mineralogy and chemistry

Ferruginous duricrust, nodules+ and pisoliths+

residual

- Preservation of bedrock structures, quartz veins or fabrics through the complete profile.
- Gradual transition between mottled saprolite and overlying duricrust.
- Angular shapes and diffuse external borders.
- Similar framework grains within nodules and matrix materials.
- Thin, goethite-rich yellowish brown cutans (may have undergone minimal transport after their formation).

transported

- Goethite and Mn-oxide rich and generally lack kaolinite and hematite e.g., slabby and vesicular duricrust.
- Presence of quartz pebbles, zircon and heavy minerals can suggest formation in distal alluvium.
- Some pisolitic or nodular duricrusts could be localised reworking (50-100 m) of laterally introduced goethite cementing pisoliths or nodules.
- Large proportion of nodules or pisoliths with chipped or worn cutans.
- Significant variability in texture and composition of clasts.

+ nodules are irregular in shape and may have a cutan around a nucleus or core. As sphericity increases, the term pisolith becomes appropriate (Anand et al., 1989).

Some examples of residual and transported duricrust are illustrated in Figures 2.1-2.5

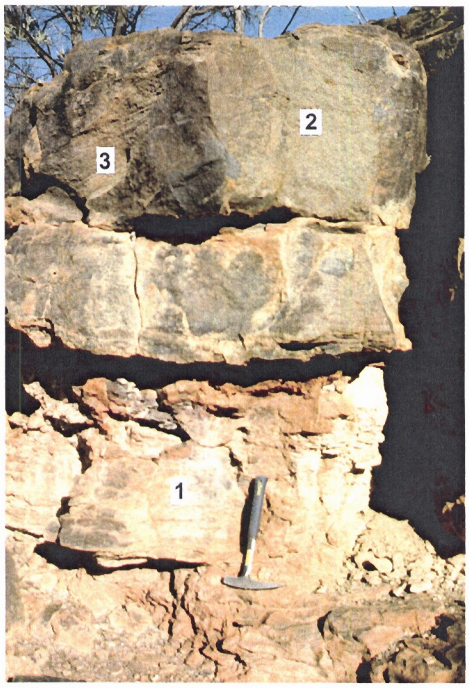

Figure 2.1. *Residual duricrust.* A gradual transition from underlying mottled saprolite (1) to massive duricrust (2). Cross-bedding structure (3) of sandstone can be seen in the duricrust. Profile on Mesozoic sandstone at Selwyn area, AMG 448000 mE, 7627450 mN, Zone 54K.

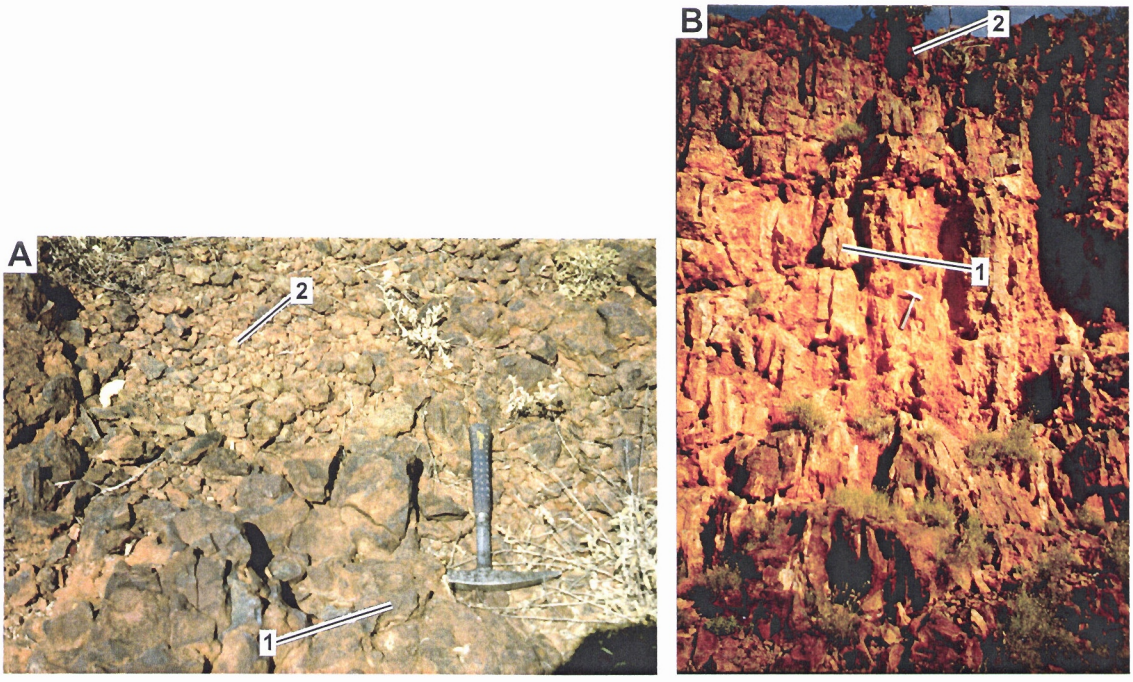

Figure 2.2. *Residual massive duricrust, nodules and pisoliths.*
A. Massive duricrust (1) with veneer of nodules and pisoliths (2).
B. Underlying ferruginous saprolite (1) (Refer Figure FM8-C,D) which shows relict vertical jointing and gradual transition upwards to massive duricrust (2). In this profile, a remnant quartz vein (not shown) trangresses the profile. Profile on Proterozoic metabasalt at Buckley River area, AMG 324600 mE, 7755410 mN, Zone 54K.

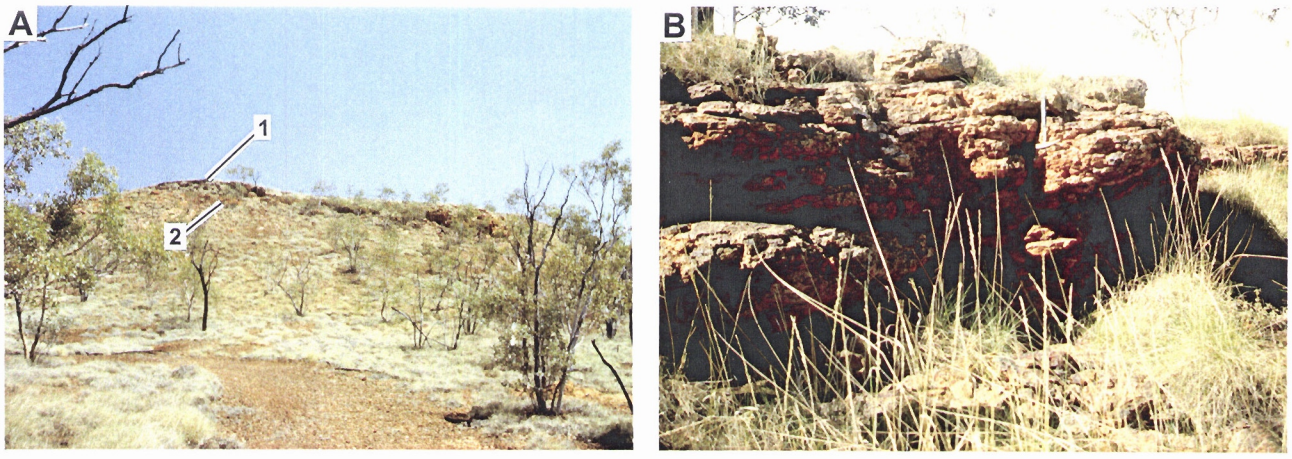

Figure 2.3. *Transported duricrust.*

A. General view of slabby duricust (1) on plateau margin, lying unconformably on mottled, silicified, Proterozoic saprolite (2). Close view of (2) is shown in Figure 2.7B. Buckley river area, AMG 307250 mE, 7756170 mN.

B. Close view of a slabby duricrust. It was formed by Fe oxide impregnation of sands at seepages on edges of valley floors. It has now become a topographic high in the present landscape. Buckley river area, AMG 303470 mE, 7759530 mN, Zone 54K.

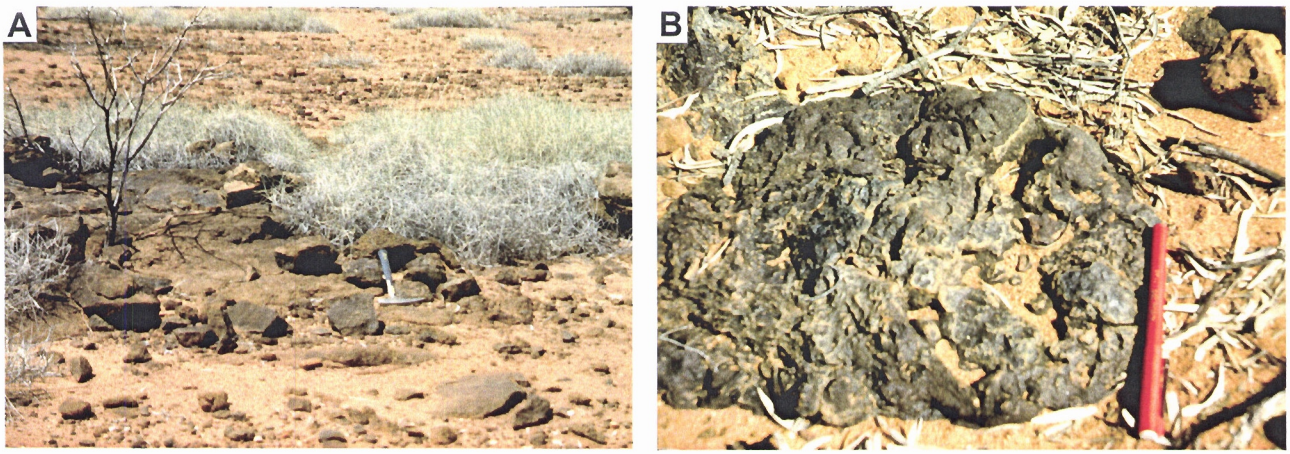

Figure 2.4. *Transported duricrust.*

A. A scattering of ferruginous duricrust on a colluvial-alluvial plain. The duricrust was formed by cementation by goethite of locally derived sands.

B. Close up view of ferruginous duricrust. Refer Figure FM6-C,D. Tringadee area, AMG 482460 mE, 7588900 mN, Zone 54K.

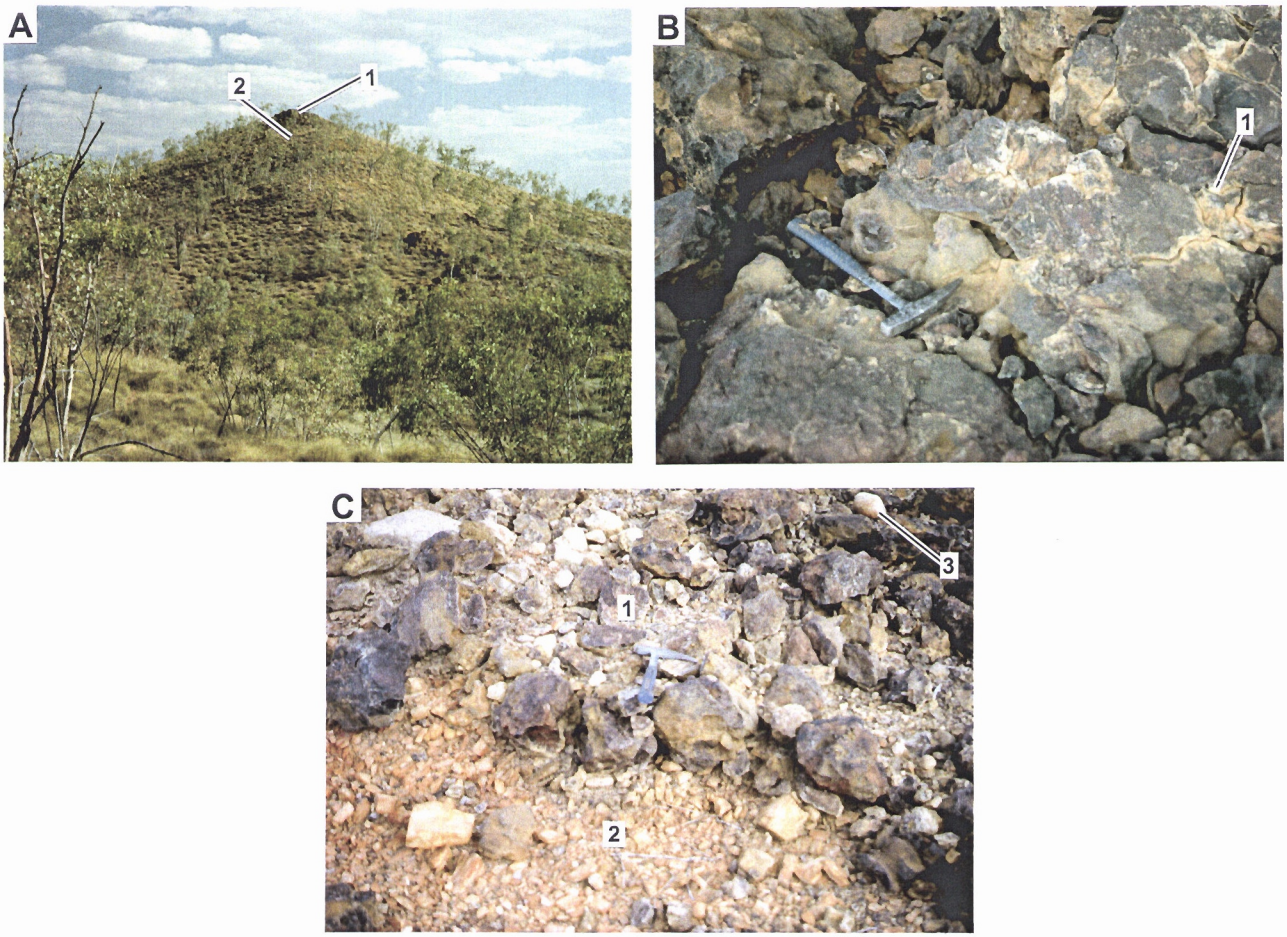

Figure 2.5. *Transported duricrust.*

A. General view of massive duricrust (1) on silicified, Proterozoic saprolite (2).
B. Close view of massive duricrust, showing some minor rounded quartz clasts (1). (Refer Figure FM6-A,B).
C. Lower part (1) of the same massive duricrust unconformably overlies silicified, Proterozoic saprolite (2). Note quartz cobble (3) is rounded. The abundances of Cu (115 ppm) and Co (55 ppm) in this massive duricrust are much greater than in the underlying silicified saprolite (1 ppm Cu), suggesting the two units are not genetically related. Probably the massive duricrust was formed in a low position, in an undulating landscape, with Fe and Cu derived laterally from groundwater. The topography has since been inverted (Anand *et al.*, 1996).

2.2 HAND SPECIMENS AND PHOTOMICROGRAPHS OF FERRUGINOUS DURICRUSTS

FIGURE FM1
FERRUGINOUS DURICRUST

Pisolitic ferruginous duricrust

A. Pisolitic ferruginous duricrust in Proterozoic dolomitic siltstone. Pisoliths of varying sizes are closely packed. Interstices are filled with Fe oxide-stained kaolinite (1) or in places, occur as a conglomerate of kaolinite spherules (2). Rare, subrounded quartz is found in the interstices (3). *C.f.* Figure FM1-B. Polished specimen BR-2 from Buckley River area, AMG 304220 mE, 7757070 mN, Zone 54K.

B. Detail of Figure FM1-A. The pisoliths have multi-layered goethite-rich cutans (1) and a porous, hematite-rich core (2), some of which have very minor quartz grains (3) embedded in them. Some pisoliths are enclosed in a compound nodule (4) which has a reddish Fe oxide-stained matrix. Interstices are dominantly filled by goethite-stained kaolinite (5) that contains tiny, black, hematite-rich fragments. Close up photograph in oblique reflected light.

C. Pisolitic ferruginous duricrust in Southern Cross Formation. Pisoliths of varying sizes are set in reddish, Fe oxide-stained, kaolinite-rich matrix (1) which contains tiny quartz grains either sporadically distributed or concentrated together (2). Rare, rounded quartz granule (3) is embedded in the matrix. *C.f.* Figure FM1-D. Polished specimen LI-82 from Red Falls, AMG 367700 mE, 7795920 mN, Zone 55.

D. Detail of Figure FM1-C. Pisolith consists of subangular quartz grains (1) cemented by hematite rich clay (2) containing vugs (3). The matrix contains many vugs (4) and an aggregation of tiny spherules (5) of goethite-stained clay with oriented, birefringent clay cutan. Photomicrograph with crossed polarizers.

Pisolitic-nodular ferruginous duricrust

E. Pisolitic-nodular ferruginous duricrust in Proterozoic shale. Pisoliths (1) and nodules (2) are hematite-rich and are set in reddish hematite-stained kaolinite (3). A ferruginous saprolite fragment (4) is present. The matrix contains a few subangular quartz granules (5). Many ghost-like pisoliths (6) can be seen which have fabrics similar to the matrix. *C.f.* Figure FM1-F. Polished specimen 4095 from Buckley River area, AMG 305095 mE, 7761500 mN, Zone 54K.

F. Detail of Figure FM1-E. Hematite-rich nodule has a concentration of hematite at the cortex (1) and fissures (2). Core contains hematite-stained kaolinite (3) with some subangular quartz grains (4) which is similar to the matrix (5). Photomicrograph in normally reflected light.

Geochemistry and mineralogy

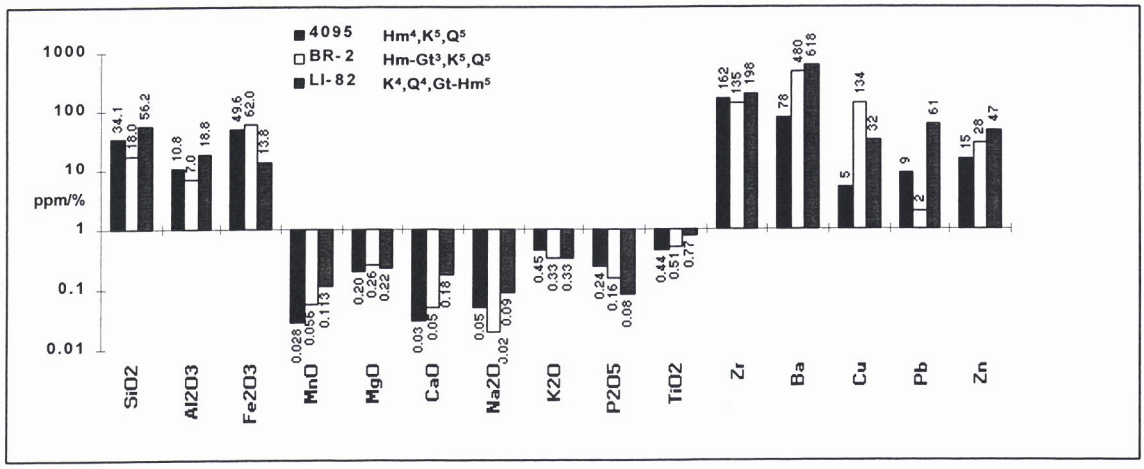

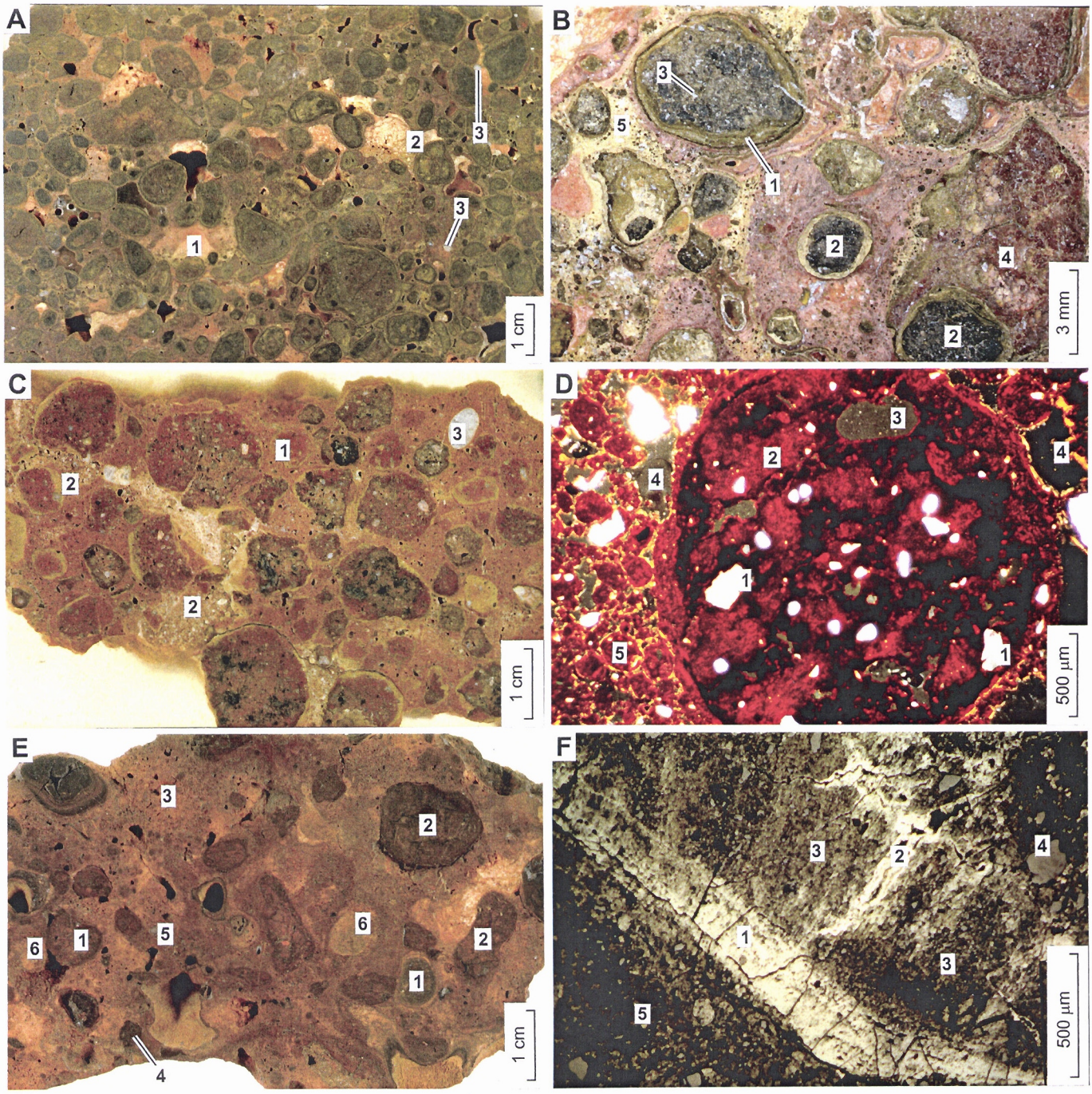
A
1
2
3
3
1 cm
B
3
5
1
2
4
2
3 mm
C
1
3
2
2
1 cm
D
3
2
4
4
1
5
1
500 µm
E
3
2
6
1
5
6
2
1
4
1 cm
F
3
2
4
1
3
5
500 µm

FIGURE FM2
FERRUGINOUS DURICRUST

Nodular-vermiform ferruginous duricrust

A. Nodular-vermiform ferruginous duricrust in Mesozoic sandstone. Hematite-kaolinite-rich nodules (1) with white spots of kaolinite set in vermiform goethite-rich matrix (2). Matrix contains numerous, tiny, goethite-stained kaolinite spherules (3). *C.f.* Figure FM2-B. Polished specimen 4145 from Drifter area, AMG 303770 mE, 7835090 mN, Zone 54K.

B. Detail of Figure FM2-A. Goethite-rich matrix contains spherules of kaolinite (1) interlinked by a thin coat of goethite (2) with abundant vugs (3). Photomicrograph in normally reflected light.

Brecciated-pisolitic ferruginous duricrust

C. Brecciated-pisolitic ferruginous duricrust in Proterozoic granite. Goethite-rich ferruginous saprolite fragments (1) contain profuse network of hematite (2) and some subangular quartz grains (3). Tiny spherules of kaolinite (4) and subrounded quartz grains with kaolinite-rich cutans (5) cement the ferruginous saprolite fragments. *C.f.* Figure FM2-D. Polished specimen TG-204 from Tringadee area, AMG 469120 mE, 7589130 mN, Zone 54K.

D. Detail of Figure FM2-C. Spherules of goethite-stained kaolinite (1), some of which have cutans of alternating hematite and goethite layers (2). Some pisoliths are cored either with quartz grains (3), hematite (4) or a mixture of hematite and kaolinitic clay spherules (5). The vugs are coated with birefringent clay (6). Photomicrograph in plain polarized light.

Geochemistry and mineralogy

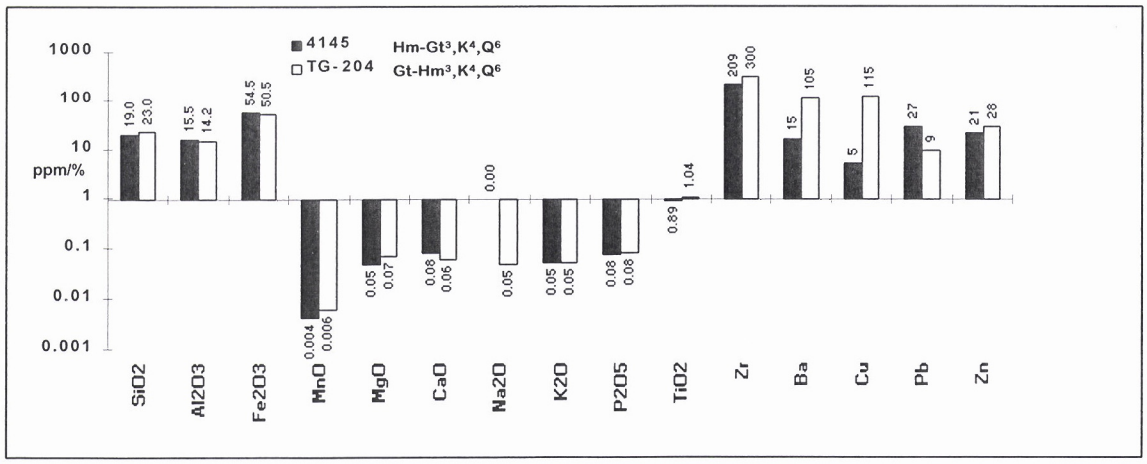

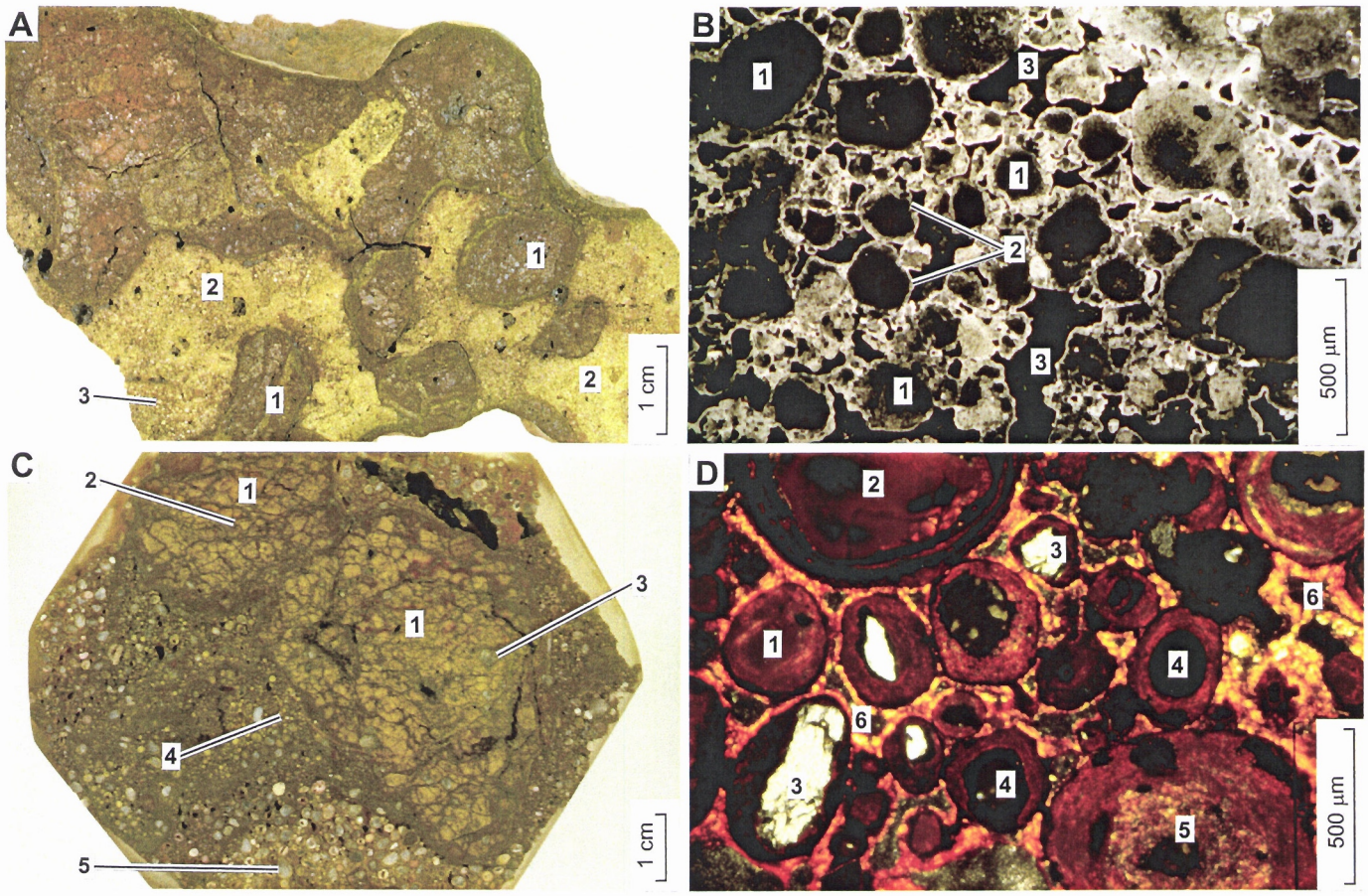
A
1
2
3
1
2
1 cm
B
1
3
1
2
3
1
500 µm
C
2
1
1
3
4
5
1 cm
D
2
3
6
1
4
6
3
4
5
500 µm

FIGURE FM3
FERRUGINOUS DURICRUST

Vermiform ferruginous duricrust

A. Vermiform ferruginous duricrust in Proterozoic sediments. Consists of goethite-rich dark-brown zone (1) with bleached zones of kaolinite (2), goethite-stained kaolinite (3) and voids (4). *C.f.* Figure FM3-B. Polished specimen DF-22 from Drifter area, AMG 308130 mE, 7823780 mN, Zone 54K.

B Detail of Figure FM3-A. Goethite-rich (1) and kaolinite-rich zones (2) contain similar, uniformly dispersed, subrounded quartz grains. The goethite zone results from Fe oxide precipitation in oxidised zones. The kaolinite-rich zone is due to reduction and leaching of Fe from the sediments. Voids (3) are a consequence of removal of kaolinite. Close up photograph in oblique reflected light.

Mottled ferruginous duricrust

C. Mottled ferruginous duricrust in Mesozoic siltstone. Hematite and kaolinite-rich mottles (1) are in intimate contact with goethite-rich mottles (2). *C.f.* Figure FM3-D. Polished specimen TG-73 from Tringadee area, AMG 482990 mE, 7581480 mN, Zone 54K.

D. Detail of Figure FM3-C. Hematite-rich mottle shows variable Fe oxide impregnation, being more intense along surfaces of fissures (1). The less impregnated area (2) shows fabric of the siltstone with fine grained quartz grains (3). Photomicrograph in normally reflected light.

Speckled ferruginous duricrust

E. Speckled ferruginous duricrust in Mesozoic siltstone. It consists of kaolinite-rich white spots (1) in a hematite-rich matrix. The pale brown patch (2) contains Fe oxide-stained spherules and fragments of kaolinite. *C.f.* Figure FM3-F. Polished specimen 4144 from Drifter area, AMG 303770 mE, 7833880 mN, Zone 54K.

F. Detail of Figure FM3-E. Hematite is concentrated in the voids (1) and as a concentration of hematite specks (2). The kaolinite (3) has scattered grains of fine quartz (4). Photomicrograph in normally reflected light.

Geochemistry and mineralogy

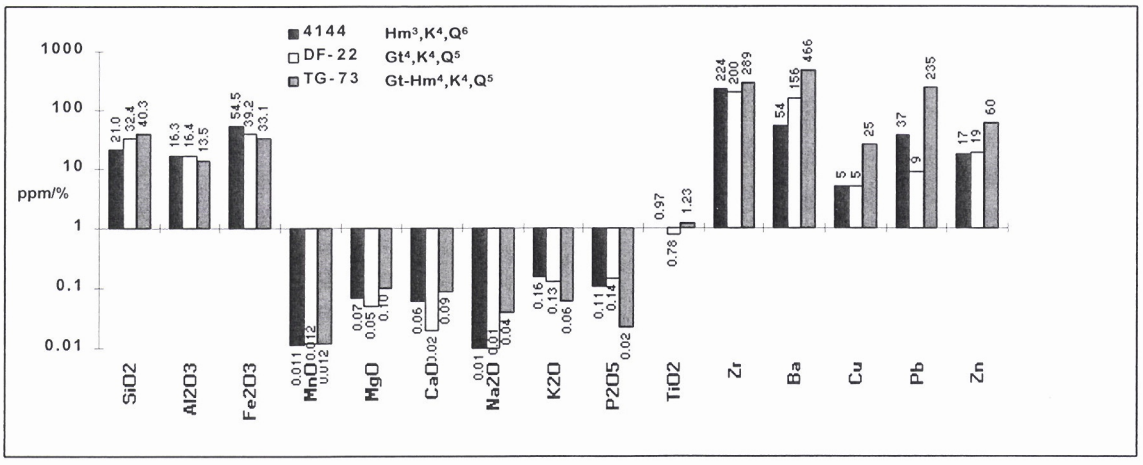

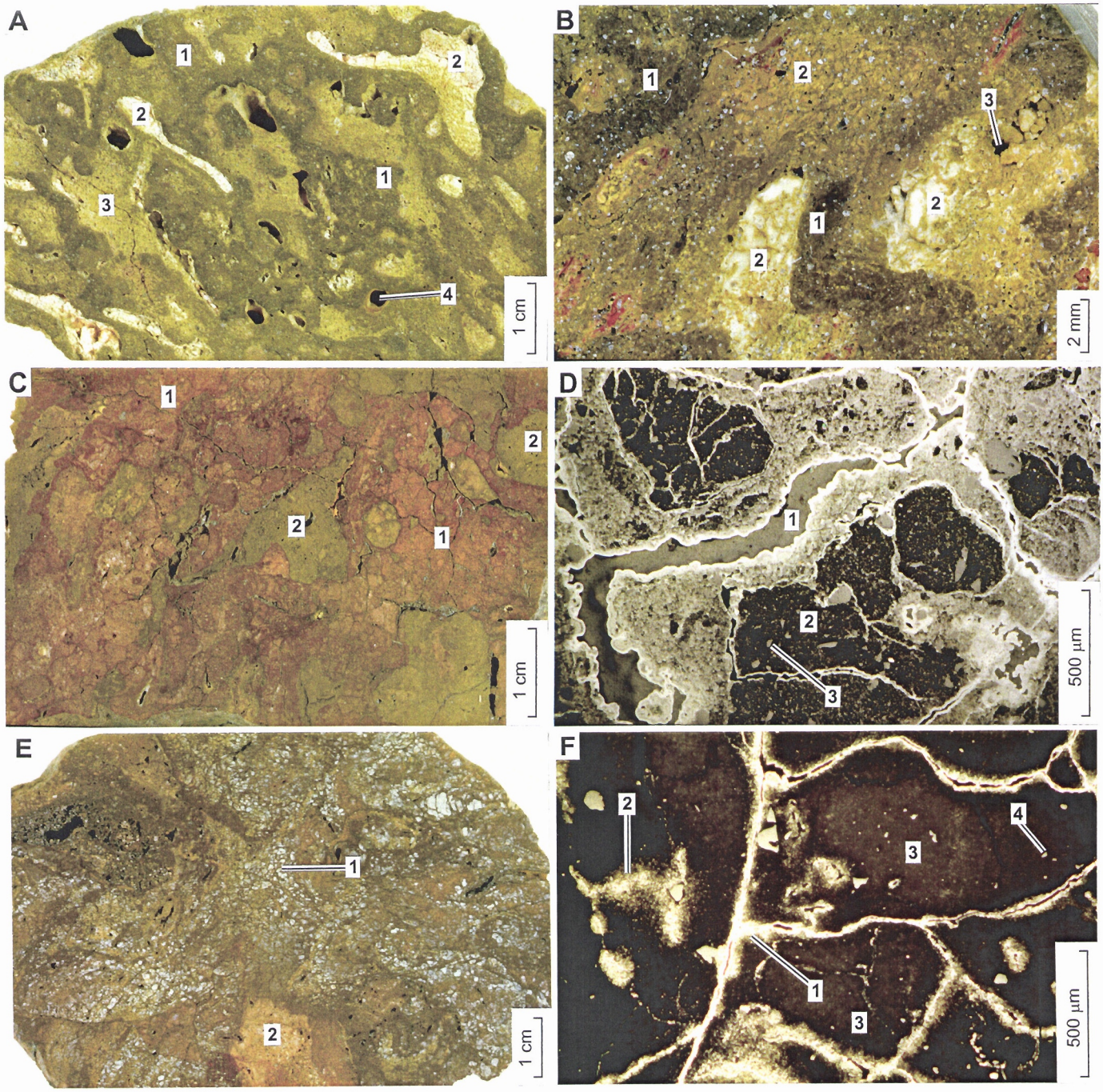
A
1
2
2
1
3
4
1 cm
B
1
2
3
1
2
2
2 mm
C
1
2
2
1
1 cm
D
1
2
3
500 µm
E
1
2
1 cm
F
2
4
3
1
3
500 µm

FIGURE FM4
FERRUGINOUS DURICRUST

Speckled-brecciated ferruginous duricrust

A. Speckled-brecciated ferruginous duricrust on Proterozoic granite with hematite-rich vein. Quartz grains (1) and hematite-rich fragments (2) with white kaolinite (3) are set in a hematite cemented clay matrix. *C.f.* Figure FM4-B. Polished specimen TG-190 from Tringadee area, AMG 479590 mE, 7588960 mN, Zone 54K.

B. Detail of Figure FM4-A. Hematite-rich fragment shows remnant trellis structure (1) indicating derivation from magnetite. Solution weathering has reduced some parts of the magnetite to skeletal structures (2) with voids (3). Photomicrograph in normally reflected light.

Variegated ferruginous duricrust

C. Variegated ferruginous duricrust overlying subcrop of Proterozoic granite in low part of the landscape. Matrix is kaolinite rich with abundant, subangular quartz derived from granite. It is stained with goethite (1) and hematite (2). Coarse rounded quartz grains (3) are evidence of some alluvial derivation. *C.f.* Figure FM4-D. Polished specimen TG-207 from Tringadee area, AMG 476500 mE, 7583940 mN, Zone 54K.

D. Detail of Figure FM4-C. Matrix shows mainly subangular to subrounded quartz grains (1), embayed quartz grains (2) and muscovite (3) in goethite impregnated kaolinite (4). Photomicrograph in normally reflected light.

Gritty ferruginous duricrust

E. Gritty ferruginous duricrust in Proterozoic sandstone and siltstone. Matrix is dominantly hematite impregnated kaolinite, (1) with a few blotches of goethite (2) and a minor sandy matrix (3). Coarse subangular quartz grains (4) give it a gritty appearance. *C.f.* Figure FM4-F. Polished specimen IS-41 from Grey Ghost area, AMG 307110 mE, 7780300 mN, Zone 54K.

F. Detail of Figure FM4-E. Hematite-rich matrix (1) contains a mixture of rounded, polycrystalline quartz grains (2), subrounded, embayed quartz grains (3) and fine-quartz grains (4). Photomicrograph with crossed polarizers.

Geochemistry and mineralogy

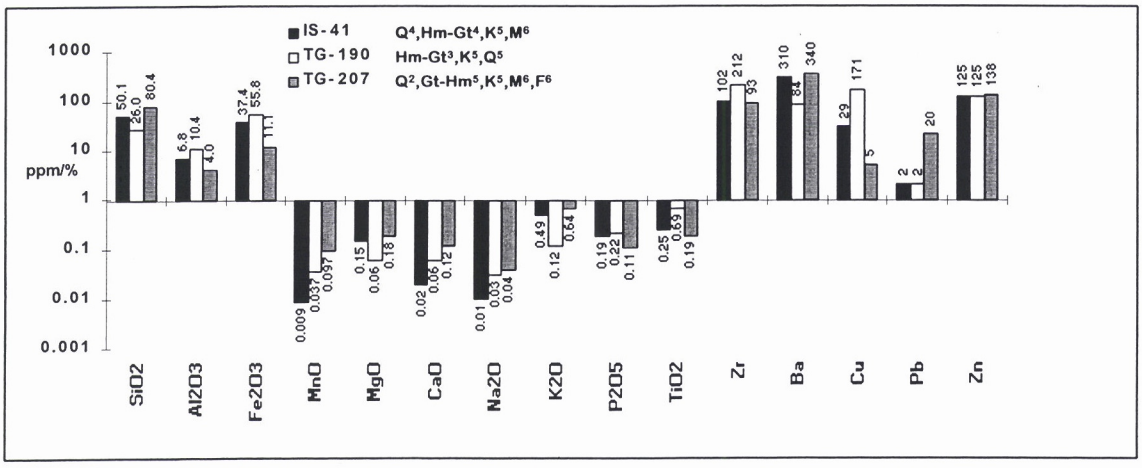

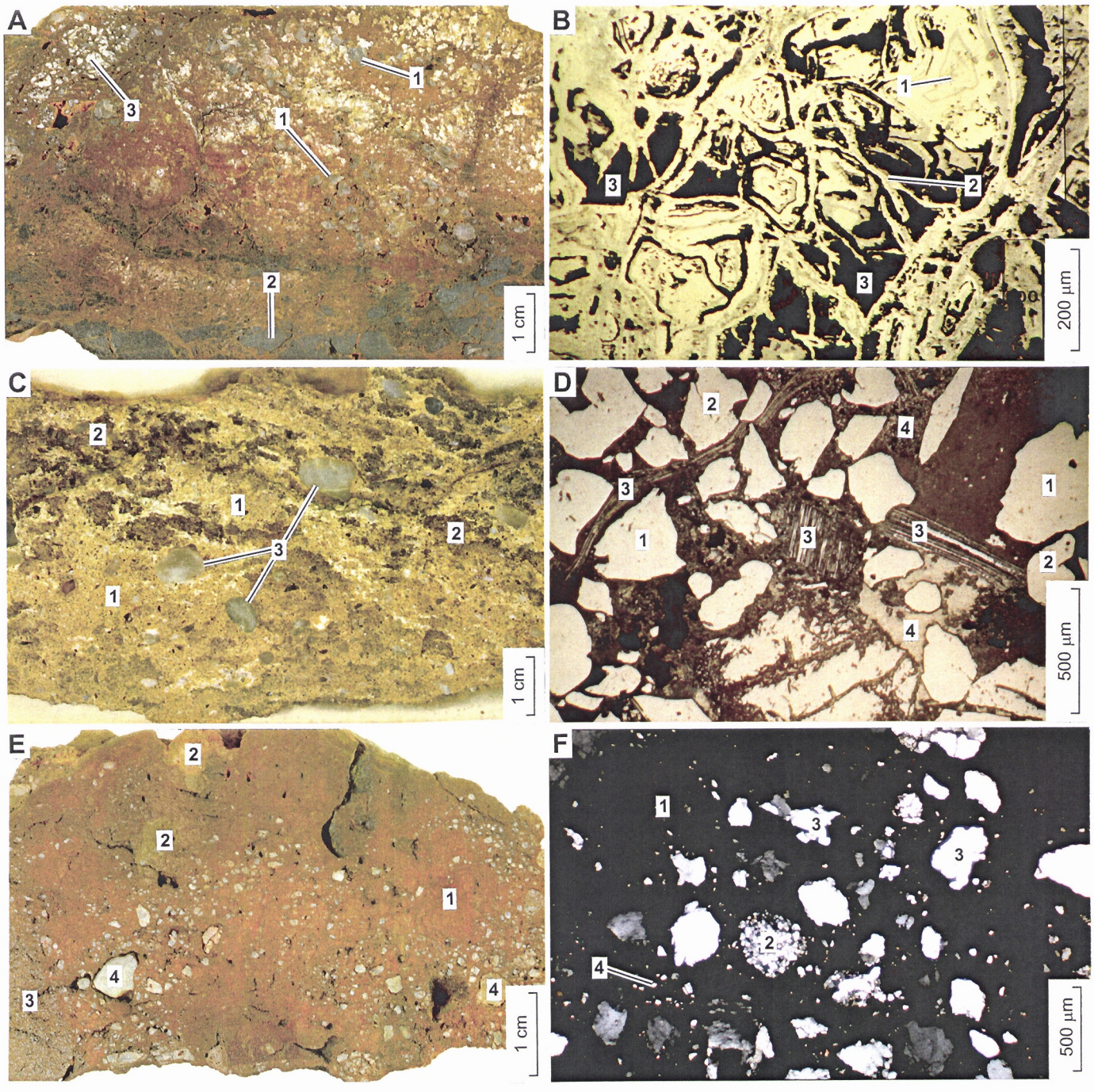
A
1
3
1
2
1 cm
B
1
3
2
3
200 µm
C
2
1
3
2
1
1 cm
D
2
4
3
1
1
3
3
2
4
500 µm
E
2
2
1
4
3
4
1 cm
F
1
3
3
2
4
500 µm

FIGURE FM5
FERRUGINOUS DURICRUST

Conglomeratic ferruginous duricrust

A. Conglomeratic ferruginous duricrust developed in ferruginised sediments. The matrix is goethite-rich and goethite is more intensely developed along fissures (1). Fragments of ferruginised sandstone (2) are cemented together by goethite with very coarse, angular quartz grains (3). *C.f.* Figure FM5-B. Polished specimen IS-38 from Grey Ghost area, AMG 308100 mE, 7775600 mN, Zone 54K.

B Detail of Figure FM5-A. Goethite is concentrated along fissures (1). The fine groundmass (2) is speckled with goethite and subangular quartz grains (3). Photomicrograph in normally reflected light.

C. Conglomeratic ferruginous duricrust developed in ferruginised sediments. Quartz pebbles (1), quartz granules (2) and sand (3) are cemented by hematite. *C.f.* Figure FM5-D. Polished specimen IS-45 from south of Drifter area, AMG 296960 mE, 7813430 mN, Zone 54K.

D. Detail of Figure FM5-C. Quartzite grain (1) with large and small angular quartz grains (2) and (4) are cemented by hematite (3). Photomicrograph with crossed polarizers.

Massive ferruginous duricrust

E. Massive ferruginous duricrust in Mesozoic sandstone. A fine to medium sand, cemented by hematite. A few orangy blotches are goethite-stained kaolinite (1). *C.f.* Figure FM5-F. Polished specimen DF-131, AMG 299220 mE, 7827090 mN, Zone 54K.

F. Detail of Figure FM5-E. Dominantly rounded quartz grain supported fabric (1), which is cemented by hematite (2). Interstices are infilled by goethite impregnated kaolinite (3). Voids (4) are abundant. Photomicrograph in normally reflected light.

Geochemistry and mineralogy

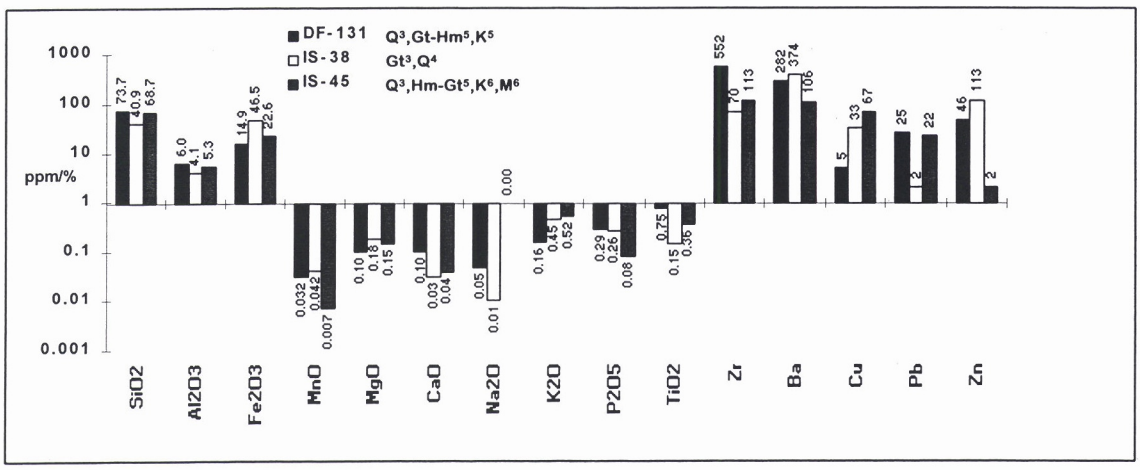

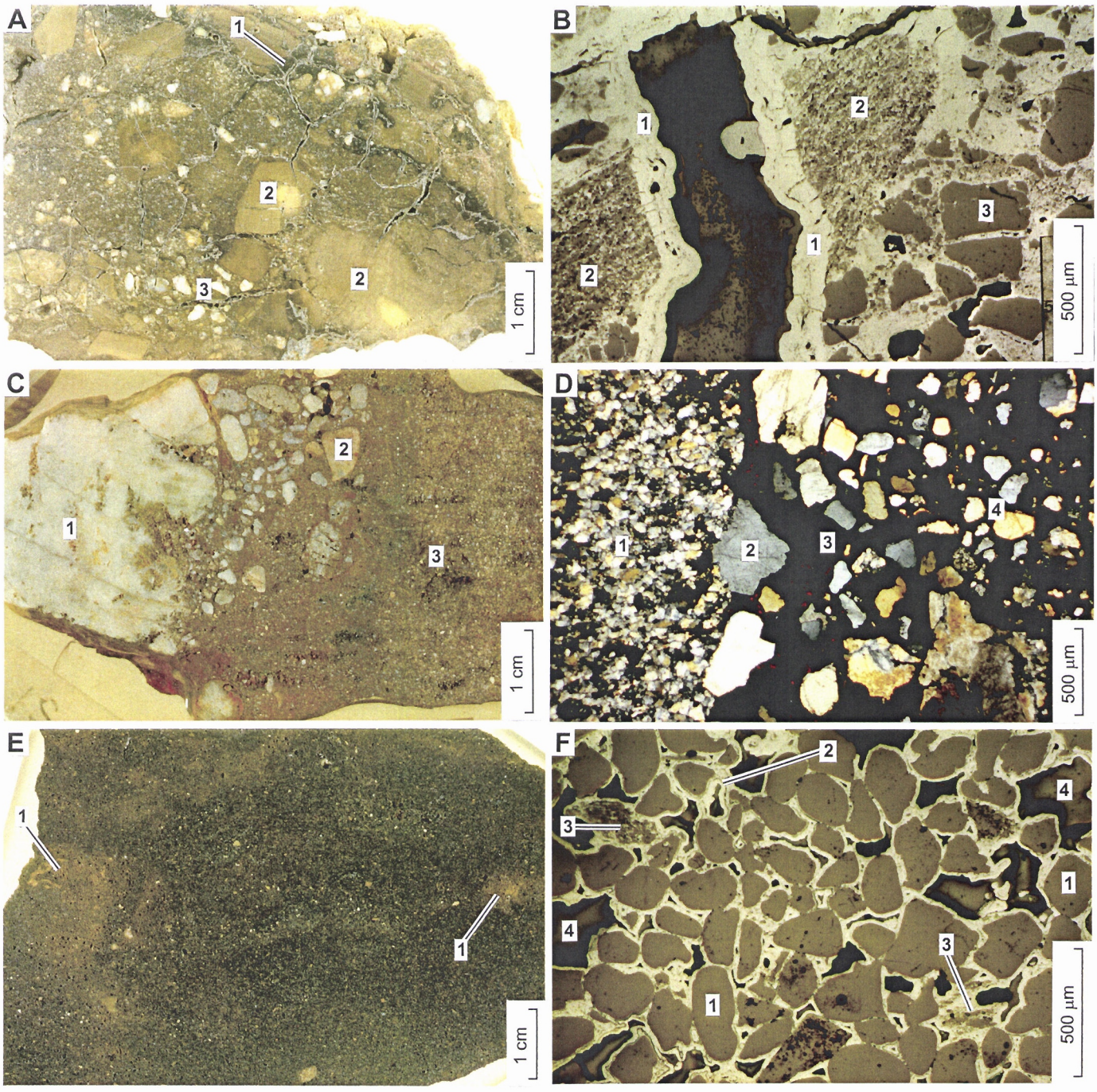
A
1
2
2
3
1 cm
B
1
2
3
1
2
500 µm
C
2
1
3
1 cm
D
4
1
2
3
500 µm
E
1
1
1 cm
F
2
4
3
1
4
1
3
500 µm

FIGURE FM6
FERRUGINOUS DURICRUST

Massive ferruginous duricrust

A. Massive ferruginous duricrust developed unconformably over Proterozoic siltstone. Slightly porous and contains medium to coarse sand, cemented by hematite and goethite. The duricrust is not genetically related to the underlying siltstone (Refer Figure 2.5-A, B, C and Figure FM6-B. Polished specimen GG-16 from Grey Ghost area, AMG 309580 mE, 7777180 mN, Zone 54K.

B Detail of Figure FM6-A. Quartz grains with embayed margins (1) are set in goethite and hematite cement (2). The quartz grains also show cross linear vesicles (3), indicating possible low temperature source. Photomicrograph in plain polarized light.

C. Massive ferruginous duricrust developed in ferruginised sediments. Refer Figures 2.4-A, B. It is goethite rich with upper surface showing goethite growth layers (1). Underlying surface (2) is more porous. *C.f.* Figure FM6-D. Polished specimen TG-504/1, from Tringadee area, AMG 482370 mE, 7588970 mN, Zone 54K.

D. Detail of Figure FM6-C. Goethite shows several generations of growth layers (1,2,3). Quartz grain (4) and plagioclase (5) are closely associated with the porous part of the matrix as shown by the voids (6). Photomicrograph with crossed polarizers.

Geochemistry and mineralogy

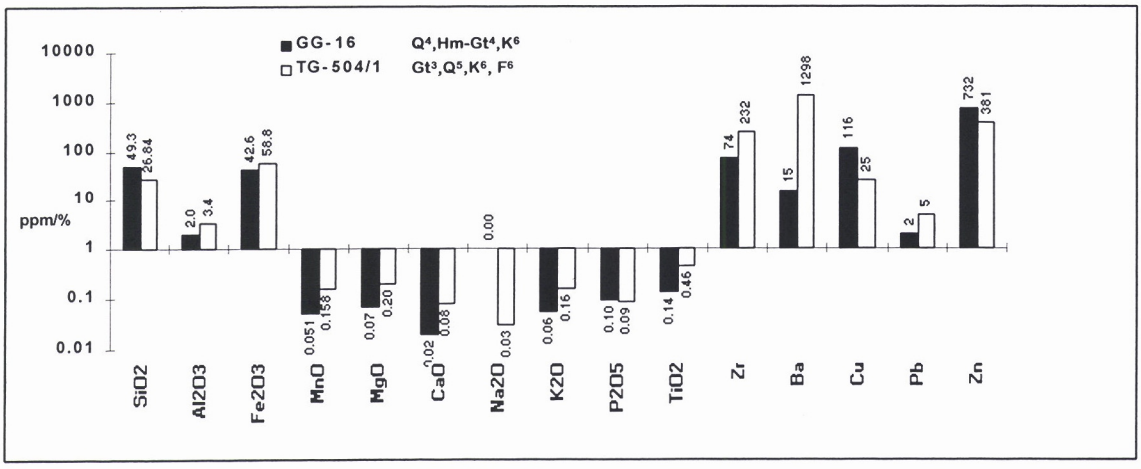

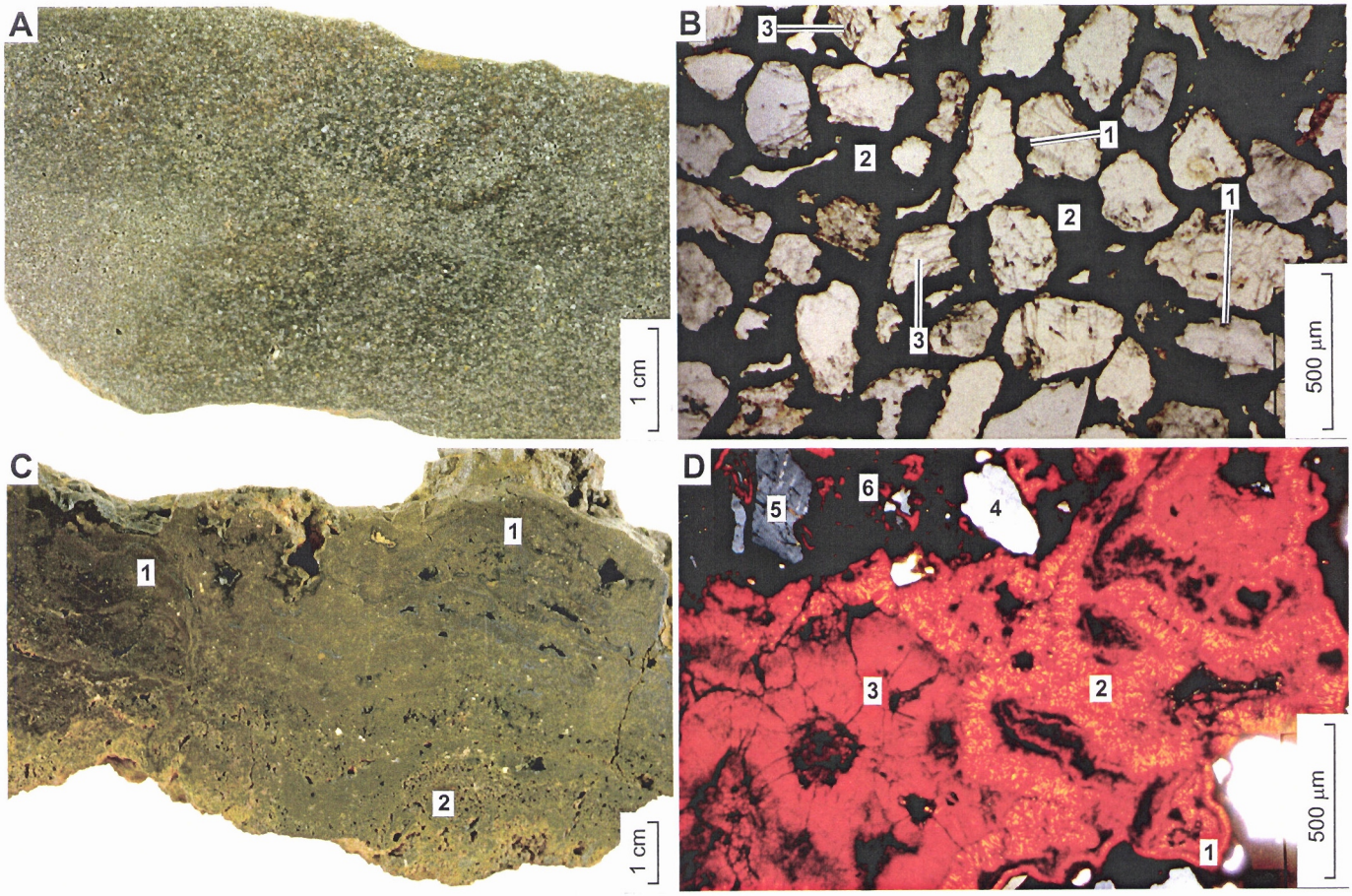
A
1 cm
B
3
1
2
2
1
3
500 µm
C
1
1
2
1 cm
D
5
6
4
3
2
1
500 µm

2.3 HAND SPECIMENS AND PHOTOMICROGRAPHS OF FERRUGINOUS PISOLITHS AND NODULES

FIGURE FM7
PISOLITHS AND NODULES

Complex ferruginous pisolith

A. Complex ferruginous pisolith from Campaspe Formation. It consists of pisoliths dominantly cemented by goethite. Pisolith (1) contains subrounded to subangular, medium to coarse quartz grains cemented by a hematite and kaolinite cement. Pisoliths (2) and (3) have similar fabrics but are more goethite rich. *C.f.* Figure FM7-B. Polished specimen LI-72 from Red Falls, AMG 367700 mE, 7795920 mN, Zone 54K.

B Detail of Figure FM7-A. Pisolith consists of hematite and kaolinite (1) cementing subangular quartz grains with smooth margins (2). Photomicrograph in plain polarized light.

Variegated ferruginous pisoliths

C. Variegated ferruginous pisoliths developed on Proterozoic granite. Goethite-rich pisolith with a thin goethite cutan (1). Hematite occurs as patches (2) or filling branching fractures in the goethite and kaolinite matrix (3). There are some quartz grains (4) in the matrix. *C.f.* Figure FM7-D. Polished specimen TG-205 from Tringadee area, AMG 469120 mE, 7589130 mN, Zone 54K.

D. Detail of Figure FM7-C. Hematite (1) is concentrated along fissures. The goethite- and kaolinite-rich matrix is shown in (2). Photomicrograph in normally reflected light with crossed polarizers.

Oblate ferruginous nodules

E. Oblate ferruginous nodules from a lag on a depositional plain. Massive and hematite-rich, with a black stain of Mn oxides. Oblate shape is probably due to saltation during sheetwash along the depositional plain. *C.f.* Figure FM7-F. Polished specimen CL3 near Cloncurry, AMG 481500 mE, 769350 mN, Zone 54K.

F. Detail of Figure FM7-E. Bright specks (1) of hematite in a greyish matrix (2) of fine quartz grains and kaolinite. Photomicrograph in normally reflected light.

Geochemistry and mineralogy

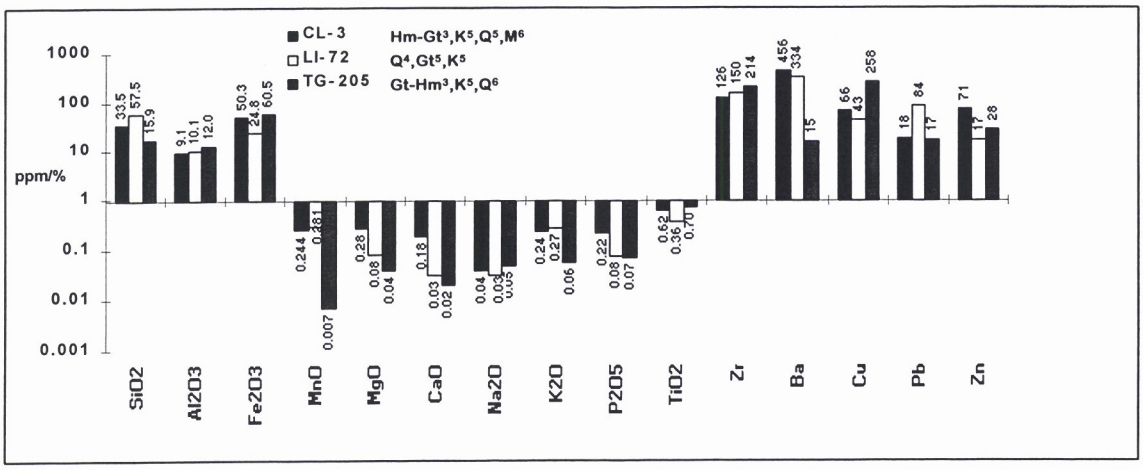

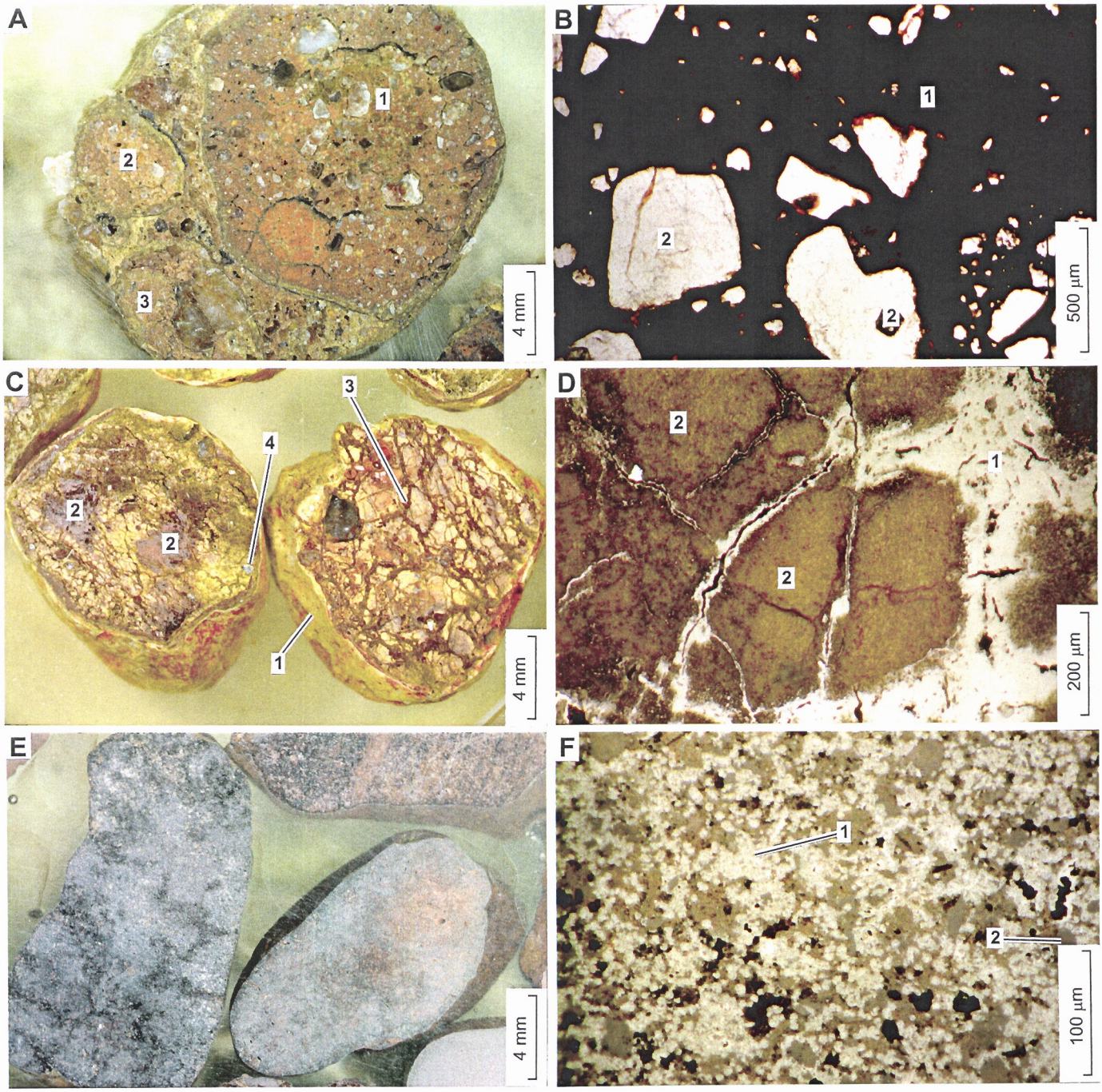
A
1
2
3
4 mm
B
1
2
2
500 µm
C
3
4
2
2
1
4 mm
D
2
1
2
200 µm
E
4 mm
F
1
2
100 µm

2.4 SELECTED FIELD PERSPECTIVES OF FERRUGINOUS SAPROLITE

Ferruginous saprolite refers to saprolite that has finely disseminated Fe oxides, commonly goethite, dispersed through the matrix (commonly clay- or quartz-rich, depending on host lithology). It can be massive, blocky, laminated, brecciated or collapsed. It can be found underlying ferruginous nodules, duricrust, mottled clays, mottled saprolite and bleached saprolite. The features of ferruginous saprolite are partly inherited from the bedrock and from weathering. In Figure 2.6, a turret of brecciated/collapsed Fe oxide-stained saprolite was produced by removal of the clay matrix by leaching, causing brecciation, fragmentation and mass wasting. Photomicrographs of Fe oxide-stained brecciated saprolite is shown in Figures FM8-A, formed in similar situations. In Figures FM8-C and FM9-A, C fractures and laminations are inherited from the bedrock. Figure 2.7 shows a cross-bedded, ferruginous saprolite of Mesozoic sediment overlying Proterozoic granite saprock and a folded ferruginous saprolite.

Iron-rich lithologies produce ferruginous saprolite as in Figure FM8-C. The movement of Fe oxide into the saprolite matrix is generally through pores and fissures. Hematite tends to coat the outer surface of the saprolite.

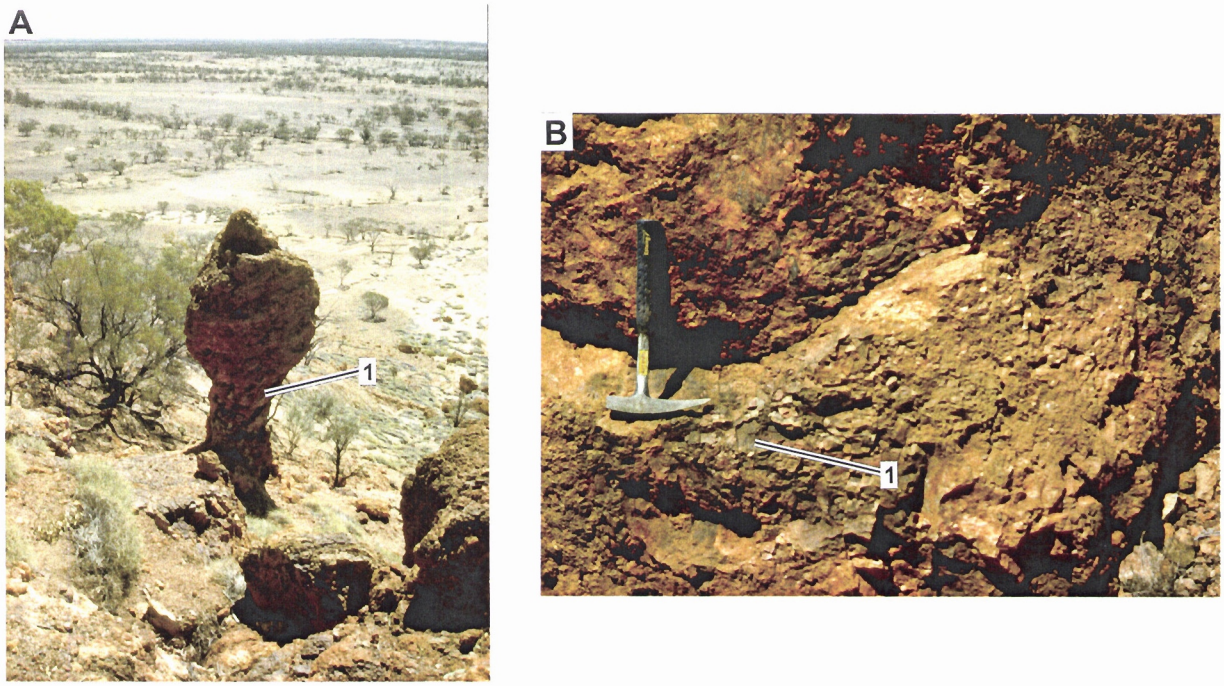

Figure 2.6. *Brecciated, Fe oxide-stained saprolite.*
A. A turret of collapsed/brecciated, Fe oxide-stained saprolite. The top part is silicified and undercutting has affected the less silicified base (1).
B. Close view of collapsed/brecciated Fe oxide-stained saprolite showing mottling (1). Tringadee area, AMG 482990 mE, 7581480 mN, Zone 54K.

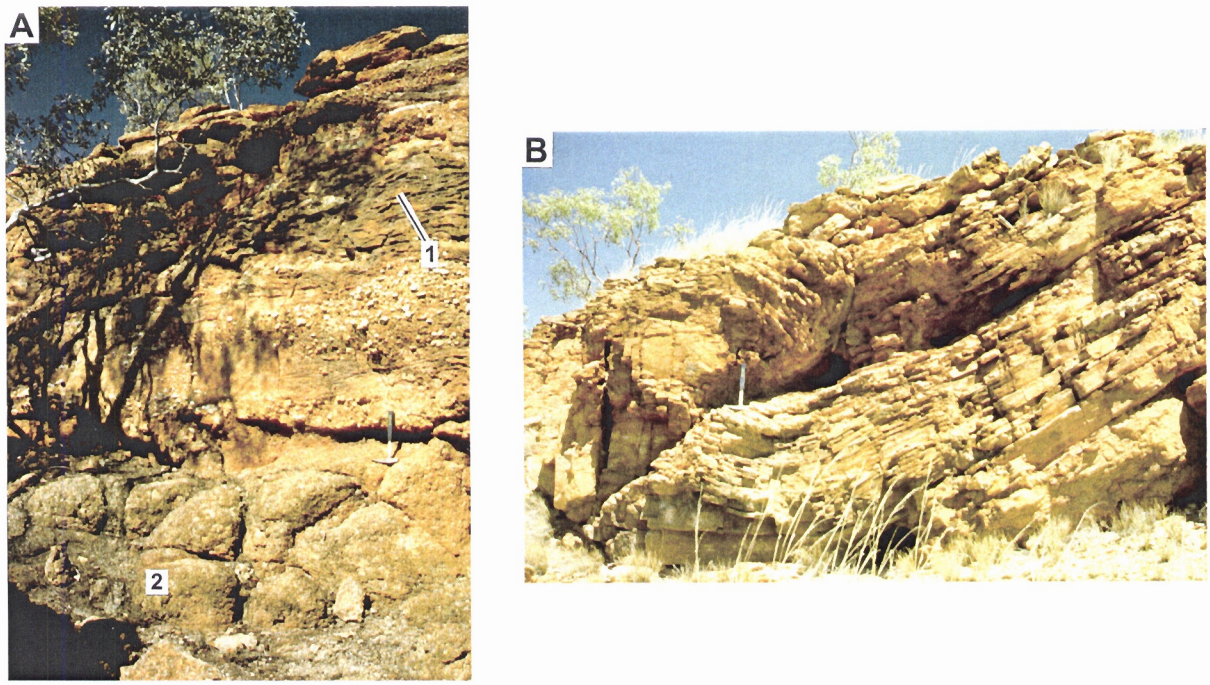

Figure 2.7. *Cross-bedded and folded ferruginous saprolite.*
A. Ferruginous saprolite on Mesozoic sediment showing cross-bedding (1) overlying Proterozoic granite saprock (2), Selwyn area, AMG 448250 mE, 7627900 mN.
B. Folded structures in ferruginous saprolite on Proterozoic sediments, showing bedding. Buckley river area, AMG 303470 mE, 7759530 mN, Zone 54K.

2.5 HAND SPECIMENS AND PHOTOMICROGRAPHS OF FERRUGINOUS SAPROLITE

FIGURE FM8
FERRUGINOUS SAPROLITE

Brecciated/collapsed, Fe oxide-stained saprolite

A. Brecciated/collapsed, silicified and dark reddish brown Fe oxide-stained saprolite of Mesozoic siltstone. The coarse Fe oxide-stained silicified clasts (1) form a skeleton in which smaller angular clasts (2) fill the interstitial spaces. The Fe tends to be leached from the edges of the angular clast (3); others (4) are more strongly leached. *C.f.* Figure FM8-A. Polished specimen TG-502 from Tringadee area, AMG 482990 mE, 7581480 mN, Zone 54K.

B. Detail of Figure FM8-A. Silicified clasts of siltstone are stained with hematite (1) with interstitial spaces (2) filled with radial and fibrous chalcedonic quartz (3). Chalcedonic quartz shows different generations of growth as revealed by the straight boundaries (4) and is lined with birefringent clay (5), indicating clay illuviation post-dated silicification. Brecciation was probably caused by collapse of the saprolite. Photomicrograph with crossed polarizers.

Blocky ferruginous saprolite

C. Blocky and dark brown ferruginous saprolite of Proterozoic metabasalt (Refer Figure 2.2B). This is hematite rich on the outer layer (1) and contains internal fractures (2). The inner part (3) is goethite rich. A remnant quartz vein (4) is cut by the fractures. *C.f.* Figure FM8-B. Polished specimen IS-11 from Buckley River area, AMG 324600 mE, 7755400 mN, Zone 54K.

D. Detail of Figure FM8-C. Hematite pseudomorphs after magnetite (1) in a matrix of Fe oxide impregnated kaolinite (2), with quartz grains (3) and voids (4). Remnant of a quartz vein is shown by (5). Photomicrograph in normally reflected light.

Massive ferruginous saprolite

E. Massive and ochre ferruginous saprolite of Proterozoic shale. It is goethite rich and porous due to a very fine sandy fabric. Larger pores are shown in (1). Hematite (2) is present as red stains on the outer edges of the sample. Finely divided mica appears as tiny bright spots under a hand lens. *C.f.* Figure FM8-F. Polished specimen LR-7 from Lady Loretta area, AMG 306200 mE, 7794350 mN, Zone 54K.

F. Detail of Figure FM8-E. Larger pores (1) are now filled with impregnating resin; small pores (2) are common. The bright patches are goethite (3) with quartz grains (4) as tiny, grey spots. Photomicrograph in normally reflected light.

Geochemistry and mineralogy

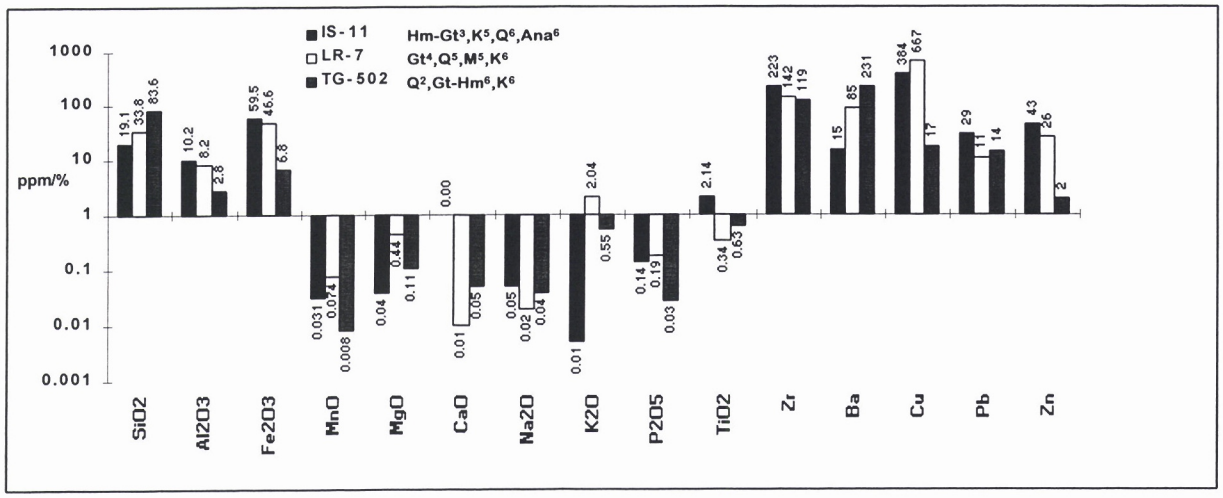

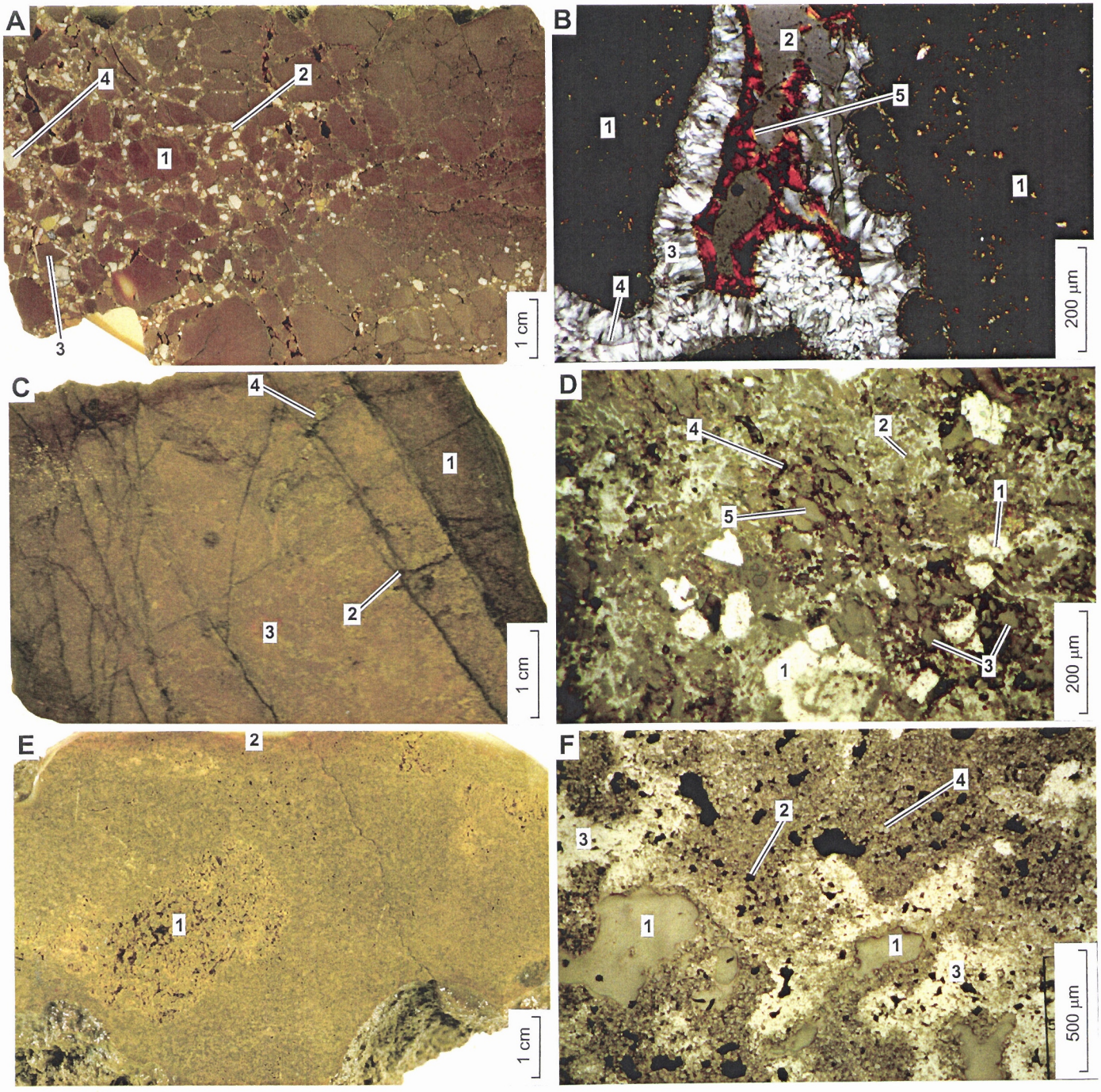
A
4
2
1
3
1 cm
B
2
5
1
1
3
4
200 µm
C
4
1
2
3
1 cm
D
4
2
1
5
1
3
200 µm
E
2
1
1 cm
F
4
2
3
1
1
1
3
500 µm

FIGURE FM9
FERRUGINOUS SAPROLITE

Laminated ferruginous saprolite

A. Red, ferruginous saprolite of laminated Mesozoic sandstone. Fine to medium quartz grains are cemented by hematite. Kaolinite forms white laminae (1). Ochre goethite stain (2) occurs around voids and the reddish stain is due to hematite. *C.f.* Figure FM9-B. Polished specimen SE-408 from Selwyn area, AMG 448250 mE, 7627900 mN, Zone 54K.

B. Detail of Figure FM9-A. Subangular quartz grains are cemented by hematite (1) with some muscovite (2). Bright brown spots within the hematite are birefringent clay (3). Photomicrograph with crossed polarizers.

C. Ochre, ferruginous saprolite of cross-bedded Mesozoic sandstone. Fine quartz grains are cemented dominantly by goethite, with minor mottles of hematite (1). White kaolinite laminae (2) accentuate the cross-bedding. *C.f.* Figure FM9-D. Polished specimen DF-410 from Drifter area, AMG 298400 mE, 77832500 mN, Zone 54K.

D. Detail of Figure FM9-C. Dominantly uniform subrounded quartz grains are cemented by goethite (1). Oblate quartz grains (2) do not show any preferred orientation. Mica flakes (3) are patchily distributed. Bright brown birefringent clay (4) occurs within the hematite cement. Photomicrograph with crossed polarizers.

Geochemistry and mineralogy

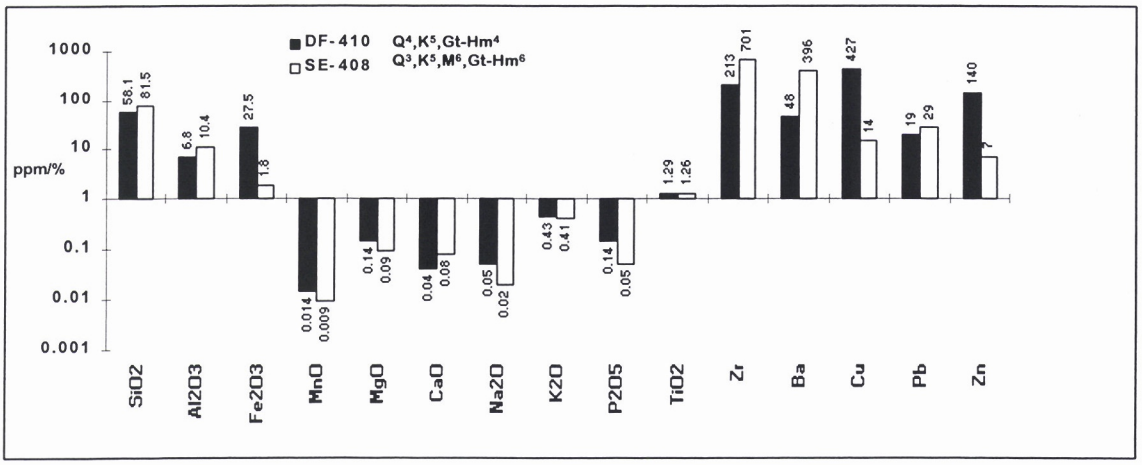

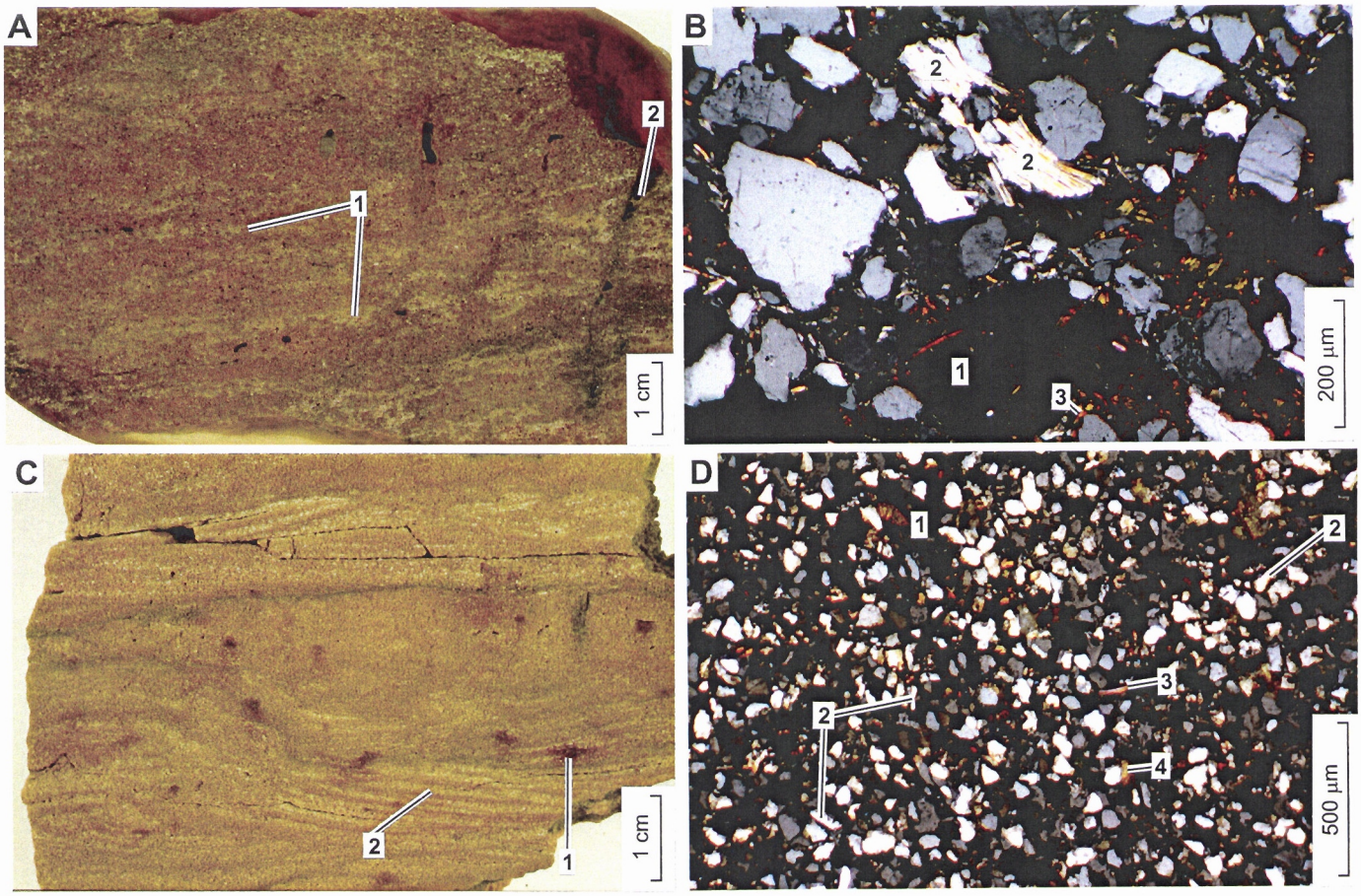
A
1
2
1 cm
B
2
2
1
3
200 µm
C
2
1
1 cm
D
1
2
3
2
4
500 µm

2.6 SELECTED FIELD PERSPECTIVES OF CEMENTED SANDS, GRITS AND SILTS

Cemented sands occur in the Cainozoic Campaspe Formation of the North Drummond Basin and the Lolworths-Ravenswood Block. Cross bedding and other sedimentary features are preserved.

At Red Falls (Figure 2.8), the Campaspe Formation consists of 14 m of coarse, quartz-rich sands that unconformably overlie the Southern Cross Formation (Scott *et al.*, 1996). Cementation of quartz grains by Fe oxides occurs at the surface of the Campaspe Formation which degrades to a lag of 2-25 mm ferruginous nodules (Figures FM7-A, B). A similar profile in the Campaspe Formation occurs at the Waterloo prospect, Pajingo and many parts of the Charters Towers - north Drummond Basin (Anand *et al.*, 1997). At 'erosion gully' at the Waterloo Prospect, the cemented sands of the Campaspe Formation are mottled (Figure 2.9).

The Southern Cross Formation, an older Cainozoic sediment, is more ferruginous, consists of gritty sandstone and lacks sedimentary structures. At Red Falls, the Southern Cross Formation contains remnants of a pisolitic duricrust (Figures FM1-C, D). In the Scott Pit at Pajingo (Figure 2.10A), there are different facies of mottled Southern Cross Formation overlying volcanic saprolite. Different types of mottling are shown in Figures 2.10B-D. In places, the matrix is cracked and the clays along these cracks have separated into very small oolitic structures (Figures FM10-F); some show hydration of hematite to goethite (Figures FM10-E). Their poor sorting and the variety of regolith materials they contain indicate very immature sediments that have been derived from a variety of regolith horizons (Robertson, 1997).

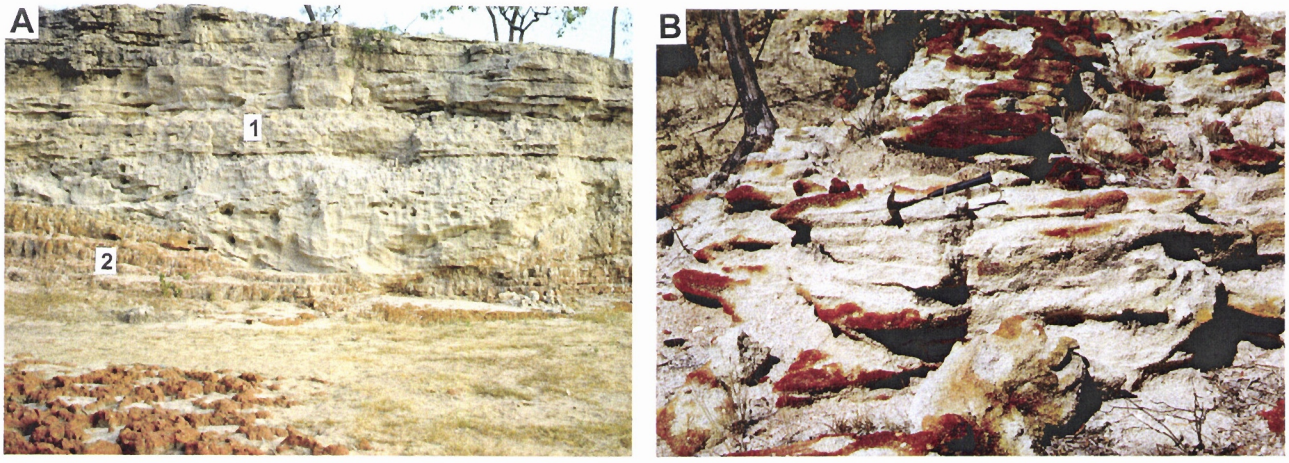

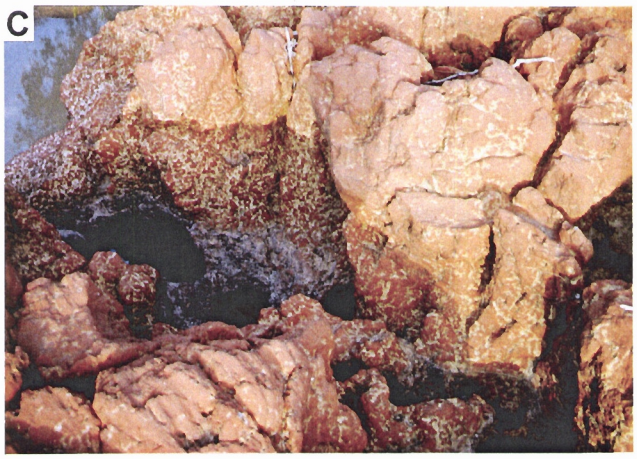

Figure 2.8. *Cemented sands of the Campaspe Formation.*

A. Cemented sands of the Campaspe Formation (1) (Refer Figures FM10-A, B) overlying the ferruginous Southern Cross Formation (2) which forms the present channel bed.
B. Close view of cemented sands showing patchy ferruginisation along bedding planes.
C. Close view of strongly mottled Southern Cross formation. Red Falls, AMG 367700 mE, 7795910 mN.

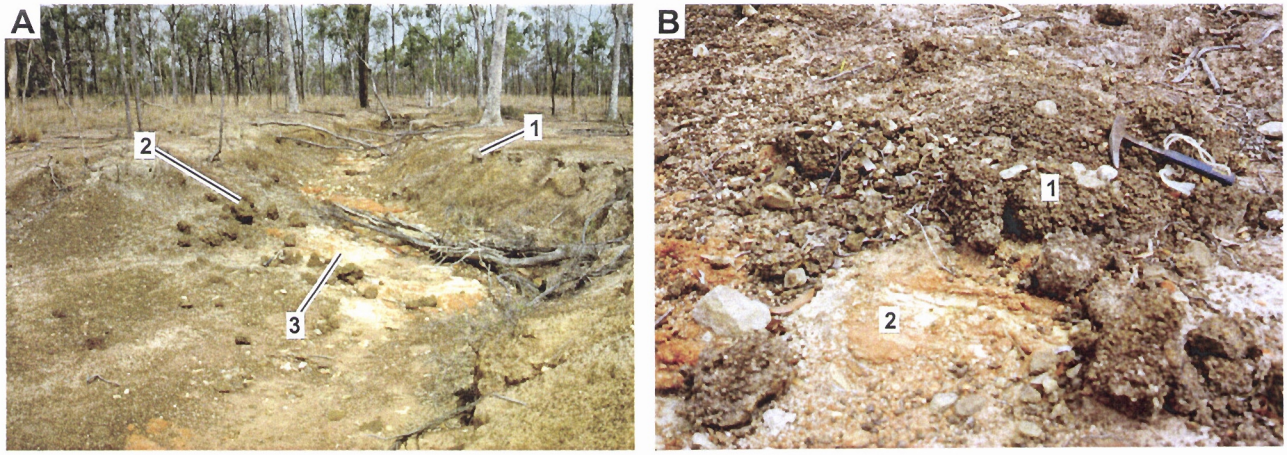

Figure 2.9. *Mottled, cemented sands of the Campaspe Formation.*

A. Grey soil (1) over weakly cemented pisoliths (2) which, in turn, overlie mottled cemented Campaspe sands (3).
B. Unconformity between weakly cemented pisoliths (1) and mottled cemented Campaspe sands (2) (Refer Figures FM10-C, D). Erosion gully at Waterloo Prospect, AMG 405500 mE, 7746150 mN, Zone 55.

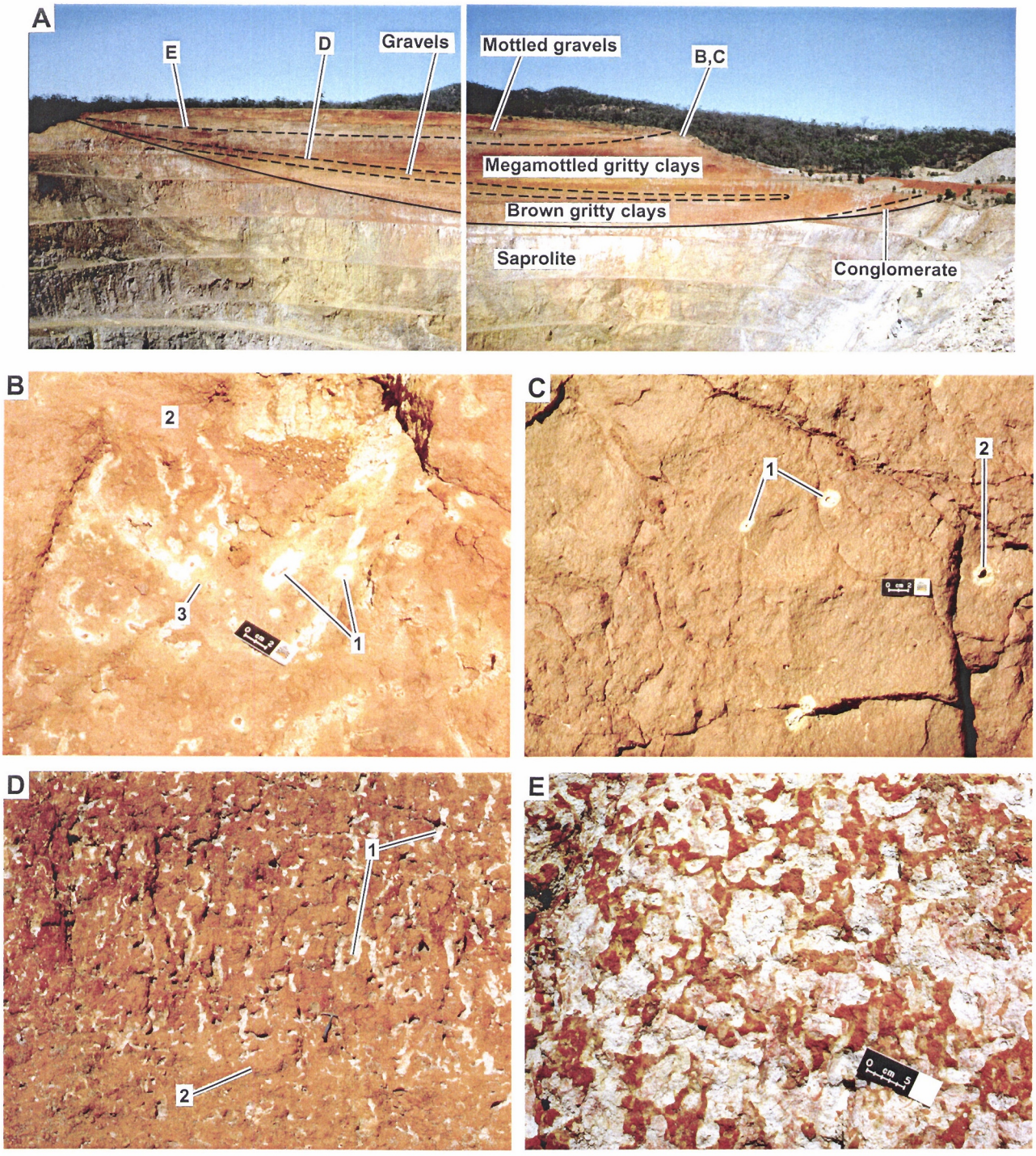

Figure 2.10. Mottled Southern Cross Formation.

A. Exposure of Southern Cross Formation at Scott Pit, Pajingo. The locations of detailed photographs are shown as B, C, D and E.
B. Details of rhizomorphic bleaching (1) of a hematite (2) and goethite-stained (3) grit from the upper, western part of the exposure.
C. Localised bleaching (1) around root tubules in a red, hematite-stained grit. The central tubule (2), once occupied by a root, is clearly visible. Upper, western part of the exposure.
D. Large rhizomorphic bleached patches (1) in brown, hematite-stained, fine-grained grits (2). Middle, eastern part of the exposure.
E. Coarse mottles near upper,eastern part of the exposure developed in a coarse-grained, immature sediment, mottled with hematite and goethite.

2.7 HAND SPECIMENS AND PHOTOMICROGRAPHS OF CEMENTED SANDS, GRITS AND SILTS

FIGURE FM10
CEMENTED SANDS, GRITS AND SILTS

A. Cemented sands in Campaspe Formation (Refer Figure 2.8A, B). It has coarse to very coarse quartz grains (1) and some pinkish alkali feldspars (2). Some of the feldspars (3) have been weathered to sericite. *C.f.* Figure FM10-B. Polished specimen LI-80 from Red Falls, AMG 367700 mE, 7795910 mN, Zone 55.

B. Detail of Figure FM10-A. Grain supported fabric of plagioclase (1), showing twinning, microcline (2), microperthite textured of alkali feldspar (3), rock fragment (4) and quartz (5). Grains and vugs are coated with birefringent kaolinite-smectitic clay (6). Photomicrograph with crossed polarizers.

C. Ferruginised/mottled cemented sands of Campaspe Formation (Refer Figure 2.8B). Very coarse, subangular quartz grains (1), rounded siltstone (2) and ferruginised lithorelics (3) set in a matrix of abundant coarse to fine quartz grains and oriented, hematite stained-clay (4). *C.f.* Figure FM10-D. Polished specimen LI-83 from erosion gully, at the Waterloo Prospect, AMG 405500 mE, 7746150 mN, Zone 55.

D. Detail of Figure FM10-C. Rock fragment contains phenocrysts of plagioclase (1) and quartz (2). Oriented clay is shown in (3) and goethite-hematite cement (4). Photomicrograph with crossed polarizers.

E. Cemented grits in Southern Cross Formation. A coarse, polymictic grit with subrounded to subangular saprolitic fragments of volcanic materials (1), vein quartz (2) and minor goethite fragments (3), set in a dominant matrix of pinkish hematitic clay (4). The clay has cracked and the hematite on the edges of the cracks has hydrated to khaki-yellow goethite (5). Close up photograph with oblique reflected light. Polished specimen RVS2002 from Scott Pit, Pajingo, Local mine grid 100038.5 mE, 101550.7 mN.

F. Cemented silts in Southern Cross Formation. A relatively fine-grained, silty material with a matrix of brown, slightly cracked kaolinitic clay (1). This is set with a few small fragments of vein quartz (2), saprolite (3), ferruginous saprolite and goethite granules (4). Where the matrix is cracked, the edges are deeper brown and is composed of clay ooliths (5). Close up photograph with oblique reflected light. Polished specimen RVS 5010 from Scott Pit, Pajingo, Local mine grid 100023.8 mE, 101531.5 mN.

Geochemistry and mineralogy

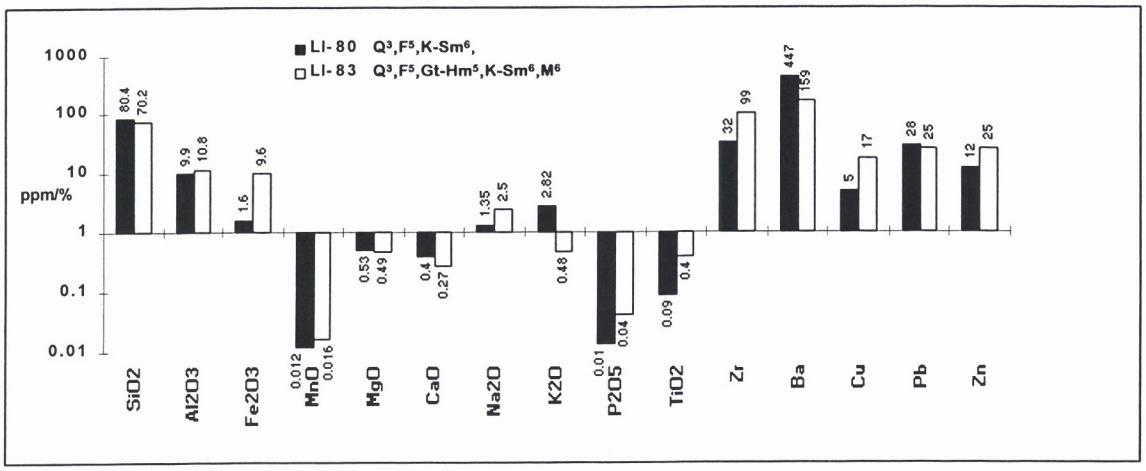

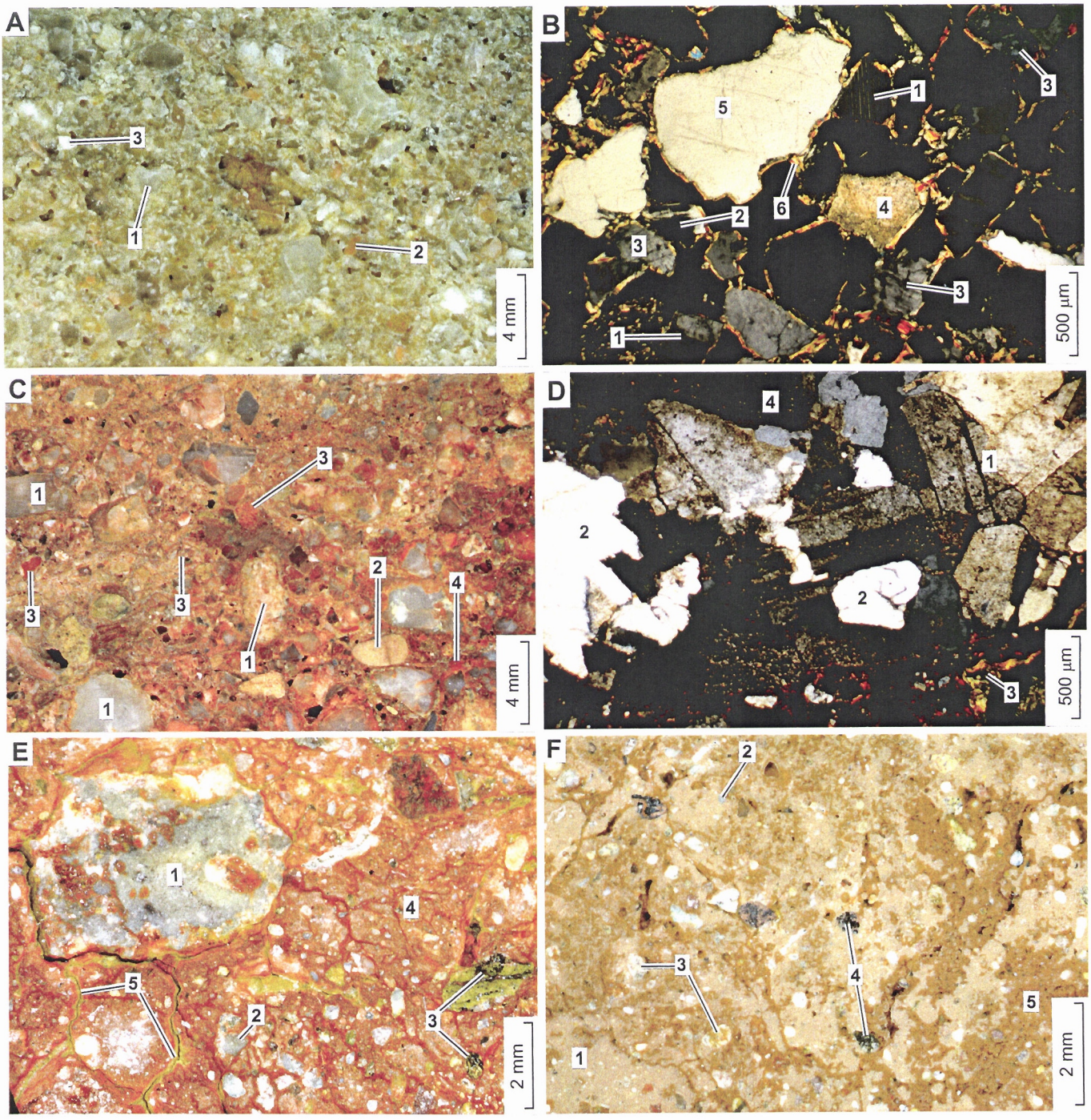
A
3
1
2
4 mm
B
5
1
3
2
6
4
3
3
1
500 µm
C
3
1
3
2
4
3
1
1
4 mm
D
4
1
2
2
3
500 µm
E
1
4
5
2
3
2 mm
F
2
3
4
5
1
2 mm

2.8 SELECTED FIELD PERSPECTIVES OF IRONSTONES

Ironstones are highly ferruginous, weathered materials consisting mainly of Fe oxides and oxyhydroxides, with variable amounts of Al hydroxides, silica and phyllosilicates that are commonly linear and follow an underlying geological unit or structure. In contrast, gossan is the weathered expression of rocks that contained substantial matrix or massive sulphide mineralisation. Because these are commonly Fe sulphides, the resultant gossans are rich in Fe oxides and oxyhydroxides and are therefore a form of ironstone. Those gossans formed by weathering of Fe-poor sulphides (e.g., carbonate-hosted Pb-Zn deposits) will give Fe-poor gossans; such gossans may be siliceous or have a high Mn-content. The term gossan has no economic connotation, nor does it describe the mode of occurrence (Butt and Zeegers, 1992).

At the Little Eva Prospect (Figure 2.11A), there are massive pods of magnetite, which are not weathering products but lenses of slightly weathered 'primary' magnetite (Robertson *et al.*, 1995). These ironstones shed lag fragments. Where this material has been incorporated into the surrounding colluvium (Figure 2.11B) following transport, the clasts have been rounded but have no cutans and, on careful examination, show a few small crystal faces on the indented parts of their worn surfaces and, particularly, on their freshly-broken surfaces. Internally, they contain included quartz.

At the Selwyn Au-Cu deposit, bands of metamorphosed Proterozoic ironstones form two parallel ridges 70 m above the local landsurface and are aligned north-south. The outcrop of the Selwyn ironstones is shown in Figure 2.12. Oxidation has formed goethite from primary chalcopyrite and altered magnetite to hematite (Wildman, 1997). Most of the Cu has been leached 50 m below the surface below which it occurs as chalcocite and native copper. At the surface, goethite after chalcopyrite contains 6,000 ppm Cu and the Au occurs as inclusions in quartz and hematite. The Selwyn ironstones can be massive, variegated or vesicular (Figure FM11-A to F).

At Tringadee (Phang *et al.*, 1997), there are ironstones fragments (Figure 2.13) consisting of hematite after magnetite related to the late-stage hydrothermal activity associated with granite emplacement.

At the Grey Ghost and Gordon prospects, ironstones which occur as stratigraphic layers within saprolitic dolomitic shales along valley floors were developed on bedrocks of weakly pyritic carbonaceous dolostone. Photomicrographs of the stratified ironstones are shown in FM12-A to D. Details of the bedrocks, the petrography of the ironstones and their geochemistry are given in Appendix II. The ironstones occur as massive ironstone pods and lenses, rich in goethite and hematite. They begin as narrow zones of ferruginous staining of the pale grey saprolite along specific beds (Figure 2.14A). These become progressively more intense to form a ferruginous saprolite (Figure 2.14B); some have parallel lenses separated by less ferruginous material (Figure 2.14C). They follow the bedding and are demonstrably parallel to thin, silty-sandy beds but are distinctly oblique to the slaty cleavage (Figure 2.14A). Where strongly developed, these beds consist of or are cored by massive goethite and hematite, with a banded structure (Figure 2.14D), and some of this is surrounded by speckles of stellate goethite (Figures 2.14E), locally referred to as 'ghostite'. At the Gordon Prospect, the upper part of this regolith material has been substantially silicified (Figure 2.14F) and the cleavage sealed. Some of these stratiform ironstones are associated with Pb and Zn anomalies (L.F. Bettenay, pers. comm., April 1994; Anand *et al.*, 1996).

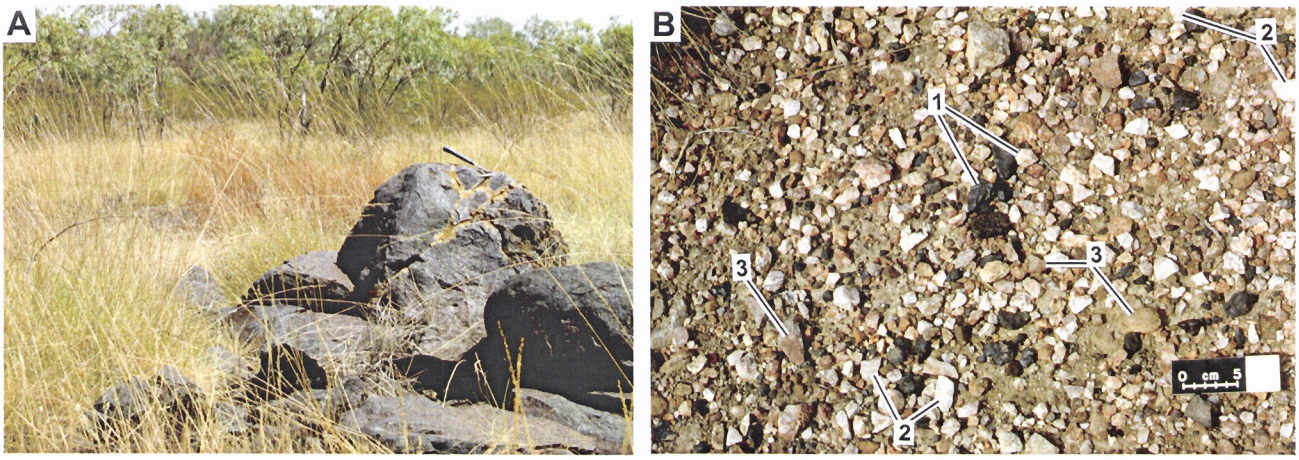

Figure 2.11. *Ironstone/ lag.*
A. A small, pod-like outcrop of magnetite at the Little Eva Prospect.
B. Round magnetite clasts (1), from weathering of similar ironstone outcrop or pods, scattered on a very pale brown, carbonate-rich soil at the Little Eva Prospect. The lag includes angular vein quartz (2) and subrounded quartzite clasts (3).

Figure 2.12. *Ironstone.*
Outcrop of blocky and massive ironstones around the mines at Selwyn.

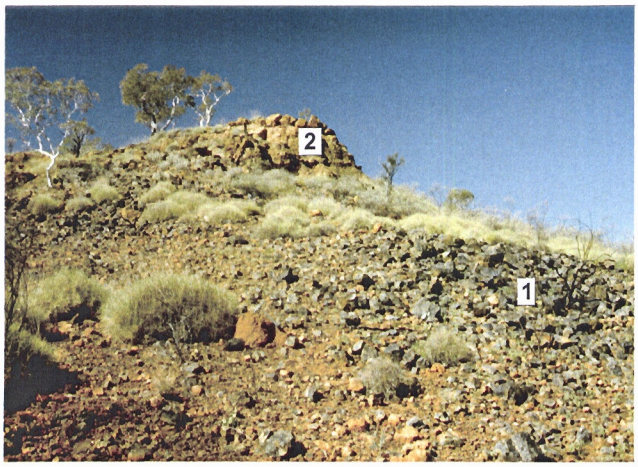

Figure 2.13. *Fragments of hematite after magnetite.*
Fragments of hematite after magnetite (1) on the flanks of a Proterozoic granitic hill. The top of the hill is covered with remnant Mesozoic sediments (2). The hematite-rich vein is related to the late-stage hydrothermal activity associated with granite emplacement. Tringadee area, AMG 475490 mE, 7588670 mN, Zone 54K.

Figure 2.14. *Stratifiform ironstone*

Initial stage.

A. Grey saprolite of carbonaceous dolostone (1) with initial thin beds of slightly ferruginous saprolite (2) along strike from a stratiform ironstone. This is cut acutely by a slatey cleavage (3). Grey Ghost Prospect.

Intermediate stage.

B. Ferruginous shale (1) in saprolitic shale (2). Grey Ghost Prospect.

C. Lens of goethitic shale (1) with parallel ferruginous bands (2) interspersed with slightly stained saprolite (3). Grey Ghost Prospect.

Advanced stage.

D. Folded bed of hematite- and goethite- impregnated saprolitic shale (1), with liesegang structures (2). Grey Ghost Prospect.

E. Core of hematite and goethite (1) in saprolite (2) surrounded by speckles of stellate hematite (3), locally referred to as 'ghostite'. Grey Ghost Prospect.

Silicification

F. Surface-silicified ferruginised saprolite (1) forming a subvertical pod in saprolite (2). Gordon Prospect.

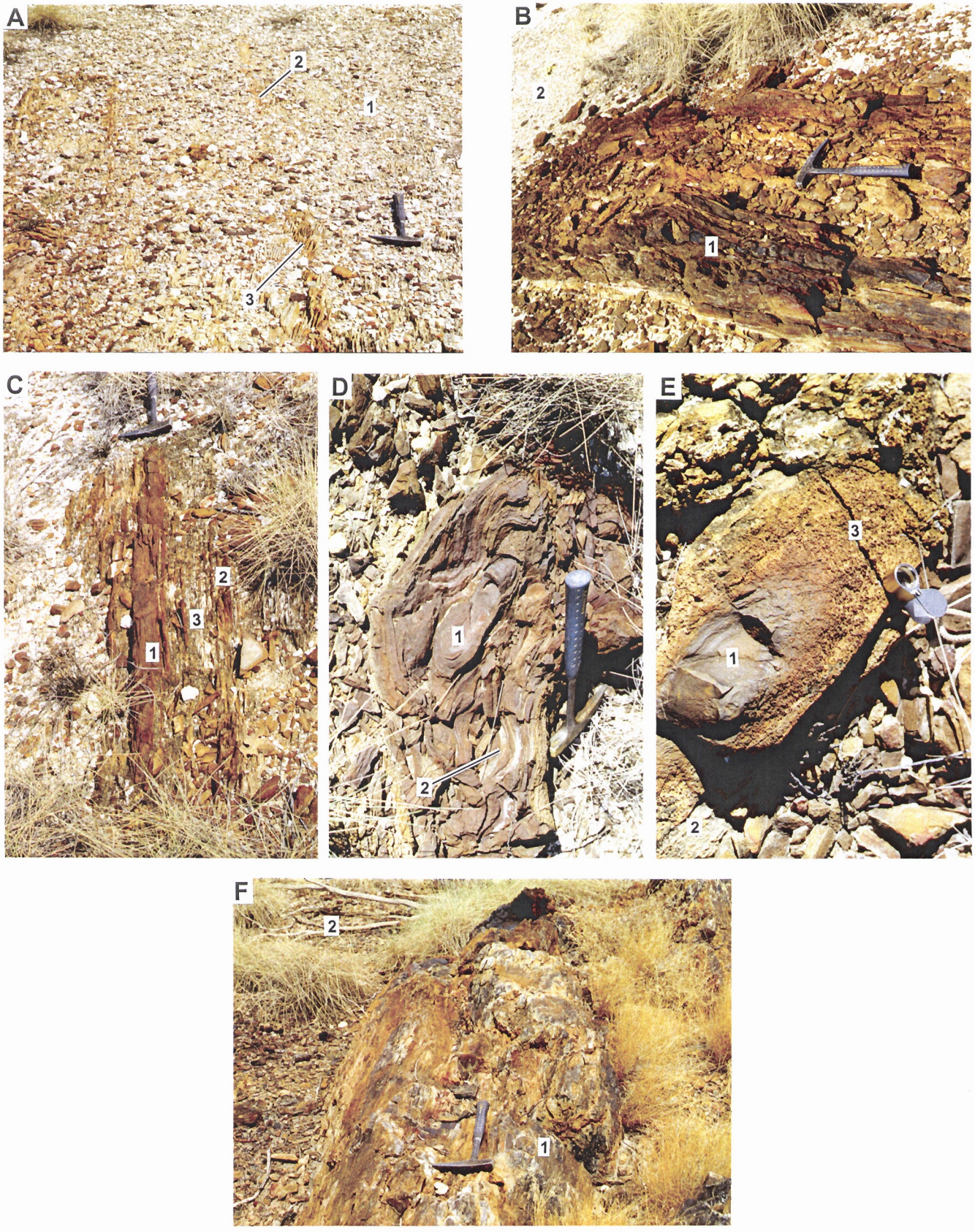
A
2
1
3
B
2
1
C
2
3
1
D
1
2
E
3
1
2
F
2
1

2.9 HAND SPECIMENS AND PHOTOMICROGRAPHS OF IRONSTONES

FIGURE FM11
IRONSTONES

Massive ironstone

A. Massive and black ironstone. It is hematite-rich with quartz veinlet (1). Goethite (2) is associated with voids. *C.f.* Figure FM11-B. Polished specimen SE-103 from Selwyn Mine Pit 257, AMG 445600 mE, 7602690 mN, Zone 54K.

B. Detail of Figure FM11-A. An elongate grain of martite (1) (magnetite pseudomorphed by hematite) has characteristic lamellae. Large, porous grains of hematite (2) are common in the ironstone. Mosaic of sutured quartz veinlet (3) appears as dark background. Photomicrograph in normally reflected light.

Variegated ironstone

C. Variegated and Mn oxide-rich ironstone. Dark patches (1) are Mn oxide rich (*c.f.* Figure FM11-D) and hematite-stained quartz (2) is red-orange. Polished specimen SE-159 from Selwyn, AMG 447200 mE, 7601550 mN, Zone 54K.

D. Detail of Figure FM11-C. Manganese oxide (cryptomelane and hollandite) has colloform fabric (1) with fine dotted texture. Hematite appears either as large, porous grains (2) or small elongate grains (3). The fibrous feature (4) is mica with Mn oxide infusion. A less weathered mica is shown at (5). Photomicrograph in normally reflected light.

Vesicular ironstone

E. Vesicular ironstone. It is hematite and quartz rich and contains 900 ppm Cu. Hematite-rich matrix (1) is punctuated by vesicles which contain a mixture of goethite, kaolinite and quartz as yellow-white patches (2). *C.f.* Figure FM11-F. Polished specimen SE-143 from Selwyn Pit 251, AMG 445450 mE, 7602100 mN, Zone 54K.

F. Detail of Figure FM11-E. Large martite grain (magnetite pseudomorphed by hematite) has bright (1) and light grey zones (2) indicating two juxtaposed pseudomorphed magnetite crystals. Part of the grain is leached and has distorted, skeletal martite lamellae (3). Mica pseudomorph after magnetite is shown in (4). Photomicrograph in normally reflected light.

Geochemistry and mineralogy

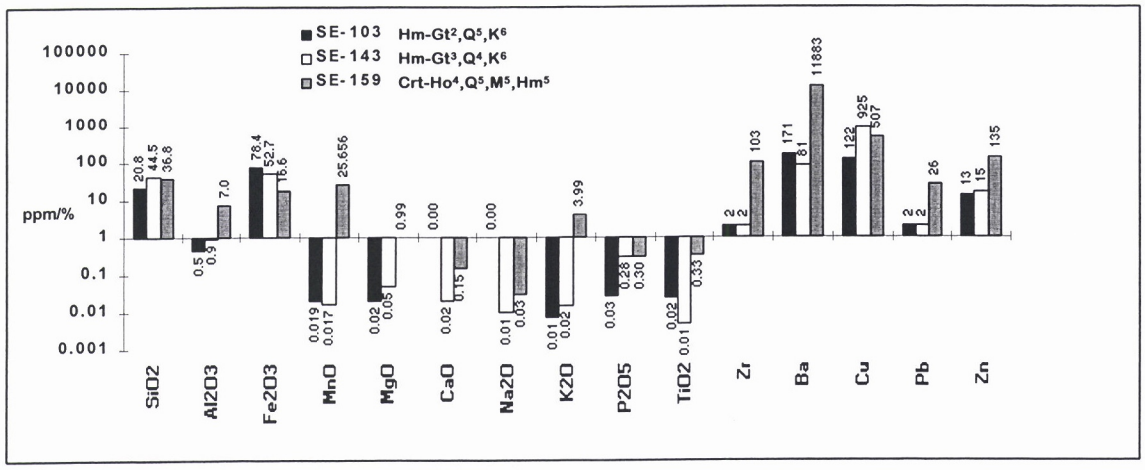

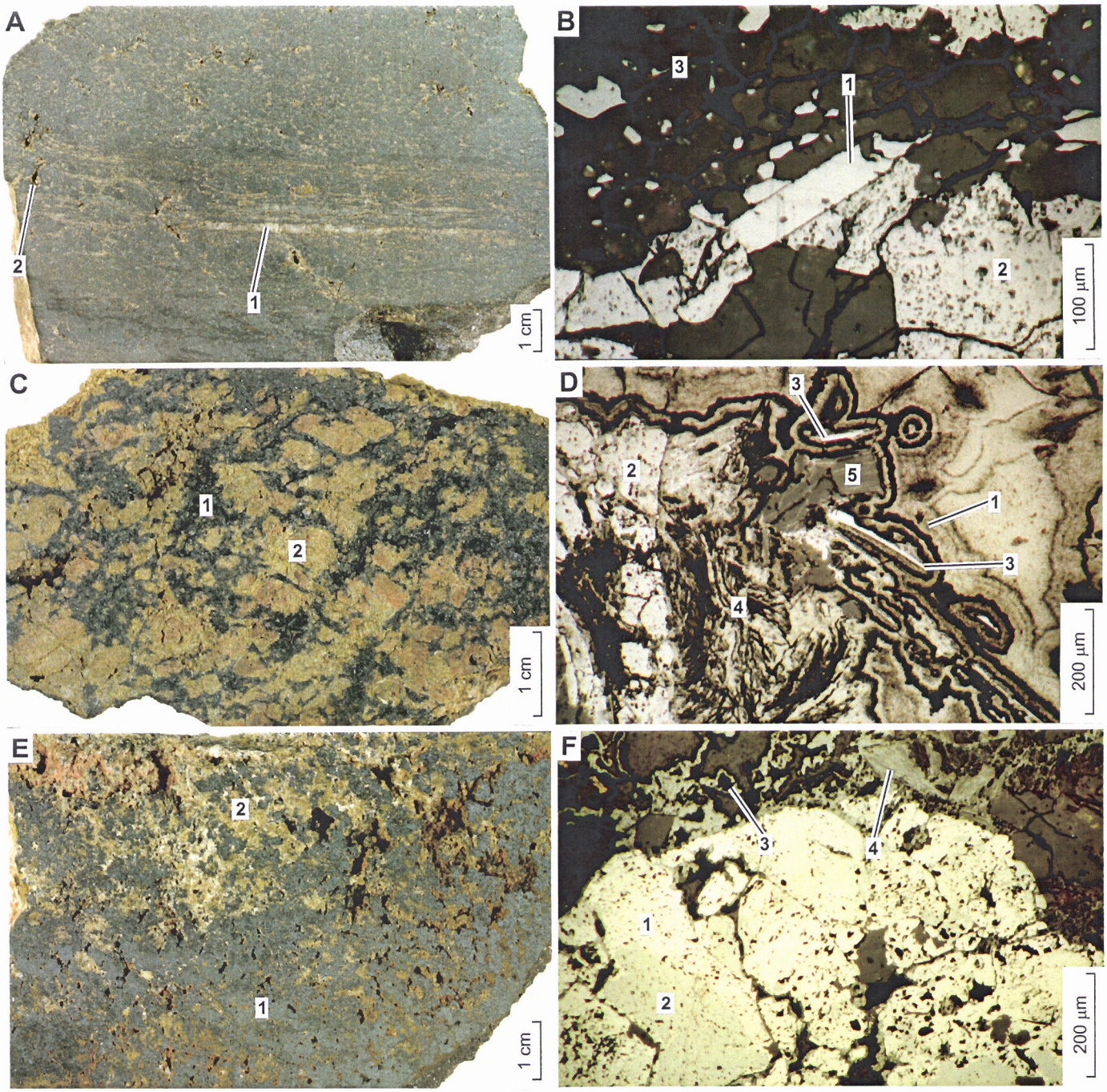
A
2
1
1 cm
B
3
1
2
100 µm
C
1
2
1 cm
D
3
2
5
1
3
4
200 µm
E
2
1
1 cm
F
3
4
1
2
200 µm

FIGURE FM12
IRONSTONES

Stratiform ironstone

A. Stratiform ironstone. Stellate clusters of dark brown goethite (1), developed after weathering diagenetic siderite, forming a typical 'ghostite' fabric. This is set in yellow, slightly iron-stained quartz and muscovite (2). Any primary lamination has been destroyed by diagenesis. C.f. Figure FM12-A. Polished specimen 08-1762 from Grey Ghost Prospect, AMG 310420 mE, 7777470 mN. Close up photograph with oblique reflected light.

B. Detail of Figure FM12-A. Hematitic goethite (1) forming a bladed, stellate structure after nailhead siderite. The siderite, now entirely replaced by goethite, has grown at the expense of muscovite (2) but contains remnant quartz (3). Specimen 08-1762. Photomicrograph in normally reflected light.

C. Stratiform ironstone. Brown, stellate goethite (1) and yellow quartz and muscovite (2) cut by a veinlet of goethite (3). Polished specimen 08-1757 from Grey Ghost Prospect, AMG 310420 mE, 7777470 mN Close up photograph with oblique reflected light.

D. Carbonate crystals of a veinlet, now altered to goethite (1), form a lens within muscovite, goethite and quartz (2). Specimen 08-1764. Photomicrograph in normally reflected light.

Geochemistry* and mineralogy**

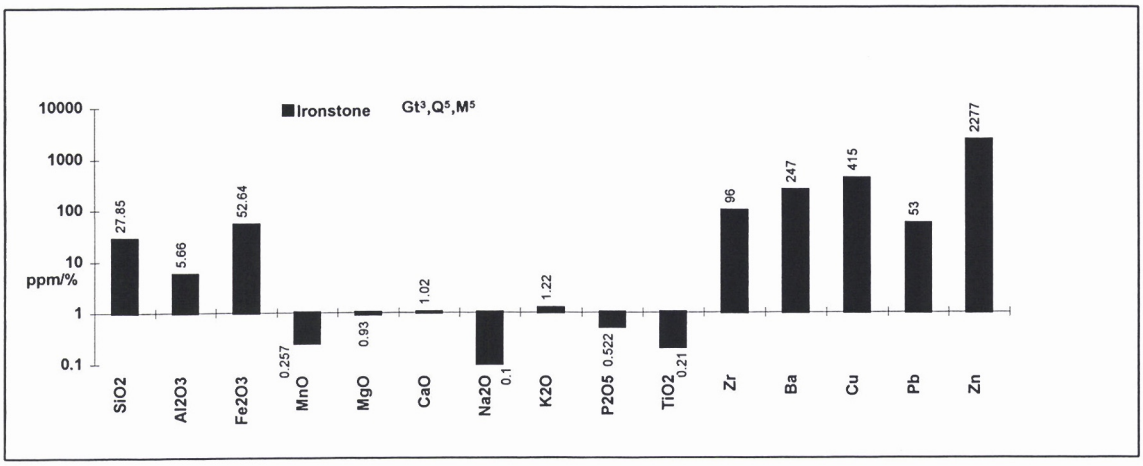

* Mean values for ironstones from Grey Ghost prospect. Refer Appendix II-Table 1 for detailed geochemistry.

** General mineralogical trend.

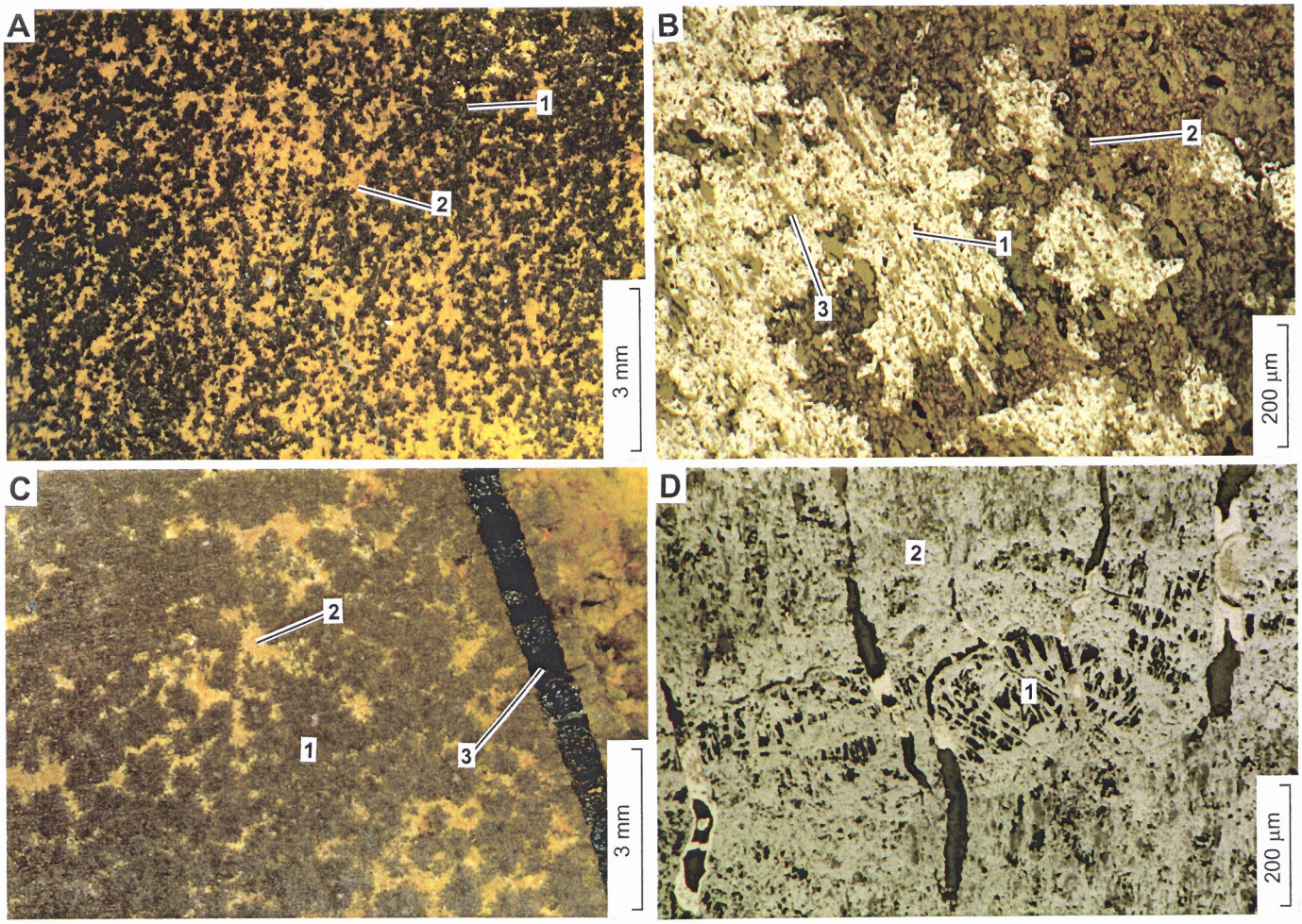
A
1
2
3 mm
B
2
1
3
200 µm
C
2
1
3
3 mm
D
2
1
200 µm

2.10 SELECTED FIELD PERSPECTIVES OF FERRUGINOUS VEINS AND BANDS

The ferruginous veins are structurally controlled and probably follow tectonically-induced cross-cutting fracture systems. They are found in the Mesozoic sediments at the Brumby Prospect (Phang *et al.*, 1997), shown in Figure 2.15. They can be massive, variegated or striated (Figure FM13-A to F). At the Brumby Prospect, these structurally controlled, subvertical, ferruginous veins in the Mesozoic give little indication of mineralisation.

The ferruginous bands are sub-horizontal and represent either redox zones or preferred pathways for induration by Fe-rich fluids in the more permeable layers of the sediments. They may accumulate trace elements related to underlying mineralisation. Figure 2.16 shows ferruginous bands in a Cambrian sediment in the Drifter area which contains up to 5000 ppm Zn. At Tringadee, goethite and Mn oxide-rich bands occur at the base of the Mesozoic mesas. Some of these bands form step-like microrelief. These ferruginous bands reflect past redox zones or permeability contrasts within the sediments associated with cyclical sedimentation (Phang *et al.*, 1997). Goethite and Mn oxides in these bands have scavenged Zn and other trace elements, so forming the Zn anomaly at the Tringadee Prospect in the Mesozoic cover. Figure FM14-E shows an example of a ferruginous band from the Tringadee area.

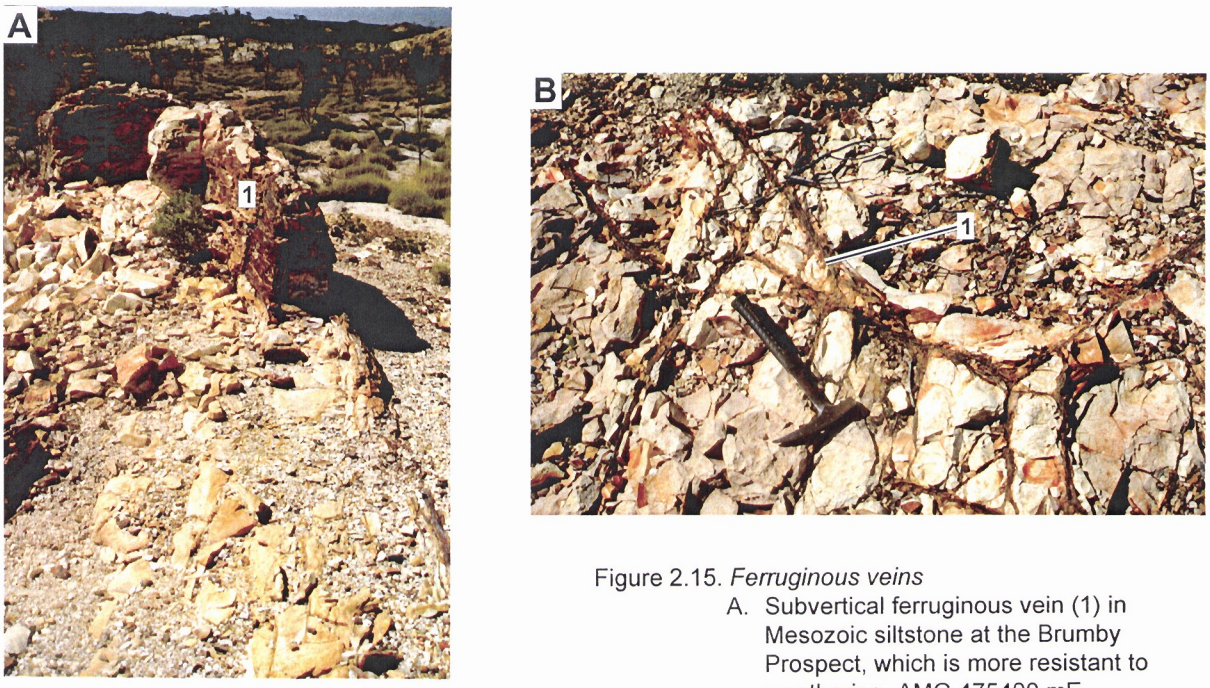

Figure 2.15. *Ferruginous veins*
A. Subvertical ferruginous vein (1) in Mesozoic siltstone at the Brumby Prospect, which is more resistant to weathering, AMG 475400 mE, 7584430 mN, Zone 54K. Refer Figure FM13-A to F.
B. Close up view of anastomosing ferruginous vein (1) which is set in Fe oxide-stained silicified saprolite.

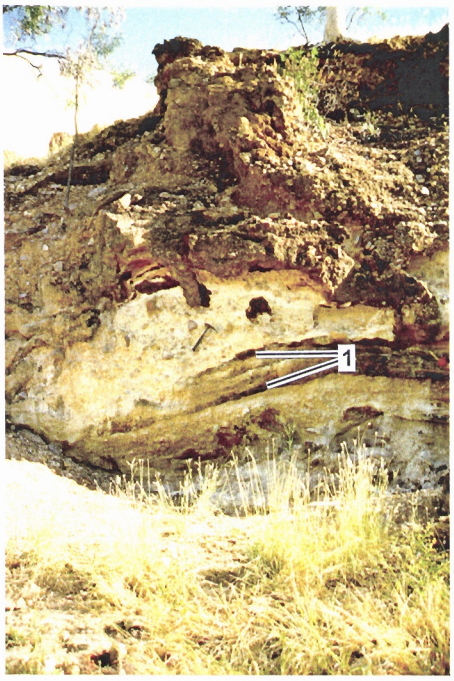

Figure 2.16. *Ferruginous bands*
Subhorizontal ferruginous bands (1) in Cambrian sediments which are goethite- and manganese oxide-rich, containing about 5000 ppm Zn. Drifter area, AMG 303800 mE, 7822450 mN, Zone 54K. Refer Figure FM14C,D.

2.11 HAND SPECIMENS AND PHOTOMICROGRAPHS OF FERRUGINOUS VEINS AND BANDS

FIGURE FM13
FERRUGINOUS VEINS AND BANDS

Massive ferruginous vein

A. Massive, subvertical, ferruginous vein in Mesozoic siltstone. Goethite-rich matrix (1) contains abundant fine quartz grains. Hematite concentrates along fissures (2) (*c.f.* Figure FM13-B) and at the exposed surface (3). Polished specimen TG-215 from Brumby Prospect, AMG 475000 mE, 7584400 mN, Zone 54K.

B. Detail of Figure FM13-A. Goethite-impregnated kaolinitic matrix (1), contains angular quartz (2) and vugs (3). Dense beady hematite coating (4) occurs along fissure. Minor mica (5) is present. Photomicrograph in normally reflected light.

Variegated ferruginous vein

C. Variegated, subvertical, ferruginous vein in Mesozoic siltstone. It is goethite rich, with dark brown patches (1) due to Mn oxides. *C.f.* Figure FM13-D. Polished specimen TG-106 from Brumby Prospect, AMG 475020 mE, 7584600 mN, Zone 54K.

D. Detail of Figure FM13-C. Leaching of goethite has left a network of martite lamellae (1), more apparent around voids (2). This probably indicates that the ferruginous vein of Figure FM12-C was derived from magnetite veins. Leaching could result from fluctuating groundwater. Photomicrograph in normally reflected light.

Striated ferruginous vein

E. Striated, subvertical, ferruginous vein in Mesozoic siltstone. Hematite is concentrated at the exposed part (1) of the ferruginous vein and along internal cracks (2). Inner part (3) is goethite rich. *C.f.* Figure FM13-F. Polished specimen TG-103 from Brumby Prospect, AMG 475050 mE, 7584600 mN, Zone 54K.

F. Detail of Figure FM13-E. Specks of goethite (1) impregnate the matrix. Hematite (2) forms a coating along a fissure. Angular quartz grains (3) are irregularly distributed. Photomicrograph in normally reflected light.

Geochemistry and mineralogy

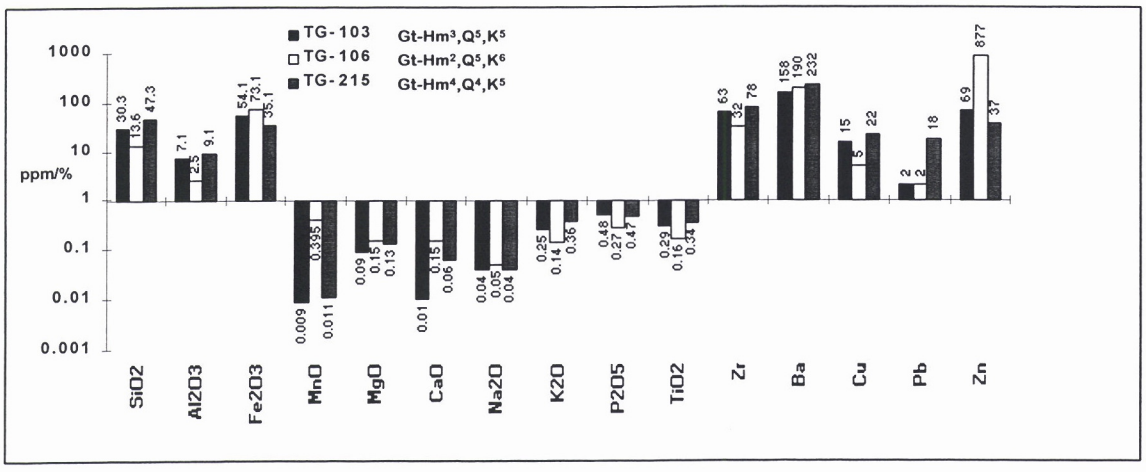

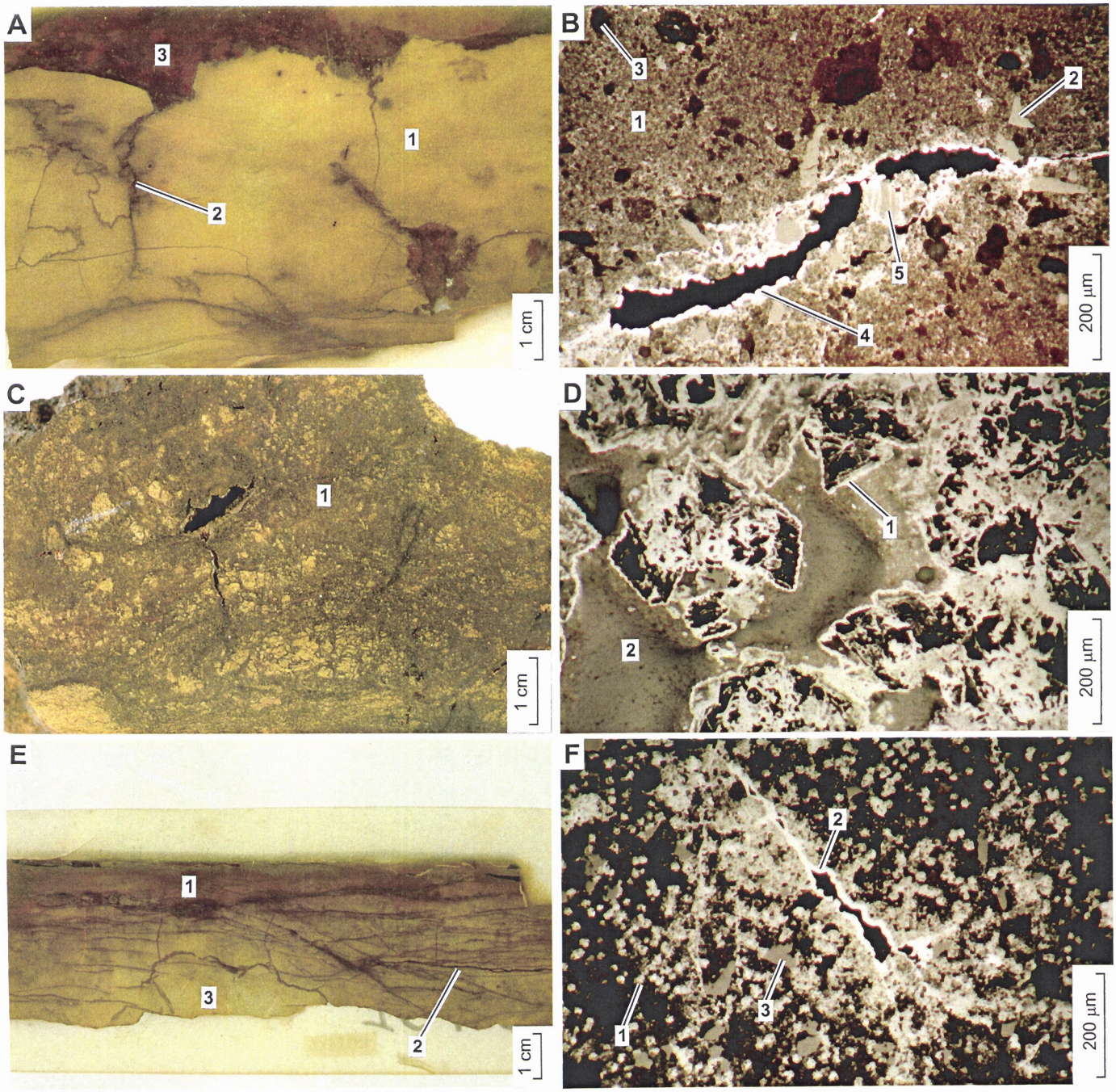
A
3
1
2
1 cm
B
3
2
1
5
4
200 µm
C
1
1 cm
D
1
2
200 µm
E
1
3
2
1 cm
F
2
3
1
200 µm

FIGURE FM14
FERRUGINOUS VEINS AND BANDS

Fragmental ferruginous vein

A. Fragmental, subvertical, ferruginous vein in Mesozoic siltstone. This is goethite rich (1) with hematite concentrations (2) along cracks. Fe oxide-stained kaolinite is shown in (3). *C.f.* Figure FM14-B. Polished specimen TG-76 from Tringadee area, AMG 482990 mE, 7581480 mE, Zone 54K.

B. Detail of Figure FM14A. Subangular fragments of goethite (1) are cemented by hematite (2). Interstitial spaces are infilled by kaolinite (3) and coated with hematite. Photomicrograph in normally reflected light.

Sinuous Ferruginous band

C. Sinuous, ferruginous band in Cambrian sediments. Zones are variously goethite-rich (1), Mn oxide-rich (dominantly hollandite) (2), calcite and apatite (3), halite (4) and chert fragments (5). Band contains approx., 25% Cl, 5000 ppm Zn. *C.f.* Figure FM14-D. Polished specimen DF-17 from Drifter area, AMG 303800 mE, 7822450 mN, Zone 54K.

D. Detail of Figure FM14-C. Goethite-rich zone (1) contains cubic voids (2) after halite crystals. This probably suggests contemporaneous precipitation of goethite and halite from pore fluids. Photomicrograph in normally reflected light.

Striated Ferruginous band

E. Striated, ferruginous band in Mesozoic sediments. It consists of dark-brown, goethite-rich zones (1) and bright yellow zones, which are formerly voids. Manganese oxides (2), dominantly lithiophorite and hollandite, infill cracks and vugs. *C.f.* Figure FM14-F. Polished specimen TG-147 from Tringadee area, AMG 483290 mE, 7582740 mN, Zone 54K.

F. Detail of Figure FM14-E. Goethite impregnated zone (1), retains siltstone fabric. The fissure is filled with growth banded lithiophorite and hollandite (2). Photomicrograph in normally reflected light.

Geochemistry and mineralogy

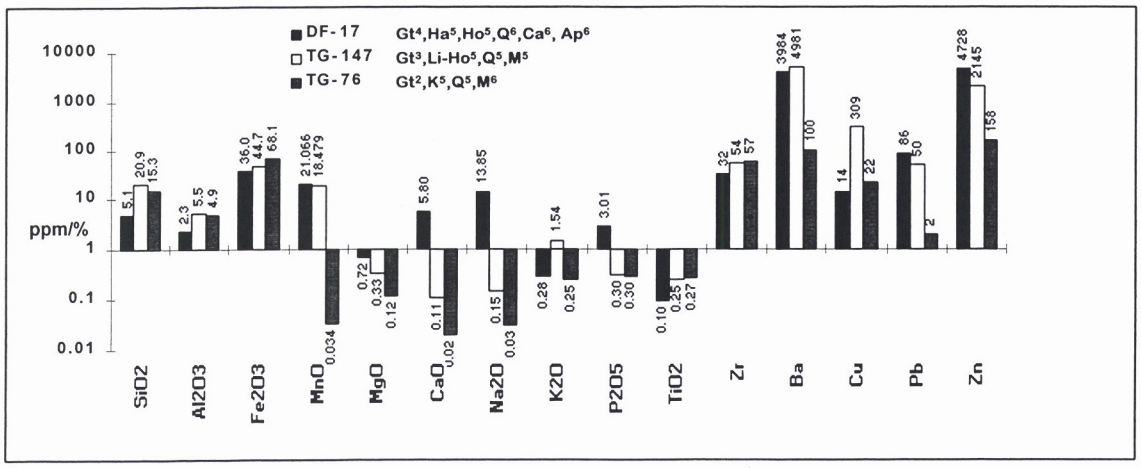

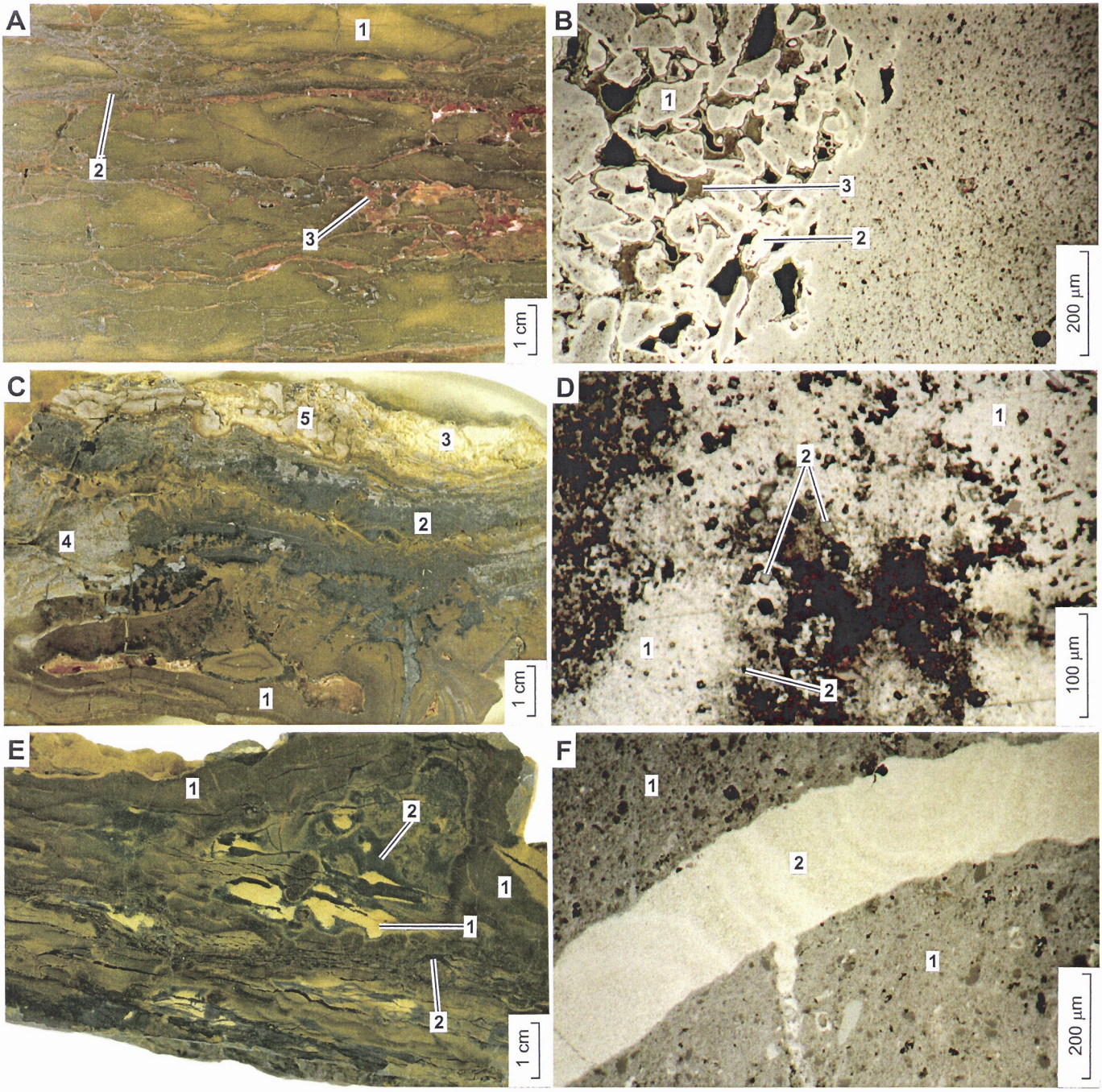
A
1
2
3
1 cm
B
1
3
2
200 µm
C
5
3
4
2
1
1 cm
D
1
2
1
2
100 µm
E
1
2
1
1
2
1 cm
F
1
2
1
200 µm

3.1 SELECTED FIELD PERSPECTIVES OF SILCRETE

The term silcrete refers to intensely silica-indurated regolith materials such as soil, sands, saprolite or rock fragments. Silcretes are formed on a variety of lithologies but are most common on siliceous materials (Anand *et al.*, 1997). In places, silica has cemented alluvial sands or sheet wash sands and gravels. They can be nodular-massive, terrazzo, brecciated, fragmental, massive and columnar, as in Figures SM1, SM2 and SM3. Columnar silcretes could indicate columnar peds of a palaeosol or shrinking and cracking of the silcrete during de-watering (Anand *et al.*, 1997).

In the Grey Ghost area, columnar silcretes can be : -

i) grey (Figure 3.1A), with a patchy, ferruginous coating (Figure 3.1B). Impregnation of Fe oxides into the silcrete is along cracks but it mainly forms a cutan, suggesting that ferruginisation post-dated silicification. Beneath the silcrete columns, silicified gravels unconformably (Figure 3.1C) overlie silicified, Proterozoic saprolite.

ii) fluted or ropy. The column in Figure 3.2A is about 3 m high with "cauliflower-like" tops and fluted or ropy features on the sides, resembling candle wax drippings. Blotchy hematitic mottles, set in a silicified, kaolinite and quartz-rich matrix, forms the mottled zone below (Figure 3.2B), which in turn overlies Proterozoic saprolite, strongly silicified towards the surface.

Massive silcretes are observed in the Buckley River area and in the Tringadee area. In the Buckley River area, massive silcrete (Figure 3.3A) locally consists of silicified gravels (Figure 3.3B) overlying silicified Proterozoic saprolite (Figure 3.3C). Bedding planes in the silicified, Proterozoic saprolite are rounded, suggesting dissolution of the Proterozoic sediments is a source of silica. Massive silcrete pods in Figure 3.4A rest unconformably on silicified, Proterozoic shale (Figure 4.4B). Quartz gravel and sand within the silcrete suggest that the original material was either river channel or sheetwash deposits (Anand *et al.*, 1995). Induration by silicification has led to differential erosion and relief inversion. In the Tringadee area (Figure 3.5), the massive silcrete is clay-rich and porcelaneous.

Silcretes in these study areas consist mainly of randomly distributed and embayed quartz grains and rock fragments cemented and supported by a microcrystalline quartz matrix. Embayment of the quartz grains suggest a possible source for silica for the matrix.

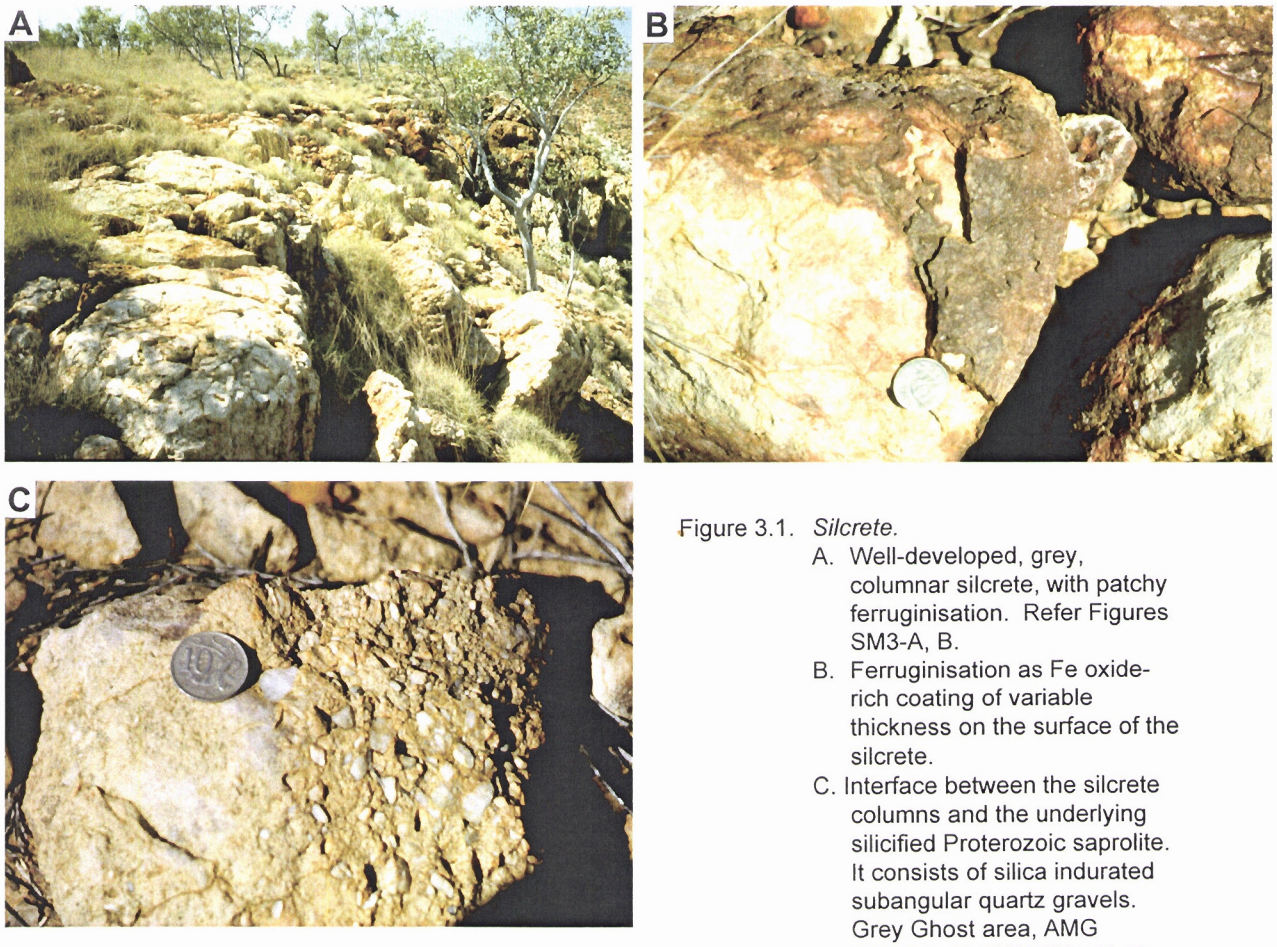

Figure 3.1. *Silcrete.*
A. Well-developed, grey, columnar silcrete, with patchy ferruginisation. Refer Figures SM3-A, B.
B. Ferruginisation as Fe oxide-rich coating of variable thickness on the surface of the silcrete.
C. Interface between the silcrete columns and the underlying silicified Proterozoic saprolite. It consists of silica indurated subangular quartz gravels. Grey Ghost area, AMG 309884mE, 7778598mN, Zone 54K.

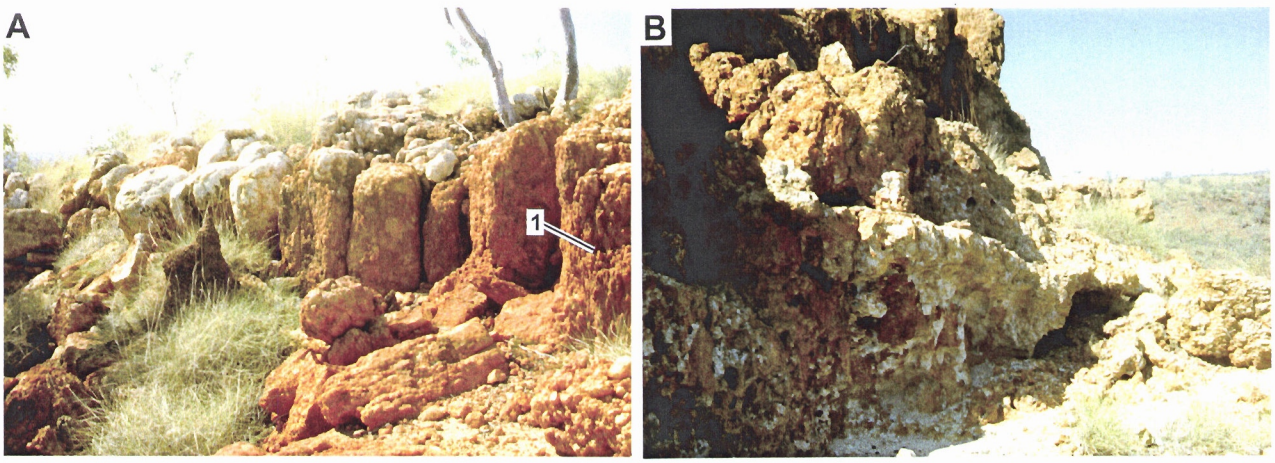

Figure 3.2. *Silcrete.*
A. Well-developed, columnar silcrete with fluted or ropy external structures (1).
B. Silicified, mottled clay zone underlying the columnar structures of (A). Grey Ghost area, AMG 310700 mE, 7777740mN, Zone 54K.

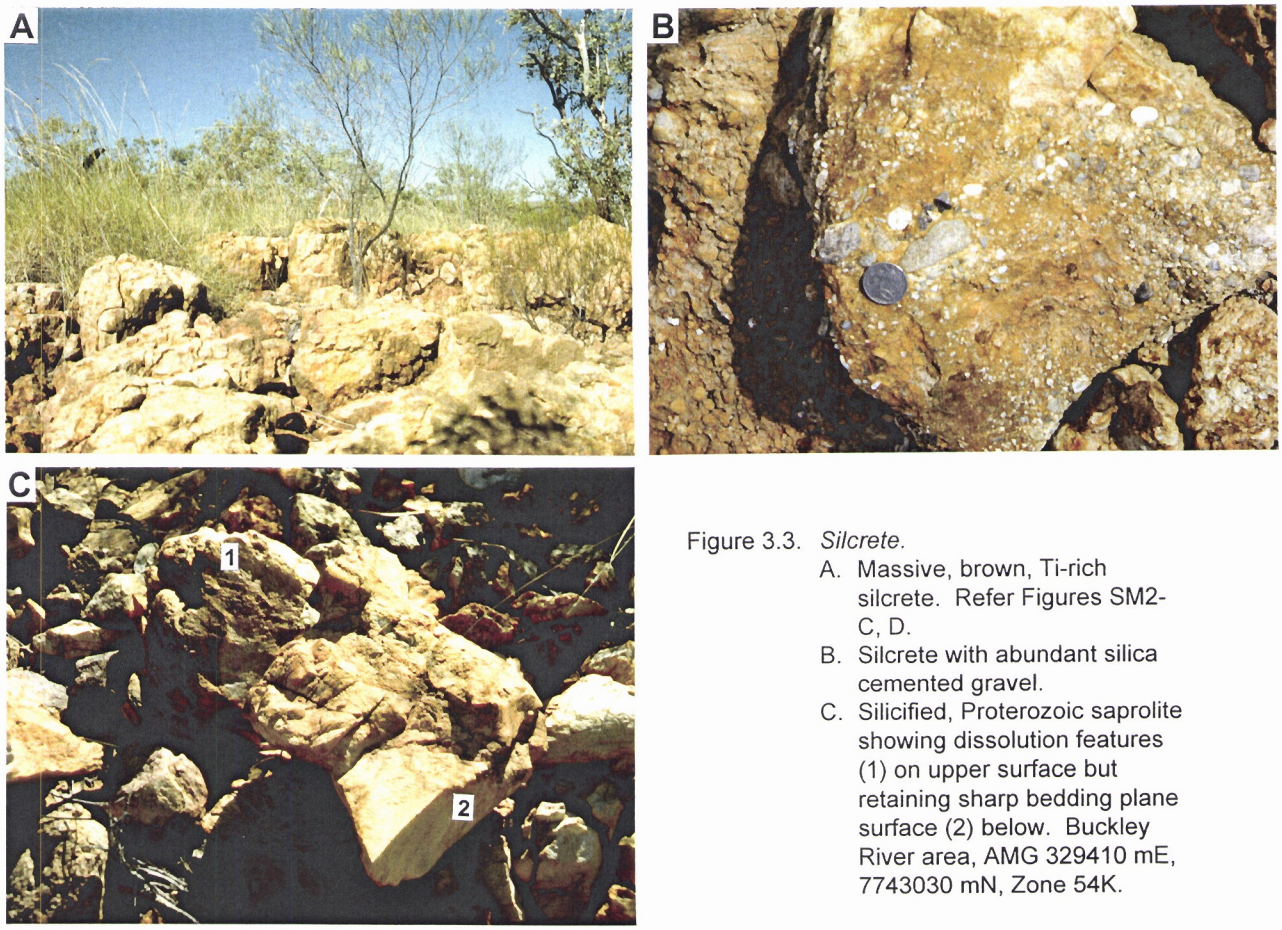

Figure 3.3. *Silcrete.*
A. Massive, brown, Ti-rich silcrete. Refer Figures SM2-C, D.
B. Silcrete with abundant silica cemented gravel.
C. Silicified, Proterozoic saprolite showing dissolution features (1) on upper surface but retaining sharp bedding plane surface (2) below. Buckley River area, AMG 329410 mE, 7743030 mN, Zone 54K.

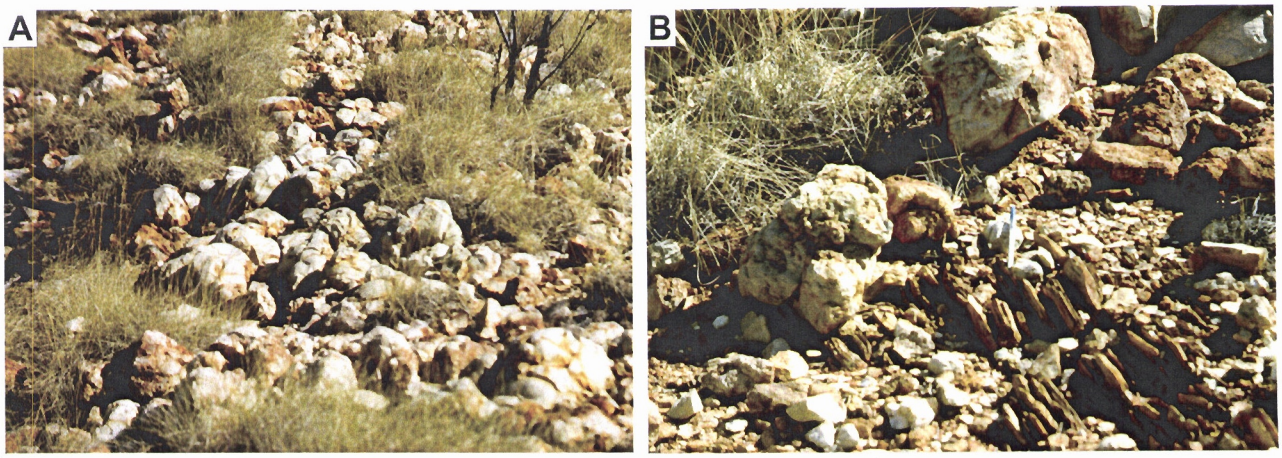

Figure 3.4. *Massive silcrete pods.*
A. Scattered silcrete pods.
B. Silcrete pods rest unconformably on silicified, Proterozoic shale. Buckley River area, AMG 305685 mE, 7756110 mN, Zone 54K.

Figure 3.5. *Massive silcrete*
Massive clay-rich porcelaneous silcrete developed in Mesozoic siltstone, with surfical Fe oxide staining. Refer Figures SM2-E, F, Tringadee area.

3.2 HANDSPECIMENS AND PHOTOMICROGRAPHS OF SILCRETE

FIGURE SM1
SILCRETE

Nodular-massive silcrete

A. Nodular-massive silcrete in Proterozoic siltstone. Some nodules are compound (1) with a few coarse, subangular quartz granules (2) in the interstices. Rutile and anatase form a grey tinge. The matrix and nodules contain a mixture of abundant fine to medium clear quartz grains and microcrystalline quartz. *C.f.* Figure SM1-B. Polished specimen LR-1 from Lady Loretta, AMG 306200 mE, 7794340 mN.

B. Detail of Figure SM1-A. Microcrystalline quartz nodule (1), is rimmed partly with titanium-oxide (2) and surrounded by embayed quartz grains (3) and subangular quartz grains. Cement is microcrystalline quartz (4). Photomicrograph with crossed polarizers.

Terrazzo silcrete

C. Terrazzo silcrete in Proterozoic sediments. Rounded (1) and subrounded (2) quartz grains in a matrix of fine to medium quartz grains and yellow-brown microcrystalline quartz (3). The quartz grains are either milky (1) or clear (2). *C.f.* Figure SM1-D. Polished surface of specimen IS-36 from Buckley River area. AMG 301790 mE, 7777660 mN.

D. Detail of Figure SM1-C. Subangular medium quartz grain (1) in near extinction with silica-anatase in planar voids (2). The silica-anatase matrix (3) cements poorly sorted, embayed quartz grains (4). Photomicrograph with crossed polarizers.

Brecciated silcrete

E. Brecciated silcrete in colluvium. A mixture of angular siltstone clasts (1), rock fragments probably of silicified sandstone (2), and subangular nodules (3) containing very fine quartz grains cemented by microcrystalline quartz. Reddish colouration is due to Ti oxide and hematite. *C.f.* Figure SM1-F. Polished specimen IS-37 from Buckley River area, AMG 306270 mE, 777470 mN.

F. Detail of Figure SM1-E. Metamorphosed siltstone fragment (1) cemented by chalcedonic quartz (2) to matrix containing silica-anatase-rutile cement with fine grained quartz grains (3). Photomicrograph with crossed polarizers.

Geochemistry and mineralogy

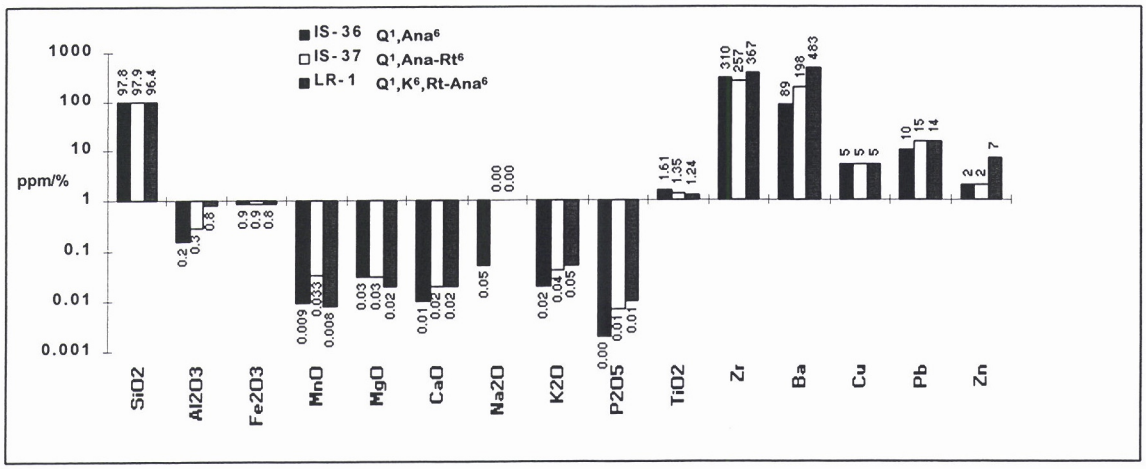

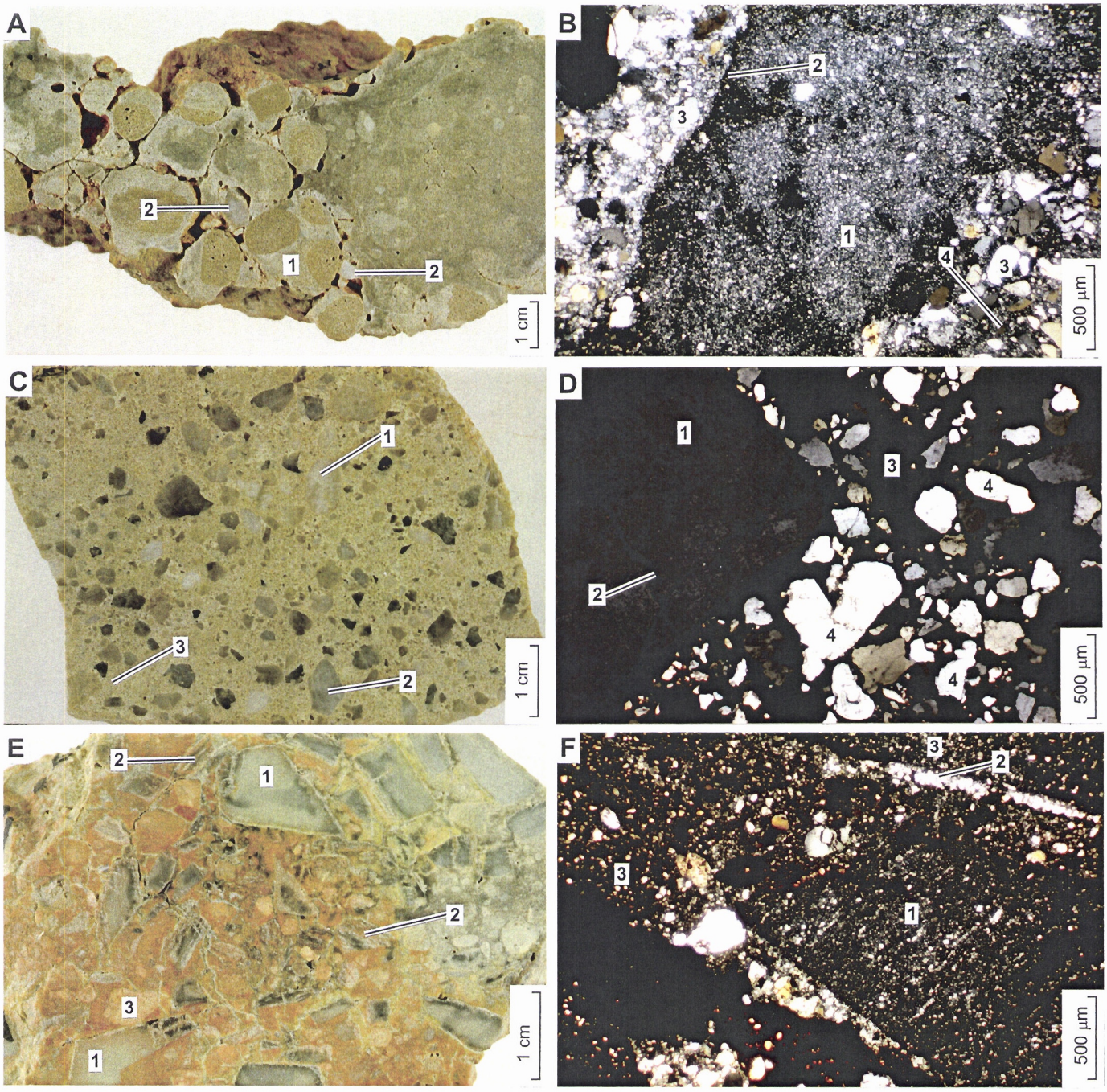
A
2
1
2
1 cm
B
2
3
1
4
3
500 µm
C
1
3
2
1 cm
D
1
3
4
2
4
4
500 µm
E
2
1
2
3
1
1 cm
F
3
2
3
1
500 µm

FIGURE SM2
SILCRETE

Fragmental silcrete

A. Fragmental silcrete in alluvium. Titanium oxide and hematite impregnate the outer surface (1) of the silcrete, and along cracks and pores. The grey matrix (2) contains fine quartz grains cemented in microcrystalline quartz with very coarse, subrounded, clear quartz grains (3) and rounded, milky quartz pebbles (4). *C.f.* Figure SM2-B. Polished specimen IS-24 from Buckley river, AMG 305540 mE, 7753730 mN, Zone 54K.

B. Detail of Figure SM2-A. Consists of microcrystalline quartzite pebble (1) with planar void and vugs filled with anatase-rutile-hematite cement (2). Subrounded (3), subangular (4) and fine grained (5) quartz grains are also present. Photomicrograph with crossed polarizers.

Massive silcrete

C. Massive silcrete in Proterozoic siltstone. (Refer Figure 3.3-A, B, C). Matrix contains medium to coarse quartz grains cemented by microcrystalline quartz enriched in anatase (7% TiO2) giving dark-brown stains (1). A few angular quartz pebbles (2) are probably derived from the underlying Proterozoic rocks. C.*f.* Figure SM2-D. Polished specimen IS-50 from Buckley River area, AMG 329410 mE, 7743030 mN, Zone 54K.

D Detail of Figure SM2-C. Consists of silica-anatase-rutile cement (1), with microcrystalline quartz (2) and various sizes of embayed quartz grains (3). Photomicrograph with crossed polarizers.

E. Massive porcelaneous silcrete in Mesozoic siltstone (Refer Figure 3.5). Pale pink and porous with fracture lines (1) near the surface. *C.f.* Figure SM2-F. Polished specimen MM-1 from Tringadee area, AMG 488450 mE, 7608880 mN, Zone 54K.

F. Detail of Figure SM2-E. Multiple fracture lines infilled by Fe oxides showing a concave pattern, probably stress related. Close up photograph with oblique reflected light.

Geochemistry and mineralogy

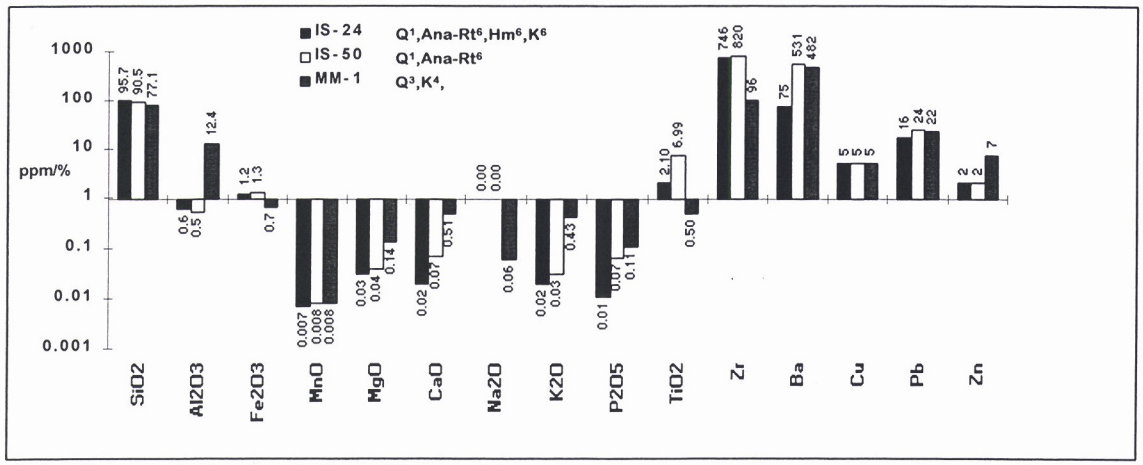

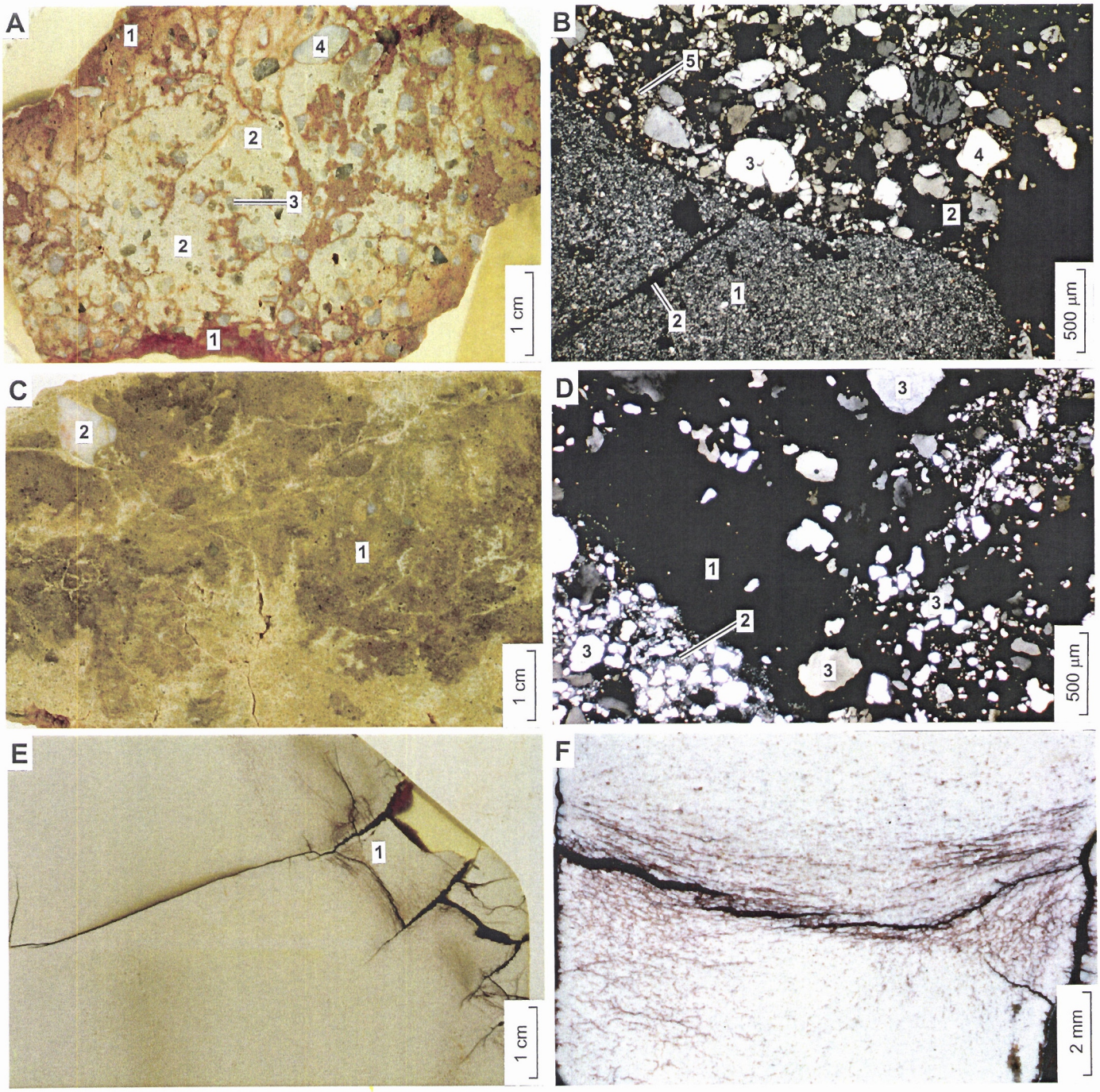
A
1
4
2
3
2
1
1 cm
B
5
3
4
2
1
2
500 µm
C
2
1
1 cm
D
3
1
2
3
3
3
500 µm
E
1
1 cm
F
2 mm

FIGURE SM3
SILCRETE

Columnar silcrete

A. Columnar silcrete over Proterozoic siltstone (Refer Figure 3.1A). The silcrete contains dense silcrete pebbles (1) of fine to medium, subangular quartz grains, cemented by silica. Some silcrete pebbles are rounded (2). The general matrix (3) is porous and contains coarse, subrounded quartz grains (4). Ferruginisation has involved mobilisation of Fe oxides into the pores and vugs (5). *C.f.* Figure SM3-B. Polished specimen GG-1 from Grey Ghost area, AMG 309890 mE, 7778600 mN, Zone 54K..

B. Detail of Figure SM3-A. Consists of subrounded polycrystalline quartz grain (1) showing angular voids (2) caused by removal of individual quartz crystals. These voids are filled with silica-anatase-rutile-hematite cement, which is also present in the matrix (3). The matrix also contains embayed quartz grains (4) and fine grained (5) quartz grains. Photomicrograph with crossed polarizers.

Geochemistry and mineralogy

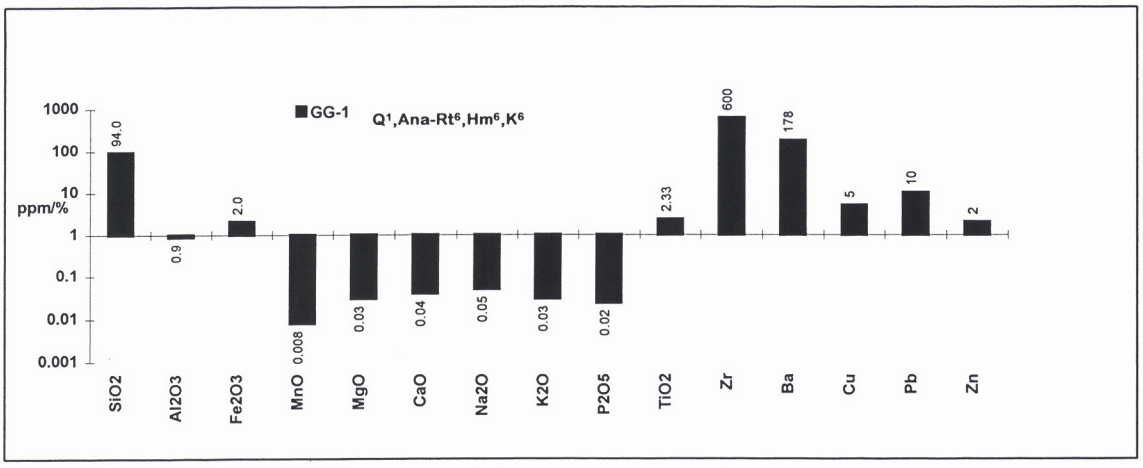

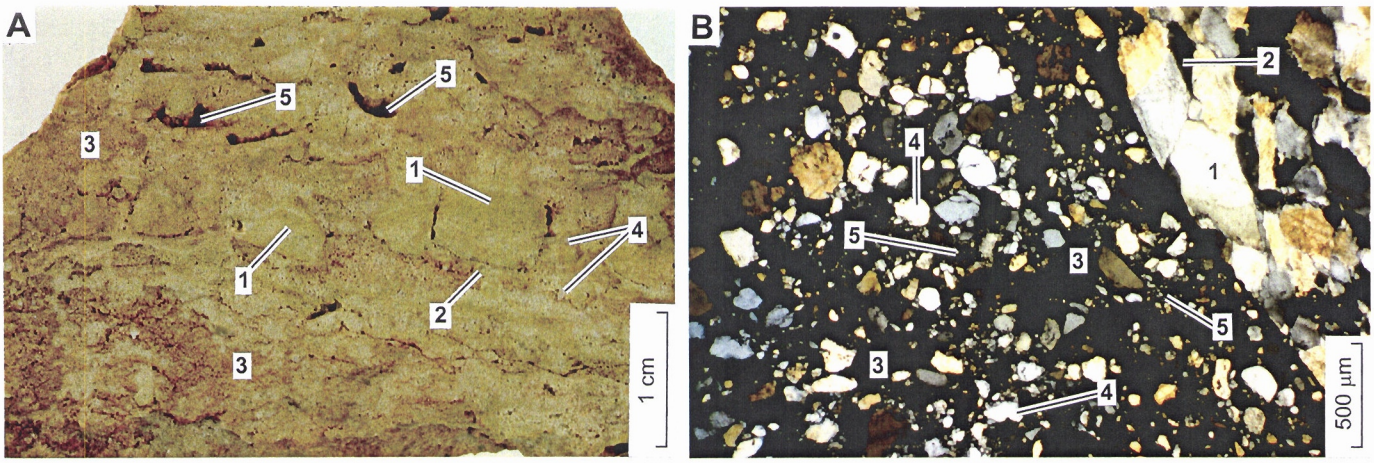
A
5
5
3
1
4
1
2
3
1 cm
B
2
4
1
5
3
5
3
4
500 µm

3.3 SELECTED FIELD PERSPECTIVES OF SILICIFIED SAPROLITE AND MOTTLED, SILICIFIED SAPROLITE

Saprolite becomes silicified by pervasive infusion of SiO_2. Silicified saprolite is preferentially found on siliceous lithologies and is associated with silcrete formation (Figure 3.6A). Silicification tends to be stronger towards the surface where the saprolite is less clay rich and more porous. Silicification leads to preservation of primary fabrics, bedding and foliation. Preferential erosion of the underlying, unsilicified saprolite causes undercutting. At Mt Coolon, silicification of the Suttor Formation forms a clay-rich, silicified saprolite (Figure 3.6B and Figure SM4-E, D).

Silicified saprolite, in places, is mottled by infusion of Fe oxides along cracks (Figure 3.6C and Figure SM5-E) or preferentially along permeable layers in the sediment (Figure SM5-A).

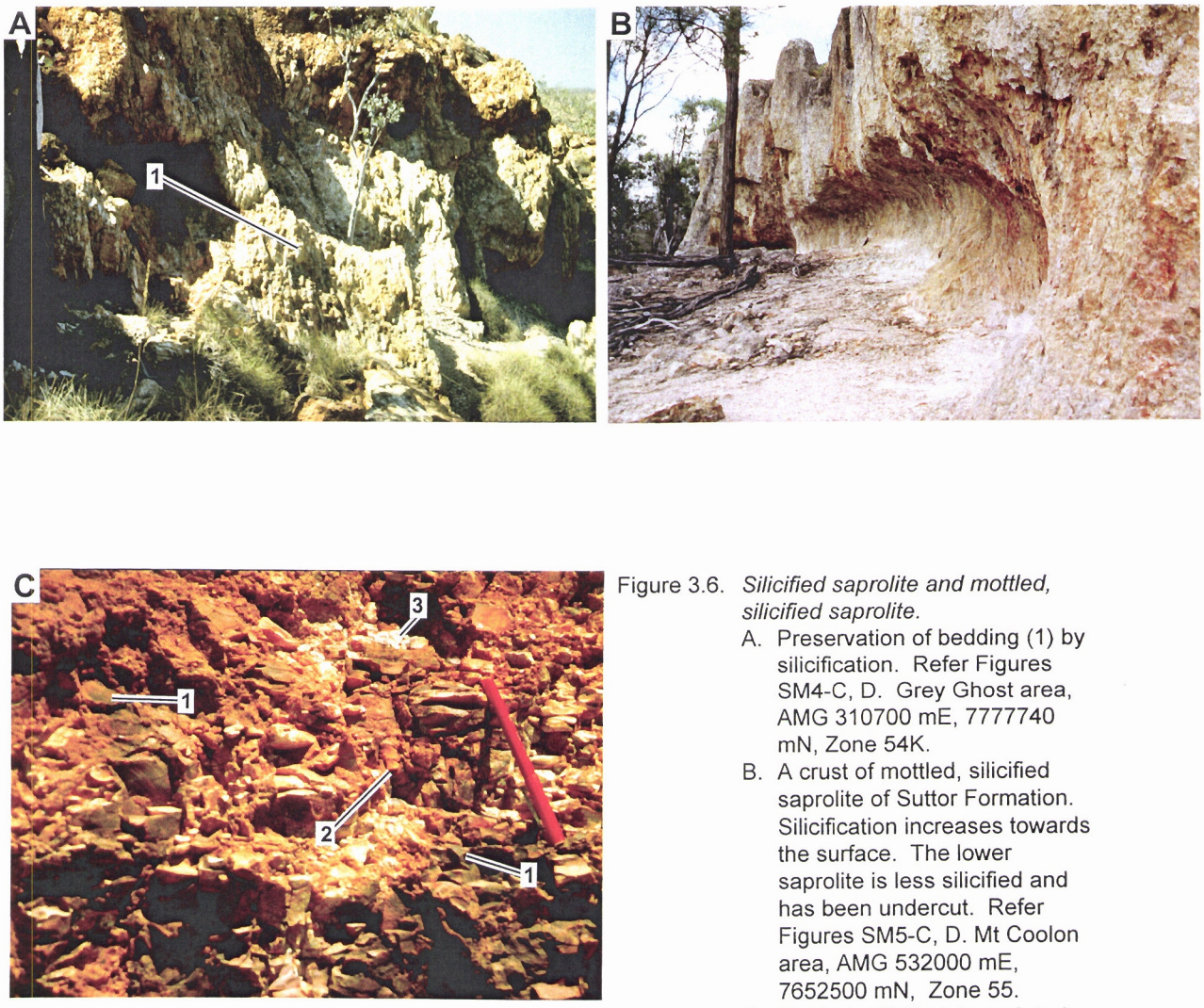

Figure 3.6. *Silicified saprolite and mottled, silicified saprolite.*

A. Preservation of bedding (1) by silicification. Refer Figures SM4-C, D. Grey Ghost area, AMG 310700 mE, 7777740 mN, Zone 54K.

B. A crust of mottled, silicified saprolite of Suttor Formation. Silicification increases towards the surface. The lower saprolite is less silicified and has been undercut. Refer Figures SM5-C, D. Mt Coolon area, AMG 532000 mE, 7652500 mN, Zone 55.

C. Mottled, silicified, brecciated saprolite developed in Mesozoic siltstone (refer Figures SM5-E, F), showing the mottles (1), Fe oxide-stained breccia (2) and pockets of pale, silicified and brecciated saprolite (3). Tringadee area, AMG 482990 mE, 7581480 mN, Zone 54K.

3.4 HAND SPECIMENS AND PHOTOMICROGRAPHS OF SILICIFIED SAPROLITE

FIGURE SM4
SILICIFIED SAPROLITE

Laminated, silicified saprolite

A. Laminated, silicified saprolite, in Proterozoic siltstone. Preferential precipitation of Ti oxide on more porous layers to form greyish bands (1). Speckles of Ti oxide are present in the finer layer (2). *C.f.* Figure SM4-B. Polished specimen LR-3 from Lady Loretta area, AMG 306210 mE, 7794340 mN, Zone 54K.

B Detail of Figure SM4-A. Lamination of the siltstone is visible as fine quartz grains in a rutile-anatase cement. Matrix has goethite staining (1) and a few voids (2). Photomicrograph with crossed polarizers.

Folded, silicified saprolite

C. Folded, silicified saprolite, in Proterozoic siltstone (Refer Figure 3.6A). It is massive and light grey, with folded bands (1). The porous part is coated (2) by goethite. *C.f.* Figure SM4-D. Polished specimen GG-5 from Grey Ghost area, AMG 309880 mE, 7778600 mN, Zone 54K.

D. Detail of Figure SM4-C. A band shows sheared and elongated quartz grains as a foliation (1), and mica flakes (2). Photomicrograph with crossed polarizers.

Speckled, silicified saprolite

E. Speckled, silicified saprolite, in Suttor Formation. It is kaolinite rich, silicified and contains many isolated fissures (1) filled with goethite. *C.f.* Figure SM4-F. Polished specimen 11-0773 from Mt. Coolon area, AMG 532000 mE, 7652500 mN, Zone 55.

F. Detail of Figure SM4-E. It is matrix supported with embayed quartz grains (1) in striated, birefringent kaolinite (2). Goethite (3) coats the outer surface of the specimen. Photomicrograph with crossed polarizers.

Geochemistry and mineralogy

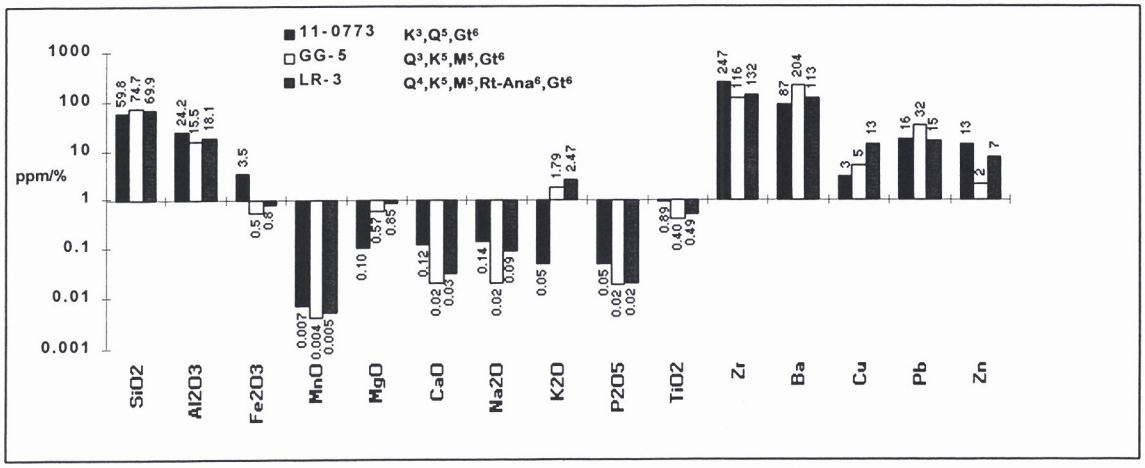

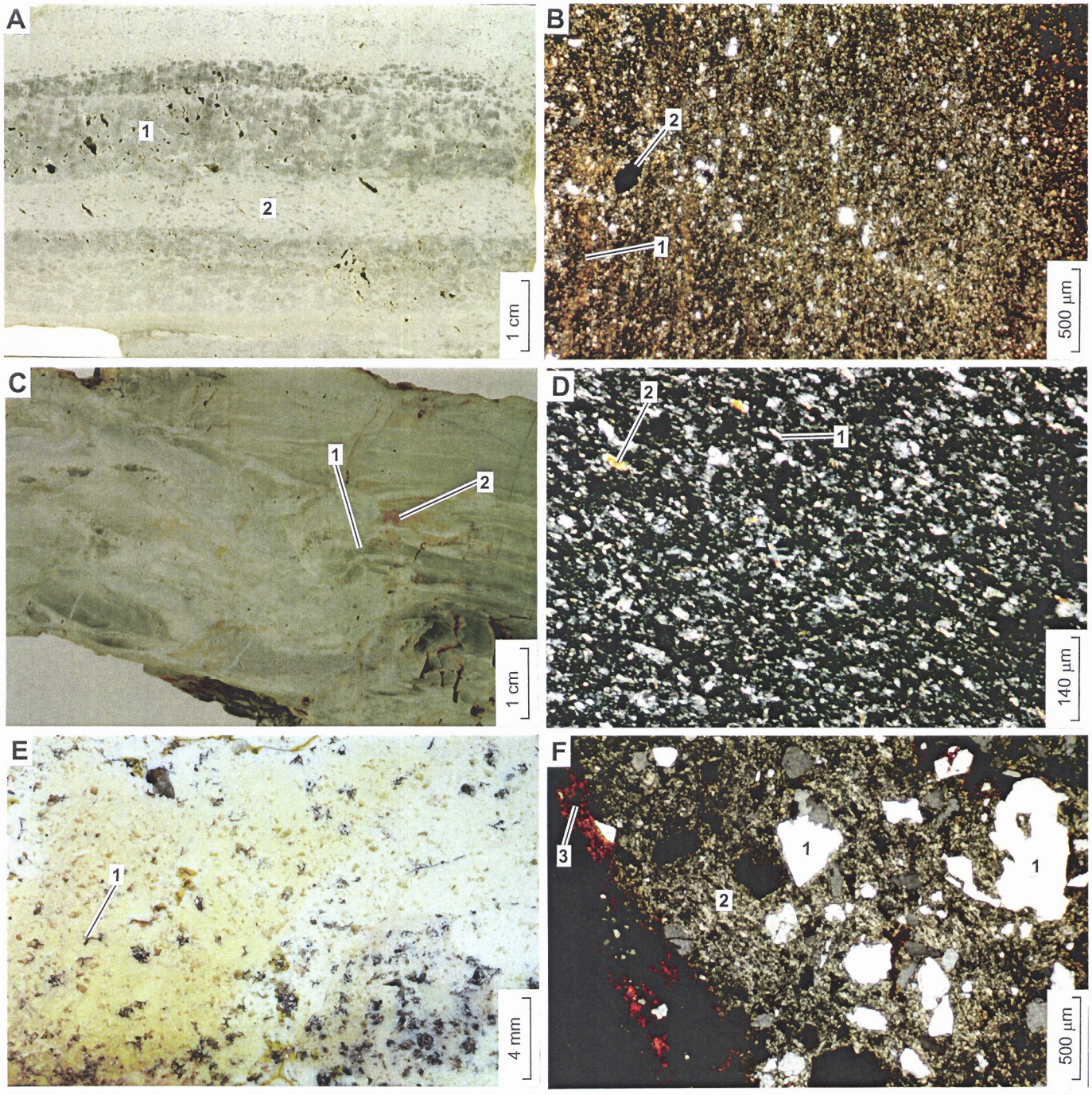
A
1
2
1 cm
B
2
1
500 µm
C
1
2
1 cm
D
2
1
140 µm
E
1
4 mm
F
3
1
1
2
500 µm

3.5 HAND SPECIMENS AND PHOTOMICROGRAPHS OF MOTTLED, SILICIFIED SAPROLITE

FIGURE SM5
MOTTLED, SILICIFIED SAPROLITE

A. Mottled, silicified saprolite of Proterozoic siltstone. A quartz vein (1) cuts across relict metasedimentary layers. Preferential impregnation by goethite is along coarser grained bands (2). *C.f.* Figure SM5-B. Polished specimen GG-6 from Grey Ghost area, AMG 309880 mE, 7778600 mN, Zone 54K.

B. Detail of Figure SM5-A. Goethite is preferentially precipitated in the coarse layers (1) and in cracks (2). The fine grained layer (3) has sheared quartz grains with tiny yellow flakes of mica. A quartz vein (4) cuts across the sedimentary layers. Photomicrograph with crossed polarizers.

C. Mottled, silicified saprolite of Suttor Formation (Refer Figure 3.6). It has abundant fine cracks and is variegated with brown, yellow and red. A few subangular, medium to coarse quartz grains (1) occur. Some of the cracks have developed into voids (2) or caused fragmentation of the saprolite into small pisoliths (3). *C.f.* Figure SM5-D. Polished specimen 11-0775 from Mt Coolon area, AMG 532000 mE, 7652500 mN, Zone 55.

D. Detail of Figure SM5-C. It is matrix supported. Consists of cross-striated birefringent clay (1), dominantly kaolinite. Goethite-hematite impregnation is shown in (2) with quartz grains (3) and voids (4). Photomicrograph with crossed polarizers.

E. Mottled, silicified saprolite after Mesozoic siltstone (Refer Figure 3.6). It is slightly brecciated, with hematite in cracks (1), as tiny dots in pore spaces giving light brown-purple stains (2) and as mottles (3). Goethite (4) occurs in some of the cracks. Silica and kaolinite dominate the matrix. *C.f.* Figure SM5-F. Polished specimen TG-75 from Tringadee area, AMG 482990 mE, 7581480 mN, Zone 54K.

F. Detail of Figure SM5-E. Hematite impregnation in a mottle is shown in the big, bright patch covering two-thirds of the photomicrograph. Within the mottle, there are vugs (1), some of which are lined with hematite (2). The light grey part (3) corresponds to a goethite-stained zone. Hematite is concentrated along channels (4). Photomicrograph in normally reflected light.

Geochemistry and mineralogy

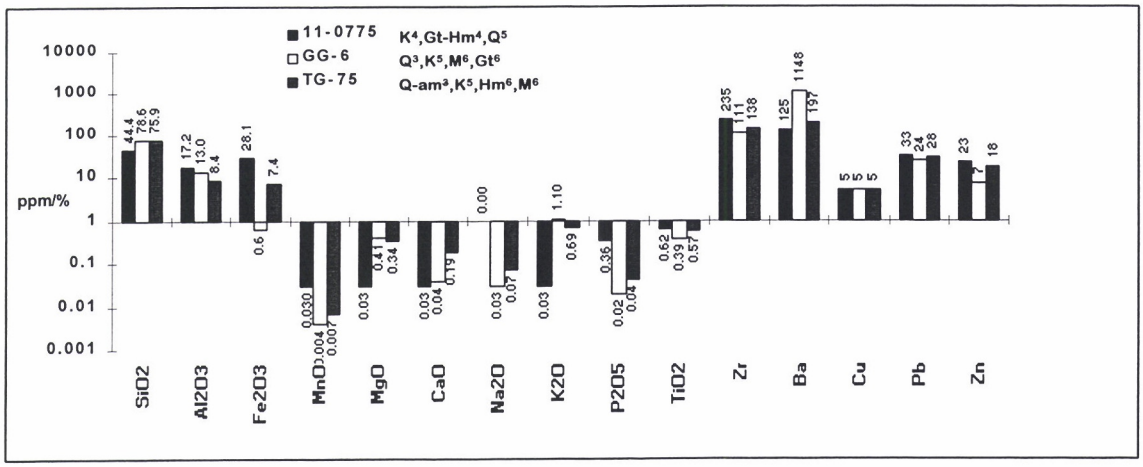

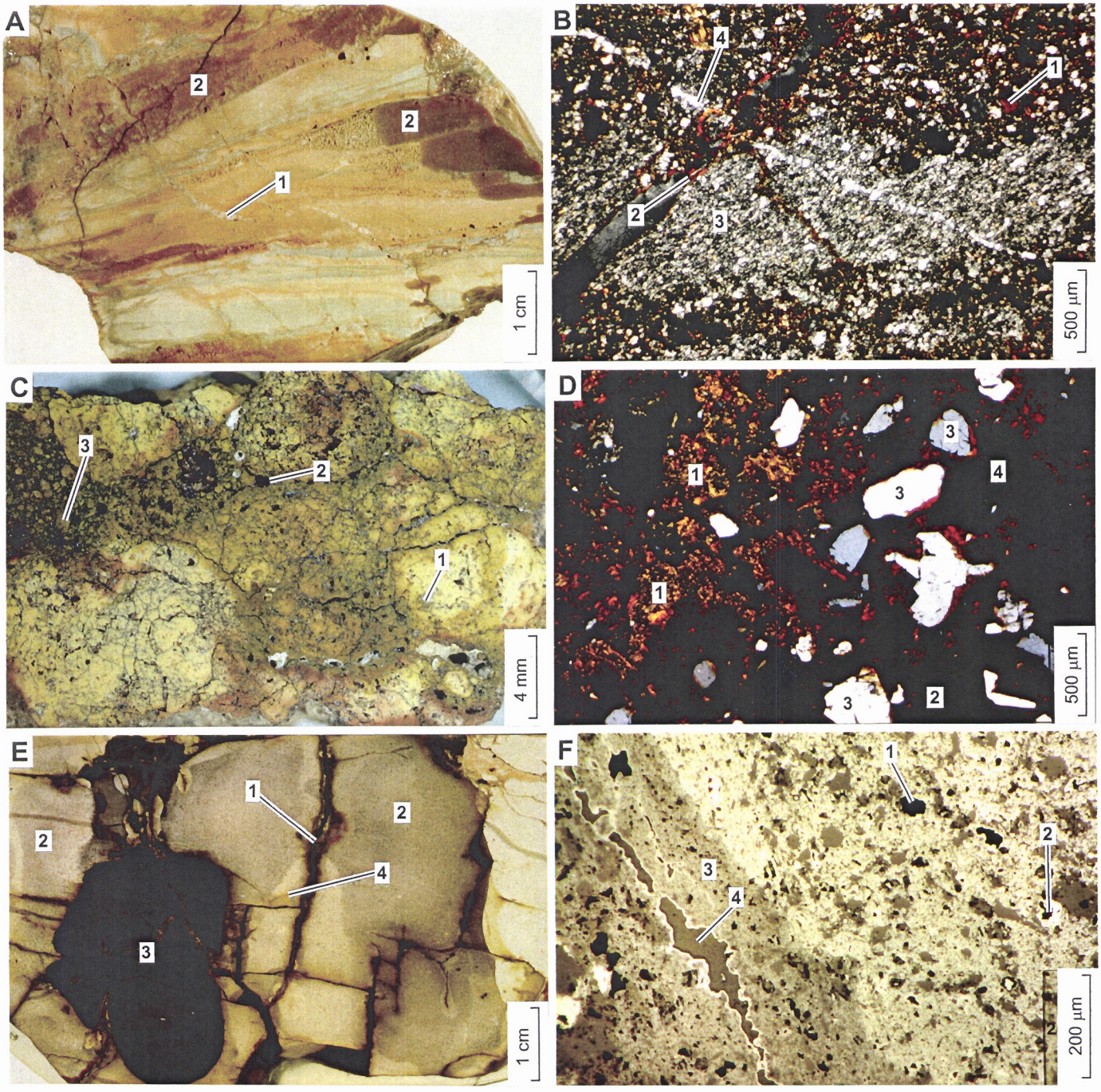
A
2
2
1
1 cm
B
4
1
2
3
500 µm
C
3
2
1
4 mm
D
3
1
3
4
1
3
2
500 µm
E
1
2
2
4
3
1 cm
F
1
2
3
4
2
200 µm

3.6 SELECTED FIELD PERSPECTIVES OF CHERTY BRECCIA

The basal unit of the Cambrian sediments is a cherty breccia. This has probably formed by weathering and removal of carbonates and clays from the original basal Cambrian sediments, resulting in collapse of the more resistant cherty parts.

At the Drifter Prospect, the cherty breccia overlies silicified, Proterozoic saprolite; forms white to reddish brown, irregular, 20-100 mm fragments and consists largely of quartz and hematite, with traces of goethite. Staining by Mn oxides is common on the surfaces of the breccia. Although hematite is generally uniformly distributed throughout the matrix, it concentrates with Mn oxides along cracks (Anand *et al.*, 1996). Figure 3.7 shows cherty breccia at the footslope of a mesa of Mesozoic sediment at Drifter area. The cherty breccia in Figures SM6-A, B shows pseudomorphs of microcrystalline quartz after radiolaria which indicates biogenic origin.

Figure 3.7. *Cherty breccia.*
A layer of cherty breccia at the footslope of a mesa of Mesozoic sediments. Drifter area, AMG 298400 mE, 7832500 mN, Zone 54K.

3.7 HAND SPECIMENS AND PHOTOMICROGRAPHS OF CHERTY BRECCIA

FIGURE SM6
CHERTY BRECCIA

A. Cherty breccia in siliceous, Cambrian sediments. Fine-grained siliceous fragment (1) cemented together with smaller, dull fragments (2) (*c.f.* Figure SM6-B). Polished specimen DF-133 from Drifter prospect, AMG 299000 mE, 7827000 mN, Zone 54K.

B. Detail of Figure SM6-A. Consists of cryptocrystalline fragments (1), some of which contain kaolinite and bright patches of microcrystalline quartz, which are pseudomorphs after radiolaria (2). The cement is hematite (3). Photomicrograph with crossed polarizers.

C. Fine-grained, partly brecciated siliceous Cambrian sediment. Fractures are coated with hematite (1). *C.f.* Figure SM6-D. Polished specimen DF-105 from Drifter prospect, AMG 298200 mE, 7827000 mN, Zone 54K.

D. Detail of Figure SM6-C. Consists of microcrystalline quartz (1) and very slightly coarser quartz (2) in a cherty breccia fragment cemented by hematite (3). Photomicrograph with crossed polarizers.

Geochemistry and mineralogy

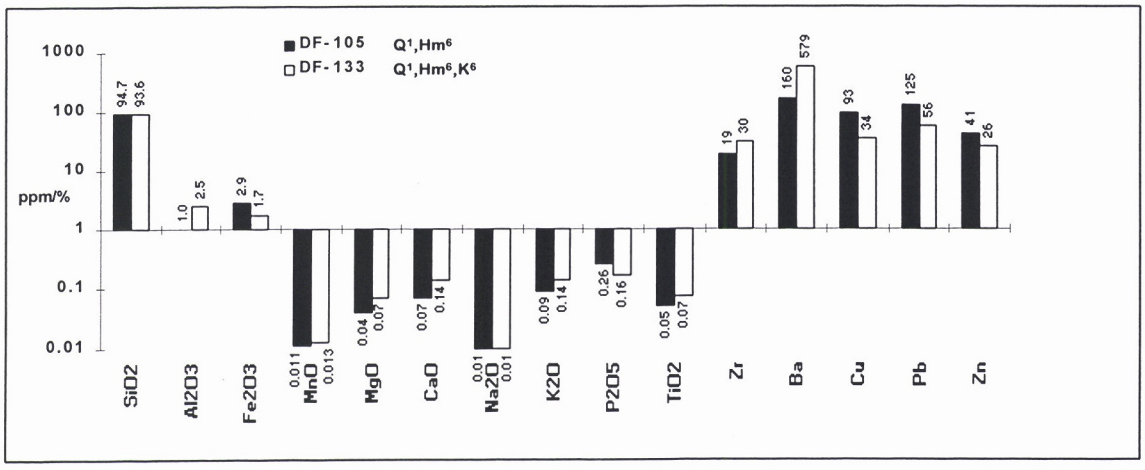

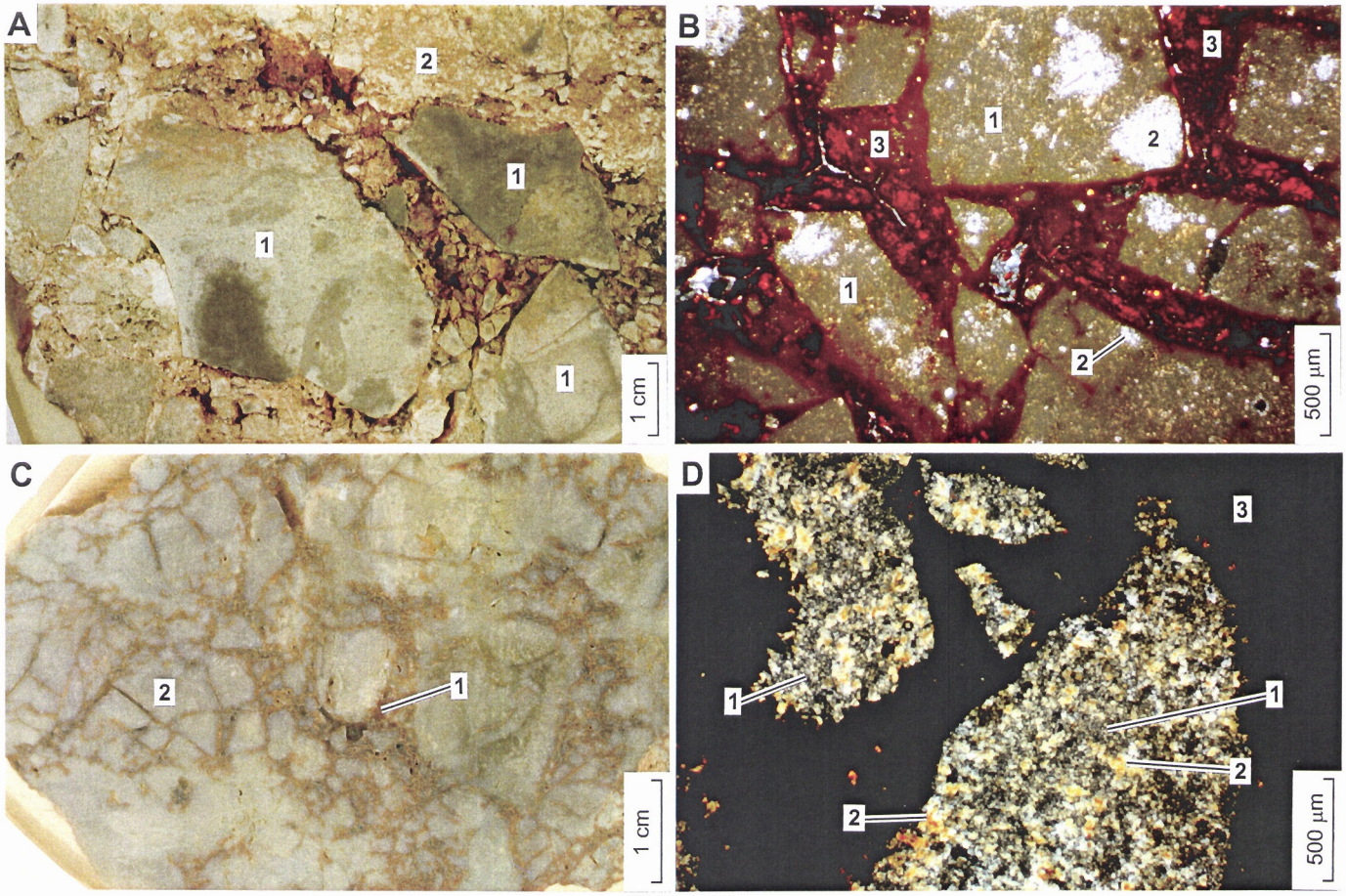
A
2
1
1
1
1 cm
B
3
1
3
2
1
2
500 µm
C
2
1
1 cm
D
3
1
1
2
2
500 µm

4. ACKNOWLEDGEMENTS

The support of sponsors of LEME-AMIRA PROJECT 417 has made this undertaking possible. Some regolith samples were collected by J. Wilford and Li Shu. Thin and polished sections were prepared by R.J. Bilz. Geochemical (XRF) and XRD analyses were by M.K.W. Hart and sample preparation was by S.L. Keppler and K. Lim. Photographs of some hand-specimens were by D. Longman, artwork was by A.D. Vartesi and document compilation was by P.J. Phillips. C.R.M. Butt and M.F. Killick provided critical review of the manuscript. All this assistance is acknowledged with appreciation.

5. REFERENCES

Anand, R.R., and Smith R.E., Innes, J., Churchward, H.M., Perdrix, J.L. and Grunsky, E.C., 1989. Laterite types and associated ferruginous materials, Yilgarn Block WA. Terminology, Classification and Atlas. CSIRO Division of Exploration Geoscience Restricted Report 60R. 90pp.

Anand, R.R., Wilford, J., Munday, T.J., Phang. C., Wildman, J.E. and Scott, K.M., 1995. Mt Isa field trip, 26-28 July, 1995. CSIRO Division of Exploration and Mining Restricted Report 156R. 41pp.

Anand, R.R., Phang, C., Wilford, J.R., Wildman, J.E., Li Shu, Robertson, I.D.M. and Munday, T.J., 1996. Regolith-landscape characteristics, evolution and regional synthesis of the Mt Isa region - Progress Report. CSIRO Division of Exploration and Mining Restricted Report 158R/CRC LEME Restricted Report 1R. 142pp.

Anand, R.R., Fraser, S.J., Jones, M.R., Li Shu, Munday, T.J., Phang, C., Robertson, I.D.M., Scott, K.M., Vasconcelos, P., Wildman, J.E. and Wilford, J., 1997. Geochemical exploration in regolith-dominated terrain, North Queensland. CSIRO Division of Exploration and Mining Restricted Report 447R/CRC LEME Restricted report 63R. 130pp.

Butt, C.R.M. and Zeegers, H., (Editors) 1992. Regolith exploration geochemistry in tropical and subtropical terrains. Handbook of Exploration Geochemistry, Volume 4. Elsevier Science Publishers B.V. Amsterdam, 607pp.

Campbell, I.D., 1996. Pajingo area. In: K.M. Scott, Li Shu, S. Fraser, I.D. Campbell, R.R., Anand and I.D.M. Robertson, Charters Towers - North Drummond Basin Field Excursion. CSIRO Division of Exploration and Mining Restricted Report 286R/CRC LEME Restricted Report 11R. 74pp.

Hancock, M.C. and Purvis, A.H., 1990. Lady Loretta silver-lead-zinc deposit. In: F.E. Hughes (Ed), Geology of the Mineral Deposits of Australia and Papua New Guinea. The Australasian Institute of Mining and Metallurgy. pp. 943-948.

Phang, C., Munday, T.J. and Wildman, J.E., 1997. Regolith-landform relationships and geochemical dispersion around Tringadee and Brumby prospects. CSIRO Division of Exploration and Mining Restricted Report 429R/CRC LEME Restricted Report 59R. 22pp.

Robertson, I.D.M., Phang, C. and Munday, T.J., 1995. Regolith geology and soil geochemistry of the Little Eva Copper Prospect, Quamby district, N.W. Queensland. CSIRO Division of Exploration and Mining Restricted Report 128R. 46pp.

Robertson, I.D.M., 1997. Dispersion into the Southern Cross Formation around the Scott and Cindy Lodes, Pajingo, N.E. Queensland. CSIRO Division of Exploration and Mining Restricted Report 449R/CRC LEME Restricted Report 65R. 41pp.

Scott, K.M and Li Shu 1996. Red Falls. In: K.M. Scott, Li Shu, S. Fraser, I.D. Campbell, R.R., Anand and I.D.M. Robertson, Charters Towers - North Drummond Basin Field Excursion. CSIRO Division of Exploration and Mining Restricted Report 286R/CRC LEME Restricted Report 11R. 74pp.

Scott, K.M., 1997. The significance of campaspe-dominated terrains in exploration within the Mt Windsor sub-province, N.E. Queensland. CSIRO Division of Exploration and Mining Restricted Report 422R/CRC LEME Restricted Report 58R. 25pp.

Wildman, J.E., 1997. The geochemical discrimination of mineralised and barren ironstones from the Selwyn Au-Cu deposit, NW Queensland. CSIRO Division of Exploration and Mining Restricted Report 341R/CRC LEME Restricted Report 35R. 21pp.

APPENDICES

APPENDIX I

Geochemistry of ferruginous and siliceous materials.

Sample No	SiO2	Al2O3	Fe2O3	MnO	MgO	CaO	Na2O	K2O	P2O5	TiO2	LOI	Ba	Ce	Co	Cr	Cu	Ga	La	Nb	Ni	Pb	Rb	S	Sr	V	Y	Zn	Zr
Unit	%	%	%	%	%	%	%	%	%	%	%	ppm	ppm	ppm	ppm	ppm	ppm	ppm	ppm	ppm	ppm	ppm	ppm	ppm	ppm	ppm	ppm	ppm
Detection	0.01	0.01	0.005	0.002	0.01	0.001	0.01	0.001	0.002	0.003		30	20	10	10	10	3	10	4	10	5	5	10	5	5	5	5	5
4095	34.1	10.8	49.6	0.028	0.20	0.03	0.05	0.45	0.24	0.44	4.49	78	59	5	50	5	14	20	2	5	9	25	440	11	73	11	15	162
4144	21.0	16.3	54.5	0.011	0.07	0.06	0.01	0.16	0.11	0.97	6.98	54	47	5	149	5	31	5	2	5	37	13	640	112	1298	8	17	224
4145	19.0	15.5	54.5	0.004	0.05	0.08	0.00	0.05	0.08	0.89	10.11	15	32	5	123	5	24	5	2	5	27	2	510	33	671	2	21	209
11-0773	59.8	24.2	3.5	0.007	0.10	0.12	0.14	0.05	0.05	0.89	10.36	87	10	5	5	3	30	10	6	5	16	2	240	63	72	7	13	247
11-0775	44.4	17.2	28.1	0.030	0.03	0.03	0.00	0.03	0.36	0.62	9.88	125	10	5	5	5	24	19	3	5	33	2	400	17	1057	8	23	235
BR-2	18.0	7.0	62.0	0.056	0.26	0.05	0.02	0.33	0.16	0.51	11.23	480	28	42	77	134	19	5	8	5	2	16	740	8	237	23	28	135
CL-3	33.5	9.1	50.3	0.244	0.28	0.18	0.04	0.24	0.22	0.62	5.15	456	93	34	241	66	20	39	8	28	18	7	310	48	1050	27	71	126
DF-17	5.1	2.3	36.0	21.066	0.72	5.80	13.85	0.28	3.01	0.10	27.01	3984	10	558	11	14	8	5	6	299	86	2	5920	174	73	12	4728	32
DF-22	32.4	16.4	39.2	0.012	0.05	0.02	0.01	0.13	0.14	0.78	11.08	156	108	14	123	5	16	46	7	5	9	2	380	38	2926	9	19	200
DF-105	94.7	1.0	2.9	0.011	0.04	0.07	0.01	0.09	0.26	0.05	1.11	160	28	5	5	93	1	12	2	5	125	5	210	55	27	7	41	19
DF-131	73.7	6.0	14.9	0.032	0.10	0.10	0.05	0.16	0.29	0.75	3.75	282	107	5	5	5	5	77	6	11	25	2	210	113	50	20	46	552
DF-133	93.6	2.5	1.7	0.013	0.07	0.14	0.01	0.14	0.16	0.07	1.65	579	26	5	5	34	3	25	2	23	56	2	320	132	49	31	26	30
DF-410	58.1	6.8	27.5	0.014	0.14	0.04	0.05	0.43	0.14	1.29	5.91	48	39	5	35	427	23	13	11	24	19	25	170	27	183	44	140	213
GG-1	94.0	0.9	2.0	0.008	0.03	0.04	0.05	0.03	0.02	2.33	0.76	178	10	5	24	5	1	5	31	5	10	2	180	12	72	20	2	600
GG-5	74.7	15.5	0.5	0.004	0.57	0.02	0.02	1.79	0.02	0.40	5.41	204	53	5	38	5	24	47	9	15	32	79	150	22	55	10	2	116
GG-6	78.6	13.0	0.6	0.004	0.41	0.04	0.03	1.10	0.02	0.39	5.19	1148	40	5	23	5	21	36	5	12	24	47	440	34	47	10	7	111
GG-16	49.3	2.0	42.6	0.051	0.07	0.02	0.00	0.06	0.10	0.14	5.76	15	61	54	15	116	1	15	2	27	2	2	720	16	61	15	732	74
IS-7	81.2	2.3	14.5	0.019	0.09	0.09	0.01	0.08	0.04	0.64	1.33	412	42	5	5	163	4	22	2	15	38	2	300	18	32	19	2	278
IS-11	19.1	10.2	59.5	0.031	0.04	0.00	0.05	0.01	0.14	2.14	8.49	15	27	5	78	384	19	5	5	11	29	5	670	2	770	12	43	223
IS-24	95.7	0.6	1.2	0.007	0.03	0.02	0.00	0.02	0.01	2.10	0.35	75	23	5	5	5	1	5	27	5	16	2	150	2	51	19	2	746
IS-36	97.8	0.2	0.9	0.009	0.03	0.01	0.05	0.02	0.00	1.61	0.01	89	10	5	5	5	1	5	16	24	10	2	120	2	22	19	2	310
IS-37	97.9	0.3	0.9	0.033	0.03	0.02	0.00	0.04	0.01	1.35	0.15	198	26	5	5	5	3	13	11	21	15	2	130	9	35	25	2	257
IS-38	40.9	4.1	46.5	0.042	0.18	0.03	0.01	0.45	0.26	0.15	7.95	374	132	39	42	33	4	49	2	34	2	21	460	20	140	35	113	70
IS-41	50.1	6.8	37.4	0.009	0.15	0.02	0.01	0.49	0.19	0.25	5.48	310	121	5	42	29	10	64	2	5	2	31	440	193	185	25	125	102
IS-45	68.7	5.3	22.6	0.007	0.15	0.04	0.00	0.52	0.08	0.36	3.14	106	116	5	44	67	9	47	2	5	22	17	270	30	181	11	2	113
IS-50	90.5	0.5	1.3	0.008	0.04	0.07	0.00	0.03	0.07	6.99	0.46	531	50	5	50	5	3	36	50	14	24	2	400	53	170	32	2	820
LI-72	57.5	10.1	24.8	0.281	0.08	0.03	0.03	0.27	0.08	0.36	6.9	334	266	28	196	43	16	14	6	35	84	30	20	12	427	19	17	150
LI-80	80.4	9.9	1.6	0.012	0.53	0.4	1.35	2.82	0.01	0.09	2.81	447	22	5	5	5	10	5	2	5	28	100	5	114	16	9	12	32
LI-82	56.2	18.8	13.8	0.113	0.22	0.18	0.09	0.33	0.08	0.77	9.74	618	131	5	78	32	21	26	9	5	61	26	100	40	257	9	47	198
LI-83	70.2	10.8	9.6	0.016	0.49	0.27	2.5	0.48	0.04	0.4	4.82	159	22	5	16	17	14	10	2	5	25	22	70	68	114	12	25	99
LR-1	96.4	0.8	0.8	0.008	0.02	0.02	0.00	0.05	0.01	1.24	0.56	483	10	5	10	5	1	11	20	5	14	2	190	8	22	18	7	367
LR-3	69.9	18.1	0.8	0.005	0.85	0.03	0.09	2.47	0.02	0.49	6.02	113	50	5	47	13	19	30	10	14	15	89	220	17	108	25	7	132
LR-7	33.8	8.2	46.6	0.074	0.44	0.01	0.02	2.04	0.19	0.34	8.25	85	60	109	102	667	9	15	2	22	11	63	200	14	277	30	26	142
MM-1	77.1	12.4	0.7	0.008	0.14	0.51	0.06	0.43	0.11	0.50	6.65	482	74	5	21	5	11	31	4	5	22	15	250	166	44	12	7	96
SE-103	20.8	0.5	78.4	0.019	0.02	0.00	0.00	0.01	0.03	0.02	0.49	171	27	19	5	122	7	16	2	5	2	2	160	13	32	28	13	2
SE-143	44.5	0.9	52.7	0.017	0.05	0.02	0.01	0.02	0.28	0.01	2.28	81	20	22	5	925	13	14	2	5	2	2	180	2	41	68	15	2
SE-159	36.8	7.0	16.6	25.656	0.99	0.15	0.03	3.99	0.30	0.33	6.34	11883	32	745	62	507	11	20	5	123	26	282	310	908	780	18	135	103
SE-408	81.5	10.4	1.8	0.009	0.09	0.08	0.02	0.41	0.05	1.26	4.29	396	72	5	29	14	16	48	57	5	29	17	160	126	64	30	7	701
TG-73	40.3	13.5	33.1	0.012	0.10	0.09	0.04	0.06	0.02	1.23	10.14	466	22	5	438	25	26	11	11	22	235	2	580	32	8914	24	60	289
TG-75	75.9	8.4	7.4	0.007	0.34	0.19	0.07	0.69	0.04	0.57	4.82	197	32	5	65	5	17	22	6	5	28	31	160	102	427	13	18	138
TG-76	15.3	4.9	68.1	0.034	0.12	0.02	0.03	0.25	0.30	0.27	9.60	100	10	45	204	22	9	5	4	89	2	10	870	36	451	5	158	57
TG-103	30.3	7.1	54.1	0.009	0.09	0.01	0.04	0.25	0.48	0.29	7.62	158	51	14	166	15	10	5	9	5	2	10	1330	72	580	8	69	63
TG-106	13.6	2.5	73.1	0.395	0.15	0.15	0.05	0.14	0.27	0.16	9.14	190	21	423	157	5	6	5	2	414	2	6	960	34	433	17	877	32
TG-147	20.9	5.5	44.7	18.48	0.33	0.11	0.15	1.54	0.30	0.25	10.9	4981	69	1678	5	309	7	16	2	1569	50	62	140	364	81	28	2145	54
TG-190	26.0	10.4	55.8	0.037	0.06	0.06	0.03	0.12	0.22	0.69	7.16	84	110	65	114	171	23	35	12	37	2	9	370	143	464	10	125	212
TG-204	23.0	14.2	50.5	0.006	0.07	0.06	0.05	0.05	0.08	1.04	10.90	105	35	12	129	115	37	5	27	5	9	2	850	12	705	7	28	300
TG-205	15.9	12.0	60.5	0.007	0.04	0.02	0.05	0.06	0.07	0.70	10.64	15	10	18	153	258	28	5	15	5	17	2	410	7	603	8	28	214
TG-207	80.4	4.0	11.1	0.097	0.18	0.12	0.04	0.64	0.11	0.19	2.89	340	33	12	5	5	7	14	2	43	20	20	350	35	69	14	138	93
TG-215	47.3	9.1	35.1	0.011	0.13	0.06	0.04	0.36	0.47	0.34	7.43	232	39	5	98	22	15	20	2	5	18	12	950	96	440	7	37	78
TG-502	83.6	2.8	6.8	0.008	0.11	0.05	0.04	0.55	0.03	0.63	2.79	231	10	5	31	17	11	5	6	5	14	27	50	28	215	8	2	119
TG-504/1	26.8	3.4	58.8	0.158	0.20	0.08	0.03	0.16	0.09	0.46	9.59	1298	93	75	30	25	7	13	8	73	5	8	540	53	81	28	381	232

APPENDIX II[1]

PETROGRAPHY AND GEOCHEMISTRY OF BEDROCKS AND IRONSTONES FROM GREY GHOST AND GORDON PROSPECTS

Bedrock

The fresh bedrocks consist of a carbonate-quartz-muscovite-chlorite assemblage with minor poppy-seed pyrite. The bedding, depicted by subtle grain-size changes, is cut acutely by a cleavage of aligned mica. Dolomite and siderite occur as coarse, diagenetic crystals in the fabric of quartz and phyllosilicates. Carbonate veins cut the bedding and contain lenses of pyrite. Microprobe analysis of the carbonates (K.M. Scott, pers. comm., 1998) reveals Mn- and Sr-rich calcite and dolomite as well as siderite which contains substantial Mn and 7000 ppm Zn.

Ferruginous saprolite, 'ghostite' and stratiform ironstone

The ferruginous saprolite consists of quartz, goethite and muscovite and shows similar bedding-cleavage relationships to the fresh rock. However, where speckles of goethite have developed ('ghostite'), the bedding is slightly deformed around them, indicating diagenetic development of what appears to originally have been carbonate in the fabric. This diagenetic carbonate developed in the fresh rock. Where the 'ghostite' structure (Figure FM12-A) is strongly developed, primary lamination is absent. Detailed investigation of the bladed, stellate structures of the 'ghostite' indicates that much of this carbonate was siderite and has since been altered to goethite, perfectly preserving the 'nailhead spar' structure (Figure FM12-B).

Where the stratiform ironstone is a deep red, the dominant minerals are very fine-grained goethite, quartz and hematite and muscovite is lacking. These rocks were probably very rich in siderite originally. Bedding is apparent and so is a crosscutting banding, probably liesegang structures.

Geochemistry

Weathering of the fresh rocks to saprolite (Table 1-Appendix II) shows the expected loss of alkalis, alkaline earths and S, with corresponding increases in Al, Si, Ba and Ce. The geochemical changes are much greater in the transition from saprolite to ironstone (Table 1-Appendix II), which is accompanied by marked increases in Fe, Mn, P, As, Cu, Sb, U, V and Zn; there are corresponding decreases in Si, Al, K, Ti, Ba, Ce, Cs, Ga, La, Rb and Th. In all, the Si-Al ratio is consistent but Fe is variable (Figure 1). Relatively stable elements, such as Zr, Ti, K and Rb, suggest some dilution of the saprolite by exogenous Fe (30-40%) but much less than implied by the Fe content. This, and the siderite content, support the contention that a proportion of the Fe content was inherited.

Many elements are strongly correlated with and have been scavenged by Fe. Although some elements (P, As and Ni) are similarly enriched with Fe at both sites (Grey Ghost and Gordon), those from the Grey Ghost Prospect are significantly proportionately richer in Zn, Cu, Sb and U (e.g. greater Zn/Fe ratio than the Gordon Prospect). Those from the Gordon Prospect are more enriched in Mn and Co in proportion to Fe.

Origin

It seems that these ironstones represent naturally Fe-rich parts of the stratigraphy. The Zn in the bedrock is, at least in part, contained in Zn-rich carbonates. One of the samples from Grey Ghost is strongly auriferous (674 ppb) and the Au is visible in polished section as very fine specs (<5 μm). The ironstones appear to have formed from layers within the dolostones that were

[1] This geochemical and petrographic investigation has not been reported elsewhere as it was too small for a formal report. It is included here for completeness.

particularly rich in diagenetic siderite and were weathered in an environment of fluctuating water tables. Weathering of pyrite may have contributed to their Fe content. A sideritic unit underlies the nearby Lady Loretta Ag-Pb-Zn Deposit (Hancock and Purvis, 1990).

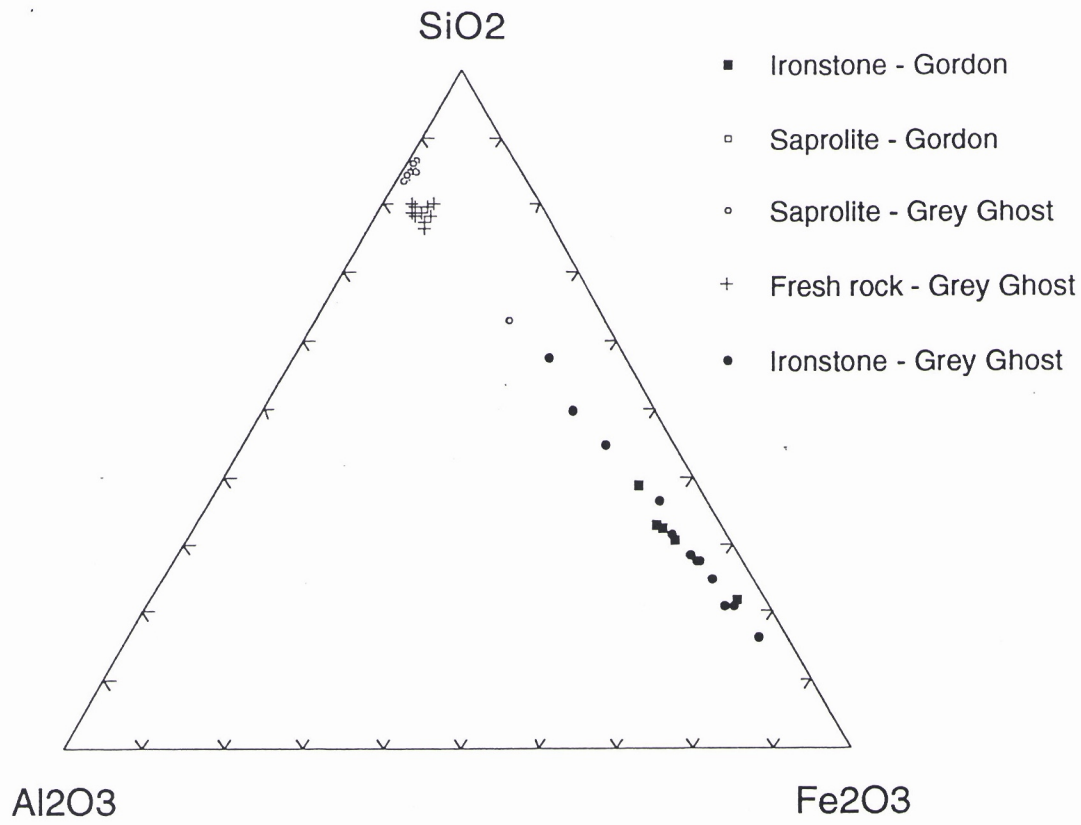

Figure 1. Ternary Si-Al-Fe diagram of the fresh rocks, saprolites and ironstones at the Grey Ghost and Gordon prospects.

APPENDIX II - Table 1

Geochemistry of fresh rocks, saprolite and stratiform ironstones from Grey Ghost and Gordon prospects.

Grey Ghost Prospect - Fresh dolomitic shales

Sampl No	Lib No	Type	SiO2 XRF %	Al2O3 XRF %	Fe2O XRF %	MgO XRF %	Ca0 XRF %	Na2O XRF %	K2O XRF %	TiO2 XRF %	MnO XRF %	P2O5 XRF %	As INAA ppm	Au INAA ppb	Ba XRF ppm	Ce INAA ppm	Co INAA ppm	Cr INAA ppm	Cs INAA ppm	Cu XRF ppm	Eu INAA ppm	Ga XRF ppm	Hf INAA ppm	La INAA ppm	Lu INAA ppm	Nb XRF ppm	Ni XRF ppm	Pb XRF ppm	Rb XRF ppm	S XRF ppm	Sb INAA ppm	Sc INAA ppm	Sm INAA ppm	Sr XRF ppm	Th INAA ppm	U INAA ppm	V XRF ppm	Y XRF ppm	Yb INAA ppm	Zn XRF ppm	Zr XRF ppm
	Detn		0.01	0.01	0.01	0.01	0.00	0.01	0.01	0.00	0.002	0.002	2	5	30	10	1	5	1	10	1	3	1	0.5	0.2	4	10	5	5	10	0.5	0.1	0.2	5	0.5	2	5	5	0.5	5	5
GD 11	08-1747	Fresh	54.31	10.97	3.80	6.74	6.14	0.02	2.59	0.42	0.076	0.203	24	<5	366	64	9	44	8	<10	1	11	4	32.6	0.3	3	28	86	148	2180	5.5	9.1	5.1	53	12.4	4	90	15	2.3	244	142
GD 12	08-1748	Fresh	61.84	13.40	4.07	3.51	2.10	0.05	3.38	0.52	0.027	0.156	33	<5	531	76	13	51	11	<4	1	16	5	39.5	0.4	1	21	69	190	7180	3.9	11.0	5.6	20	14.2	5	122	15	2.3	250	141
GD 13	08-1749	Fresh	54.63	11.29	2.92	5.64	7.41	0.02	2.88	0.40	0.062	0.136	25	<5	441	73	13	44	9	4	1	12	4	39.9	0.3	2	17	163	158	6330	4.1	9.4	5.4	58	12.5	6	93	14	2.7	209	138
GD 14	08-1750	Fresh	41.85	7.06	3.35	9.37	13.00	0.00	1.92	0.26	0.118	0.081	23	<5	303	50	9	28	6	4	1	8	3	26.3	0.2	1	15	82	109	7010	2.6	6.0	4.1	101	8.4	3	43	17	1.7	84	100
GD 15	08-1751	Fresh	51.69	11.19	3.03	5.21	9.78	0.43	2.70	0.36	0.057	0.112	22	9	385	76	11	33	9	<1	1	14	5	38.7	0.4	4	19	95	148	7030	3.3	8.0	5.8	94	13.5	5	57	20	3.1	222	135
GD 16	08-1752	Fresh	57.33	11.65	2.53	5.07	6.76	0.84	3.18	0.41	0.054	0.117	26	<5	525	71	11	48	12	<9	1	14	4	38.0	0.3	4	15	99	181	5990	3.5	10.3	5.0	68	12.4	4	101	14	2.1	564	125
GD 17	08-1753	Fresh	38.45	7.34	3.51	10.18	14.63	0.57	1.64	0.27	0.117	0.085	18	<5	288	54	8	28	5	<21	1	10	4	27.0	0.3	4	9	49	89	4080	2.2	6.4	4.7	131	9.4	3	54	17	2.0	102	110
GD 18	08-1754	Fresh	37.16	7.66	3.22	7.55	18.39	0.72	1.69	0.25	0.104	0.088	22	<5	283	60	7	25	5	<12	1	5	3	31.6	0.3	5	7	72	86	5020	2.3	6.1	5.1	180	8.8	4	47	19	2.3	112	101
GD 19	08-1755	Fresh	40.40	8.63	3.77	9.94	12.76	0.72	1.75	0.31	0.103	0.091	15	<5	269	47	8	26	7	5	1	11	4	23.8	0.3	1	11	49	102	4460	2.5	6.5	4.1	118	10.9	4	47	22	2.0	115	143
GD 20	08-1756	Fresh	44.49	8.13	3.31	8.64	12.33	0.77	1.70	0.29	0.095	0.092	14	<5	273	48	8	31	6	5	1	8	3	24.1	0.2	0	9	45	101	4220	1.9	6.5	4.2	116	9.9	4	63	18	1.7	195	114
Mean	-	-	48.22	9.73	3.35	7.19	10.33	0.41	2.34	0.35	0.081	0.116	22	9	366	62	10	36	8	5	1	11	4	32.2	0.3	3	15	81	131	5350	3.2	7.9	4.9	94	11.2	4	72	17	2.2	210	125

Grey Ghost Prospect - Saprolitic shales

Sampl No	Lib No	Type	SiO2	Al2O3	Fe2O	MgO	Ca0	Na2O	K2O	TiO2	MnO	P2O5	As	Au	Ba	Ce	Co	Cr	Cs	Cu	Eu	Ga	Hf	La	Lu	Nb	Ni	Pb	Rb	S	Sb	Sc	Sm	Sr	Th	U	V	Y	Yb	Zn	Zr
GD 01	08-1737	Weathered	55.08	10.79	21.29	2.59	0.12	0.06	2.72	0.41	0.152	0.195	53	<5	513	83	136	49	9	153	1	12	3	44.8	0.3	3	226	187	157	190	6.3	11.6	7.2	64	12.0	4	129	26	2.7	1599	131
GD 02	08-1738	Weathered	74.30	13.10	0.85	2.88	0.05	0.06	3.93	0.44	0.006	0.058	4	8	669	89	2	53	12	27	1	16	3	46.0	0.3	6	11	200	223	100	2.6	11.3	7.3	62	11.2	3	80	17	2.2	70	110
GD 03	08-1739	Weathered	77.21	12.23	1.38	1.54	0.03	0.06	3.05	0.47	0.011	0.053	8	<5	546	96	8	54	9	46	1	13	6	47.3	0.4	2	24	178	178	110	8.0	11.7	8.8	47	15.3	5	115	25	3.1	217	178
GD 04	08-1740	Weathered	79.65	11.48	0.74	1.31	0.03	0.03	3.27	0.43	0.009	0.016	2	<5	552	61	5	49	11	8	1	15	3	32.8	0.3	2	10	53	189	70	1.7	10.3	4.1	11	11.8	3	73	18	2.1	89	106
GD 05	08-1741	Weathered	76.74	11.83	0.88	1.55	0.03	0.05	3.76	0.42	0.012	0.017	2	<5	592	61	3	50	11	<1	1	15	3	33.0	0.3	0	9	51	227	60	1.3	10.6	4.2	12	11.0	3	75	16	1.9	47	102
GD 06	08-1742	Weathered	76.68	12.88	0.51	1.48	0.54	0.04	3.61	0.43	0.005	0.019	2	<5	578	86	<1	45	10	<2	1	16	4	47.0	0.3	6	2	64	211	120	1.2	10.7	4.9	15	12.6	3	60	19	2.1	15	114
GD 07	08-1743	Weathered	78.90	12.19	0.50	1.18	0.03	0.04	3.63	0.38	0.005	0.013	1	<5	570	74	<1	48	12	<3	1	16	3	39.4	0.3	4	2	47	211	80	0.9	11.0	4.7	9	10.8	<2	71	13	1.9	17	93
GD 08	08-1744	Weathered	76.38	13.26	0.58	1.57	0.05	0.04	3.95	0.45	0.008	0.042	2	<5	688	113	<1	47	12	<2	1	15	4	59.4	0.4	7	2	217	230	140	2.0	11.2	8.2	31	14.2	3	76	22	2.7	16	127
GD 09	08-1745	Weathered	74.29	13.92	0.61	1.65	0.05	0.04	3.37	0.47	0.005	0.032	2	<5	590	97	1	48	11	2	1	16	5	51.4	0.4	6	8	93	194	90	2.6	10.8	6.9	25	14.8	3	87	21	2.8	28	147
GD 10	08-1746	Weathered	76.62	13.52	0.57	1.36	0.03	0.04	4.02	0.39	0.006	0.043	2	<5	731	121	1	47	12	2	1	17	3	66.3	0.3	0	7	205	233	80	1.8	10.5	7.5	28	12.5	3	85	15	2.0	26	93
Mean	-	-	74.59	12.52	2.79	1.71	0.10	0.05	3.53	0.43	0.022	0.049	8	8	603	88	22	49	11	40	1	15	4	46.7	0.3	4	30	130	205	104	2.8	11.0	6.4	30	12.6	3	85	19	2.3	212	120

Grey Ghost Prospect - Stratiform ironstones

Sampl No	Lib No	Type	SiO2	Al2O3	Fe2O	MgO	Ca0	Na2O	K2O	TiO2	MnO	P2O5	As	Au	Ba	Ce	Co	Cr	Cs	Cu	Eu	Ga	Hf	La	Lu	Nb	Ni	Pb	Rb	S	Sb	Sc	Sm	Sr	Th	U	V	Y	Yb	Zn	Zr
GD 21	08-1757	SIGGhost	21.78	4.52	61.22	0.51	0.08	0.06	0.94	0.16	0.275	0.554	154	13	159	32	148	40	4	263	1	4	2	15.3	0.3	12	237	18	52	340	12.7	8.8	5.4	10	7.9	42	111	25	2.9	2122	83
GD 23	08-1759	SIGGhost	18.13	4.85	63.10	0.82	0.51	0.13	0.97	0.17	0.291	0.451	151	<5	205	18	110	43	3	318	1	6	2	9.2	-0.2	13	151	24	54	1750	11.8	8.1	3.4	24	5.9	33	126	17	2.3	1371	75
GD 24	08-1760	SIGGhost	50.68	8.75	28.10	1.10	0.82	0.05	2.08	0.34	0.120	0.263	55	<5	370	62	72	50	6	180	1	12	4	31.7	0.4	3	149	48	115	180	11.5	11.2	6.3	26	11.1	18	122	24	3.0	905	155
GD 25	08-1761	SIGGhost	18.21	4.08	65.34	0.49	0.07	0.46	0.77	0.16	0.468	0.533	297	<5	202	26	341	64	4	515	1	4	2	11.8	0.3	11	561	27	39	1960	69.2	11.0	5.4	9	6.7	58	218	30	3.1	2392	83
GD 26	08-1762	SIGGhost	24.48	5.34	56.17	0.56	0.26	0.07	0.93	0.20	0.187	0.750	183	<5	208	43	138	46	3	635	1	8	2	22.2	0.4	3	279	22	54	970	13.2	7.6	5.7	37	6.4	40	131	27	3.3	2219	95
GD 27	08-1763	SIGGhost	13.96	3.12	67.99	0.77	0.66	0.07	0.62	0.13	0.450	0.499	174	<5	158	24	208	43	4	372	1	4	2	10.6	-0.2	8	222	33	39	320	20.9	7.3	3.8	16	4.3	36	149	11	1.5	2975	61
GD 28	08-1764	SIGGhost	24.20	4.85	57.61	0.56	0.14	0.05	1.11	0.18	0.256	0.596	180	<5	217	35	166	39	4	506	1	5	2	17.0	0.3	6	212	38	65	380	10.0	7.5	5.5	13	6.6	24	126	27	3.0	2776	88
GD 30	08-1766	SIGGhost	23.71	4.67	57.21	1.28	1.00	0.04	1.03	0.18	0.233	0.491	99	674	278	47	158	64	2	566	1	7	2	25.5	-0.2	5	240	65	57	520	43.1	10.7	4.8	34	7.4	37	174	16	1.8	2137	86
GD 31	08-1767	SIGGhost	37.58	7.55	38.65	1.16	3.35	0.07	1.62	0.27	0.160	0.419	78	<5	289	40	114	64	5	393	1	10	4	20.3	0.3	2	202	60	87	260	25.1	11.3	4.5	17	11.0	29	148	22	2.5	1915	132
GD 32	08-1768	SIGGhost	41.49	8.93	32.29	1.40	3.13	0.02	1.92	0.30	0.131	0.461	85	<5	369	78	153	81	5	534	2	7	4	41.4	0.5	7	285	226	108	250	49.2	18.6	8.3	23	12.0	35	292	42	4.3	2449	143
GD 33	08-1769	SIGGhost	32.42	5.25	50.89	0.75	0.61	0.05	1.47	0.18	0.348	0.563	119	<5	261	42	160	37	4	390	1	6	2	22.0	0.2	10	195	21	86	500	13.7	8.8	3.9	15	5.3	25	127	12	1.7	2721	57
GD 34	08-1770	SIGGhost	27.60	6.02	53.15	1.78	1.59	0.07	1.14	0.25	0.167	0.685	133	<5	247	53	119	39	4	304	1	8	3	25.8	0.3	10	133	54	67	340	17.9	8.4	6.0	38	8.5	38	147	28	2.8	3341	99
Mean	-	-	27.85	5.66	52.64	0.93	1.02	0.10	1.22	0.21	0.257	0.522	142	343	247	42	157	51	4	415	1	7	3	21.1	0.2	8	239	53	69	648	24.9	9.9	5.3	22	7.8	34	156	23	2.7	2277	96

Gordon Prospect - Saprolite

Sampl No	Lib No	Type	SiO2	Al2O3	Fe2O	MgO	Ca0	Na2O	K2O	TiO2	MnO	P2O5	As	Au	Ba	Ce	Co	Cr	Cs	Cu	Eu	Ga	Hf	La	Lu	Nb	Ni	Pb	Rb	S	Sb	Sc	Sm	Sr	Th	U	V	Y	Yb	Zn	Zr
BR 02	08-1775	SIGordon	75.48	13.73	0.70	1.58	0.03	0.05	4.79	0.47	0.011	0.017	3	<5	657	79	3	51	5	1	1	17	4	42.0	0.4	7	4	17	235	80	0.7	12.2	5.5	9	15.6	6	64	26	2.9	18	140

Gordon Prospect - Stratiform ironstones

Sampl No	Lib No	Type	SiO2	Al2O3	Fe2O	MgO	Ca0	Na2O	K2O	TiO2	MnO	P2O5	As	Au	Ba	Ce	Co	Cr	Cs	Cu	Eu	Ga	Hf	La	Lu	Nb	Ni	Pb	Rb	S	Sb	Sc	Sm	Sr	Th	U	V	Y	Yb	Zn	Zr
BR 01	08-1774	SIGordon	19.24	3.29	65.41	0.30	0.04	0.02	0.64	0.13	0.314	0.753	230	<5	163	41	317	58	<1	498	2	5	2	17.4	0.7	7	250	21	31	140	17.2	21.4	8.4	6	6.2	16	380	53	5.7	1288	61
BR 03	08-1776	SIGordon	34.43	6.89	46.75	0.65	0.03	0.05	1.49	0.23	0.762	0.350	44	<5	510	44	230	43	4	83	1	6	3	21.8	0.4	3	203	30	61	180	8.9	9.5	5.3	13	8.9	16	210	34	3.6	757	96
BR 04	08-1777	SIGordon	26.95	6.09	54.26	0.60	0.05	0.03	1.41	0.23	0.647	0.691	169	<5	599	67	226	60	10	370	3	6	2	30.6	1.0	7	220	80	75	100	15.5	17.5	10.7	16	6.6	13	483	67	7.2	967	75
BR 05	08-1778	SIGordon	28.77	6.92	52.42	0.64	0.09	0.03	1.45	0.25	0.603	0.563	76	<5	353	43	382	29	4	97	1	7	3	21.1	0.4	7	246	10	59	190	4.0	7.3	4.7	17	8.8	8	111	22	2.6	1415	89
BR 06	08-1779	SIGordon	29.04	7.18	51.75	0.73	0.13	0.04	1.50	0.28	0.590	0.543	51	<5	513	43	217	45	3	151	2	9	2	19.5	0.8	5	197	20	67	440	8.3	11.4	7.2	22	8.9	13	155	54	6.2	1240	79
Mean	-	-	27.69	6.07	54.12	0.58	0.07	0.03	1.30	0.22	0.583	0.580	114	-	428	47	274	47	5	240	2	7	2	22.1	0.7	6	223	32	59	210	10.8	13.4	7.3	15	7.9	13	268	46	5.1	1133	80